Driver lines for studying associative learning in *Drosophila*

Yichun Shuai[1*], Megan Sammons[1,2], Gabriella Sterne[1,3], Karen Hibbard[1], He Yang[1], Ching-Po Yang[1,4], Claire Managan[1], Igor Siwanowicz[1], Tzumin Lee[1,4], Gerald M. Rubin[1], Glenn Turner[1], Yoshinori Aso[1*]

[1] Janelia Research Campus, Howard Hughes Medical Institute, 19700 Helix Drive, Ashburn, VA 20147, USA

[2] Current address: Technion-Israel Institute of Technology, 1 Efron St., Haifa 32000, Israel.

[3] Current address: Department of Biomedical Genetics, University of Rochester Medical Center, Rochester, NY, USA.

[4] Current address: Life Sciences Institute, University of Michigan, Ann Arbor, USA.

[*] Correspondence to: shuaiy@janelia.hhmi.org asoy@janelia.hhmi.org

Abstract

The mushroom body (MB) is the center for associative learning in insects. In *Drosophila*, intersectional split-GAL4 drivers and electron microscopy (EM) connectomes have laid the foundation for precise interrogation of the MB neural circuits. However, investigation of many cell types upstream and downstream of the MB has been hindered due to lack of specific driver lines. Here we describe a new collection of over 800 split-GAL4 and split-LexA drivers that cover approximately 300 cell types, including sugar sensory neurons, putative nociceptive ascending neurons, olfactory and thermo-/hygro-sensory projection neurons, interneurons connected with the MB-extrinsic neurons, and various other cell types. We characterized activation phenotypes for a subset of these lines and identified a sugar sensory neuron line most suitable for reward substitution. Leveraging the thousands of confocal microscopy images associated with the collection, we analyzed neuronal morphological stereotypy and discovered that one set of mushroom body output neurons, MBON08/MBON09, exhibits striking individuality and asymmetry across animals. In conjunction with the EM connectome maps, the driver lines reported here offer a powerful resource for functional dissection of neural circuits for associative learning in adult *Drosophila*.

Introduction

In the insect brain, the mushroom body (MB) serves as the center for associative learning (Davis, 2023; Figure 1A-C; reviewed in (Davis, 2023; Heisenberg, 2003; Modi et al., 2020; Owald and Waddell, 2015; Rybak and Menzel, 2017). Information about sensory inputs such as odor and color which can serve as a conditioned stimulus (CS), comes into the calyx of the MB. In *Drosophila*, approximately 2,000 Kenyon cells (KCs), the MB's primary intrinsic neurons, represent the identity of sensory stimuli by their sparse activity patterns (Honegger et al., 2011; Perez-Orive et al., 2002; Turner et al., 2008). Dopaminergic neurons (DANs) transmit signals related to the unconditioned stimulus (US), such as sugar rewards or electric shock punishments, to the MB (Burke et al., 2012; Kirkhart and Scott, 2015; Liu et al., 2012; Mao and Davis, 2009; Schwaerzel et al., 2003). DANs and MB output neurons (MBONs) collectively form 15 compartmental zones that tile down the length of the KC axons in the MB lobes (Aso et al., 2014a; Tanaka et al., 2008). Memories are stored as altered weights of synaptic connections between KCs and MB output neurons (MBONs) in each compartment (Hige et al., 2015a; Owald et al., 2015; Pai et al., 2013; Plaçais et al., 2013; Séjourné et al., 2011). Relative activity levels of MBONs across compartments represent the valence of the learned CS and drive memory-based behaviors (Aso et al., 2014b; Owald et al., 2015).

The recently completed electron microscopy (EM) connectomes of the *Drosophila* brain in larvae and adults revealed thousands of interneurons upstream of DANs, which convey reinforcement signals to the MB, and downstream of MBONs, which link the MB to premotor pathways and other higher-order brain centers (Dorkenwald et al., 2023; Eichler et al., 2017; Eschbach et al., 2020; Hulse et al., 2021; Li et al., 2020a; Scheffer et al., 2020; Winding et al., 2023; Zheng et al., 2018). Functional investigation of these interneuron cell types has been limited by the lack of cell-type-specific driver lines.

Using the intersectional split-GAL4 method (Luan et al., 2020, 2006), we previously generated 93 split-GAL4 driver lines that allowed for precise genetic access to 60 MB cell types, including most of the KCs, DANs, MBONs and other modulatory neurons in the MB lobe regions (Aso et al., 2014a). These lines have been instrumental in revealing the neural circuit logic by which the MB forms associative memories (Aso et al., 2019, 2014b; Awata et al., 2019; Berry et al., 2018; Dolan et al., 2018; Felsenberg et al., 2017; Handler et al., 2019; Hattori et al., 2017; Hige et al., 2015a, 2015b; Ichinose et al., 2015; König et al., 2019; Martinez-Cervantes et al., 2022; Masek et al., 2015; McCurdy et al., 2021; Pavlowsky et al., 2018; Plaçais et al., 2017; Sayin et al., 2019; Shyu et al., 2017; Tsao et al., 2018; Vogt et al., 2016; Wu et al., 2017; Yamada et al., 2023; Zhang et al., 2019).

Since the MB split-GAL4 lines were generated, new genetic and computational tools have expanded the cell types that can be targeted and facilitated the split-GAL4 design. Critically, a new collection of ZpGAL4DBD and p65ADZp hemidrivers became available (Dionne et al., 2018; Tirian and Dickson, 2017). Moreover, the expression patterns of the original GAL4 driver lines were imaged with higher-resolution confocal microscopy and Multi-Color-Flip-Out (MCFO) labeling method to reveal the morphology of individual neurons (Meissner et al., 2023; Nern et al., 2015). Additionally, advanced tools for computational

neuroanatomy were developed to aid the design of split-GAL4 driver lines (Bogovic et al., 2020; Costa et al., 2016; Masse et al., 2012; Meissner et al., 2023; Otsuna et al., 2018). Using these tools and resources, additional collections of split-GAL4 lines were generated for the atypical MBONS, which have dendritic input both within the MB lobes and in adjacent brain regions (Rubin and Aso, 2024). In this report, we introduce a novel collection of approximately 800 split-GAL4 lines, covering sensory neurons for sugar, wind and nociception, projection neurons for olfactory, thermo/hygro-sensory and gustatory signals, ascending neurons from ventral nerve cord (VNC), cell types within the MB, and interneurons that connect with DANs and/or MBONs. While our primary objective was to generate driver lines for studying associative learning, the collection also includes cell types tailored for various other functions. We provide a lookup table (Supplementary File 1) that maps the corresponding EM neurons in the hemibrain connectome for these drivers to facilitate connectome-guided investigation of neural circuits. This expanded collection of driver lines will be instrumental for many future studies of associative learning and beyond.

Results and Discussions

Split-GAL4 design and anatomical screening

We screened the expression patterns of over 4,000 intersections of split-GAL4 hemidrivers to identify lines potentially labeling neurons of interest (Figure 1D). From this we selected 1,183 split-GAL4 lines for further characterization using both higher resolution imaging, and MCFO to visualize the individual neurons that compose each split-GAL4 pattern. For these lines, we employed higher resolution confocal microscopy and visualized the individual neurons that compose each split-GAL4 pattern with the MCFO method. We eventually identified 828 lines that we deemed experimentally useful based on their specificity, intensity and consistency. These fly lines are now publicly available through the webpage of the Janelia Flylight team project (http://www.janelia.org/split-gal4), where we have deposited a total of 28,376 confocal images from 6,374 tissue samples to document their expression patterns. We included lines with off-target expression, as they can be valuable for anatomical, developmental or functional imaging experiments, even if not suitable for behavioral experiments. Additionally, we retained drivers that serendipitously had specific and likely useful labeling of cell types we were not intentionally screening for. Examples of confocal microscopy images are shown in Figure 1F and Figure 1-figure supplement 1.

We have annotated our split-GAL4 lines by matching the labeled neurons to their counterparts in the hemibrain connectome volume (Scheffer et al., 2020). We utilized confocal images registered to a standard brain, and matched neuronal cell types in each split-GAL4 line with those present in other lines and with the EM-reconstructed neurons (Figure 2A-D, see Materials and Methods). This light microscopy (LM) to EM matching process allows us to locate the cell type of each driver line in the connectome map, enabling users to select driver lines for further functional investigations based on their upstream and downstream synaptic partners (Figure 2E; Figure 2-figure supplement 1-20).

Figure 1E provides an overview of the categories of covered cell types. Among the 828 lines, a subset of 355 lines, collectively labeling at least 319 different cell types, exhibit highly specific and non-redundant expression patterns are likely to be particularly valuable for behavioral experiments. Supplementary File 1 lists 859 lines (including split-LexA) and their detailed information, such as genotype, expression specificity, matched EM cell type(s), and recommended driver for each cell type. A small subset of 47 lines from this collection have been previously used in studies (Aso et al., 2023; Dolan et al., 2019; Gao et al., 2019; Scaplen et al., 2021; Schretter et al., 2020; Takagi et al., 2017; Xie et al., 2021; Yamada et al., 2023). The newly generated LexA, Gal4DBD and LexADBD lines are listed in Supplementary File 2.

Drivers for the MB cell types, MBON-downstream and DAN-upstream

Our initial efforts to identify cells of interest started prior to the completion of the EM connectome. At this early stage, we attempted to identify cell types either downstream of MBONs or upstream of DANs using confocal images of GAL4 drivers registered to a standard brain (Bogovic et al., 2020). We searched for GAL4 drivers containing cell types with potential connections to MBONs or DANs by quantifying the number of voxels overlapping with MBON axons or DAN dendrites (Otsuna et al., 2018). We then built split-GAL4 intersections from selected pairs of drivers from the established hemidriver library (Dionne et al., 2018; Tirian and Dickson, 2017).

Once EM information became available, we matched the neurons identified with this approach to EM-reconstructed neurons to yield split-GAL4 drivers encompassing 110 cell types that connect with the DANs and MBONs (Figure 3). Several of the cell types originally selected by LM were found to be not directly connected with MBONs or DANs. Nevertheless, these lines can be valuable for other types of investigations. For example, one such line, SS32237, was found to exhibit robust female-female aggression when activated (Schretter et al., 2020).

In the hemibrain EM connectome, there are about 400 interneuron cell types that have over 100 total synaptic inputs from MBONs and/or synaptic outputs to DANs. Our newly developed collection of split-GAL4 drivers covers 30 types of these ‘major interneurons’ of the MB (Supplementary File 3). While this constitutes a small fraction, it includes cell types with remarkable connectivity patterns. For instance, CRE011, present as a single neuron per hemisphere, integrates over 2,000 inputs from 9 types of MBONs. This is the highest number of synaptic inputs from MBONs among all interneurons (Figure 3C). CRE011 provides cholinergic input to reward DANs (Figure 2E) and neurons in the lateral accessory lobe, a premotor center housing dendrites of multiple descending neurons (Kanzaki et al., 1994; Namiki et al., 2018). Another notable example is SMP108, which receives inputs from multiple glutamatergic MBONs and makes the highest number of cholinergic connections to DANs involved in appetitive memory (Figure 3C). We recently reported on SMP108’s role in second-order conditioning (Yamada et al., 2023) and its upstream neurons labeled in SS33917 in transforming appetitive memory into wind-directed locomotion (Aso et al., 2023). Supplementary File 3 contains connectivity information of MBON-downstream and DAN-

upstream neurons, along with the predicted neurotransmitters (Eckstein et al., 2023) and the available driver lines.

The current collection also contains over 180 lines for cell types that have innervations within the MB (Figure 3-figure supplement 1, Supplementary File 4 and 5). These lines offer valuable tools to study several prominent cell types that previously are not genetically accessible. Notably, SS85572 enables the functional study of LHMB1, which forms a rare direct pathway from the calyx and the lateral horn (LH) to the MB lobes (Bates et al., 2020). SS48794 labels OA-VUMa2 octopaminergic neurons, which are the *Drosophila* counterparts to the honeybee OA-VUMmx1 neurons, the first neurons identified as mediating US signals in an insect brain (Hammer, 1993). Moreover, several drivers in this collection provide improved specificity. When combined with previous collections (Aso et al., 2014a; Rubin and Aso, 2023), we now have coverage for 7 types of Kenyon cells and 62 out of 87 total cell types within the MB (excluding PNs). Overall, this amounts to over 70% coverage for non-PN cell types within the MB and about 10% coverage for MBON-downstream and DAN-upstream cell types (Supplementary File 3 and 5, Figure 3B-C).

Drivers for the antennal lobe projection neurons

In *Drosophila*, the primary CS pathway to the MB involves the antennal lobe PNs that convey olfactory signals. We have developed a set of driver lines for PNs and other cell types in the antennal lobe (Supplementary File 1). This set includes 191 lines, covering more than 48 of the approximately 190 PN types identified through EM connectome and LM studies (Bates et al., 2020; Li et al., 2020b; Lin et al., 2007; Tanaka et al., 2004; Zheng et al., 2022). This set encompasses both uni- and multi-glomerular PNs (Figure 4 and 5; Supplementary File 6).

The antennal lobe, in addition to the 51 olfactory glomeruli, contains 7 glomeruli involved in processing thermo- and hygro-sensory information (Enjin et al., 2016; Frank et al., 2015; Gallio et al., 2011; Jenett et al., 2012; Liu et al., 2015; Marin et al., 2020; Stocker et al., 1990; Tanaka et al., 2012). We provide 8 lines that cover sensory neurons projecting into these non-olfactory glomeruli and 18 lines covering the projection neurons emanating from them (Figure 6; Supplementary File 1 and 6).

Although less abundant than the olfactory input, the MB also receives visual information from the visual projection neurons (VPNs) that originate in the medulla and lobula and project to the accessory calyx (Li et al., 2020a; Vogt et al., 2016). A recent preprint described the full collection of split-GAL4 driver lines in the optic lobe, which includes the VPNs to the MB (Nern et al., 2024).

Drivers for reinforcement pathways

Our understanding of the neural pathways that encode the US has been greatly advanced by experiments that have tested the sufficiency of various neuronal cell types to substitute for the US (Aso et al., 2010; Aso and Rubin, 2016; Burke et al., 2012; Chiang et al., 2011; Claridge-Chang et al., 2009; Hige et al., 2015a; Huetteroth et al., 2015; Liu et al., 2012; Saumweber et al., 2018; Schroll et al., 2006; Yamagata et al., 2015). These experiments leveraged

194 thermogenetic or optogenetic tools expressed in specific neuronal cell types, especially DANs,
195 to assess their functions in associative learning. The approach to directly stimulate DANs,
196 although valuable, bypasses the earlier US processing pathways and potential feedback in the
197 circuit. Because of this experimental caveat, it is preferable to activate neurons at the sensory
198 level of reward or punishment pathways to faithfully replicate the natural activity of these
199 DANs. In that way, DANs can be regulated by both US sensory pathways and feedback
200 pathways from MBONs. That is likely to be essential for the successful execution of more
201 complex learning tasks in which flies update memories based on the current and past
202 experiences (Felsenberg et al., 2018, 2017; Jiang and Litwin-Kumar, 2021; McCurdy et al.,
203 2021; Otto et al., 2020; Rajagopalan et al., 2022).

204 Our collection identified several useful genetic tools that advance this approach
205 further. For example, we generated drivers for the cell types in the thermo-sensory pathways,
206 as well as PNs for odors with innate preference, such as CO2 and cVA (Datta et al., 2008; Lin
207 et al., 2013; Suh et al., 2004). These cell types are candidates to convey the reinforcement
208 signals to the MB and other brain regions for associative learning.

209 We had a particular interest in developing a driver panel for gustatory sensory
210 neurons. Although they play a central role in reward signaling, they convey those signals to
211 the MB through largley uncharacterized pathways (Bohra et al., 2018; Burke et al., 2012;
212 Deere et al., 2023; Kim et al., 2017; Miyazaki et al., 2015; Sterne et al., 2021). GAL4 driver
213 lines that recapitulate expression patterns of gustatory receptors (GRs) have been generated
214 and utilized for functional studies (Dahanukar et al., 2007; Harris et al., 2015; Miyamoto et
215 al., 2012; Wang et al., 2004; Yavuz et al., 2014). However, these driver lines tend to contain a
216 morphologically and functionally heterogeneous set of sensory neurons (see for examples:
217 Chen et al., 2022; Thoma et al., 2016) and may have off-target expression. To address these
218 limitations, we have developed split-GAL4 drivers specific to different subsets of gustatory
219 sensory neurons by generating hemidrivers for GR-gene promoters and screening
220 intersections with existing hemidrivers (Figure 7A).

221 In fruit flies, sugar is detected by sensory neurons located on different taste organs of
222 the body and also inside the brain (Fujii et al., 2015; Hiroi et al., 2002; Miyamoto et al., 2012;
223 Rodrigues and Siddiqi, 1978). Gr64f-Gal4, in which Gal4 is expressed under the control of the
224 promoter of the sugar receptor gene *Gr64f*, broadly labels sugar sensory neurons (Dahanukar
225 et al., 2007 and Figure 7 – figure supplement 1). Gr64f-Gal4 expression can be found in
226 heterogeneous sets of sensory neurons in the labellum, the tarsi and the labral sense organ
227 (LSO) located along the pharynx. In addition, Gr64f-Gal4 also labels subsets of olfactory
228 receptor neurons and neurons innervating the abdominal ganglion (Park and Kwon,
229 2011)(Figure 7-figure supplement 1). Whether these cells endogenously express Gr64f is yet
230 to be confirmed. However it seems likely that the heterogeneity of Gr64f-Gal4 expression
231 could limit its usage in generating fictive rewards in complex associative learning.

232 To refine Gr64f-Gal4 expression, we intersected Gr64f-GAL4DBD with various AD lines
233 selected to have overlapping expression with a subset of the projection patterns of the
234 original Gr64f-GAL4. We obtained 16 stable split-GAL4 lines with labeling in distinct subsets

235 of the original expression pattern (Figure 7). We examined the ability of these lines to serve
236 as US in olfactory learning (Aso and Rubin, 2016) and their potency to drive local search
237 behaviors, another memory-based behavior induced by appetitive stimuli (Corfas et al.,
238 2019)(Figure 8 and Figure 8-figure supplement 1). Additionally, we measured the walking
239 speed of flies, as flies decrease walking while feeding (Thoma et al., 2016). (Aso and Rubin,
240 2016)

241 Among the Gr64f-split-GAL4 lines, SS87269 emerged as the best driver for substituting
242 sugar reward in olfactory learning given its anatomical specificity as well as its effectiveness
243 throughout long training protocols (Figure 8E). SS87269 expresses in the labellum and in at least
244 two types of tarsal sensory neurons, namely the ascending (atGRN) and the non-ascending
245 segment-specific (stGRN) types (Figure 7E-F). The driver does not label pharyngeal sensory
246 neurons, and importantly, it lacks expression in abdominal ganglion and olfactory sensory
247 neurons, which could reflect off-target expression from the original Gr64f-GAL4. When odor
248 presentation was paired with the activation of SS87269 neurons, flies formed robust
249 appetitive memories even after extended training with high LED intensity (Figure 8E, Figure
250 8-figure supplement 1 and Video 1). Furthermore, and consistent with the idea that this
251 subset of sensory neurons encodes appetitive food-related taste information, activating
252 these neurons elicited proboscis extension and slowed flies (Figure 8F-I; Figure 8-figure
253 supplement 2, Video 2 and 4). These flies also showed robust local search behavior during
254 the post-activation period, i.e., an increased probability of revisiting the area where they
255 experienced the activation (Video 3). Notably, the revisiting phenotype of SS87269 was
256 stronger than any other Gr64f-split-GAL4 drivers (Figure 8F and Figure 8-figure supplement
257 2A) and the original Gr64f-GAL4 even after 180 repetitive activation trials (Figure 8-figure
258 supplement 3).

259 Two other lines SS88801 and SS88776, which label stGRNs or stGRNs along with labial
260 sensory neurons, respectively (Figure 7K-L,I), similarly showed appetitive learning and
261 reduced locomotion during activation (Figure 8E-F). Interestingly, however, the activation of
262 stGRNs with SS88801 did not induce significant local search behaviors (Figure 8F and Figure
263 8-figure supplement 2A). This finding could be valuable for understanding circuits underlying
264 local search behavior and invites further investigation to compare pathways from labial and
265 tarsal sensory neurons to the MB and the central complex.

266 In contrast to SS87269, two other lines, SS87278 and SS87279, express in cells that
267 appear to convey aversive signals. Activation of these lines induced an increase in walking
268 speed during activation and reduced the probability of revisiting where flies received
269 activation LED light (Figure 8F and Figure 8-figure supplement 2). Also, flies became
270 progressively less mobile during the inter-trial interval period (Figure 8G). We made a similar
271 observation with the original Gr64f-GAL4 (Figure 8G) as well as with a bitter-taste driver,
272 Gr66a-GAL4 (data not shown). With extended training using SS87278 and SS87279, the
273 preference to the paired odor eventually became negative (Figure 8E). These drivers label
274 distinct subsets of sensory neurons projecting to the abdominal ganglion (Figure 7O,P). The
275 innervation of SS87278 inside the abdominal ganglion is similar to that of Gr66a-GAL4 (Figure

7Q) (Dunipace et al., 2001), which is known to label multidendritic sensory neurons in the adult *Drosophila* abdomen (Shimono et al., 2009). Examining projection patterns in fly bodies with whole-animal agar sections, we found that sensory neurons in SS87278 also project to the abdominal body surface (Figure 7J), likely representing the class IV multidendritic neurons that detect multimodal nociceptive stimuli (Hwang et al., 2007; Ohyama et al., 2015). The expression in these aversive sensory neurons therefore may complicate the interpretation of appetitive learning with the original Gr64f-GAL4.

Overall, the refinement of Gr64f-Gal4 expression with SS87269 now allows for specific manipulation of the rewarding subset of gustatory sensory neurons and permits training with an extended number of trials. While we have not yet conducted extensive anatomical screening, LexADBD lines generated with Gr64f, Gr43a, Gr66a, Gr28b.d promoters (Figure 7A) should allow for comparable refinement of driver lines to target sensory neurons expressing these receptors. For instance, we generated split-LexA drivers specific for internal fructose sensory neurons (Miyamoto et al., 2012) or a subset of bitter taste neurons (Figure 7-figure supplement 2). We also made a small number of lines for cell types in the subesophageal zone (SEZ) area (Figure 7-figure supplement 3), which complement previous collections of drivers for gustatory interneurons (Otto et al., 2020; Sterne et al., 2021).

Lastly, we generated driver lines for putative ascending nociceptive pathways. We tested whether optogenetic activation would drive avoidance related behaviors using the circular arena, where an activating LED illuminated two quadrants of the arena, and the other two remained dark. We determined the quadrant preference for 581 combinations of ZpGAL4DBD and p65ADZp hemidrivers. We found one driver, SS01159, which showed the most robust avoidance of the illuminated quadrants, and exhibited behavioral features characteristic of nociception, including backward walking, turning, increased speed, and jumping upon activation (Figure 9B-D, and Video 5). This driver labels a group of ascending neurons (Figure 9E), which likely carry nociceptive signals from the body and legs to the brain. We then generated drivers for subsets of these ascending neurons guided by single neuron morphologies of cells in SS01159 determined by MCFO stochastic labeling (Nern et al., 2015). The collection in total contains approximately 100 split-GAL4 lines covering ascending neurons. While not completely matched to EM cell types due to only a portion of their morphologies being available in the hemibrain volume, these lines serve as a valuable resource for querying the reinforcement pathways.

Morphological individuality and asymmetry

Neuronal morphology can vary, and the randomness of developmental processes can ultimately result in differences in behavior among individuals (Linneweber). The recent landmark study systematically examined morphological variability of neurons using the EM connectomic data (Schlegel 2023), but it will only be possible to examine relatively few individual brains for the foreseeable future. As a part of Janelia Flylight team project to generate cell-type-specific driver lines, we have imaged over 6,000 fly brains for the present study. While annotating those confocal images, we occasionally encountered samples with

317 atypical morphologies (Figure 10). For example, one V_l2PN neuron, which typically projects
318 to the lateral horn of the ipsilateral hemisphere, exhibited a peculiar morphology in one brain
319 sample, where its axon crossed the midline and projected to the contralateral hemisphere,
320 yet it still reached the correct target area within the lateral horn of the opposite side (Figure
321 10A). Another instance involved a DPM neuron, the sole serotonergic neuron of the MB lobes.
322 While typical brain samples contain only one DPM neuron per hemisphere, we found a brain
323 with two DPM neurons in one hemisphere (Figure 10B). In this case, the DPM projections
324 exhibited an atypical innervation of the calyx of the mushroom body. We also found examples
325 involving MBONs. The dendrites of MBON-α1 are typically confined to the α lobe of the MB,
326 but we discovered a case where this cell in addition sent projections to the ellipsoid body
327 (Figure 10C). MBON-α3 displayed striking variability in soma positions, but only subtle
328 variability in axonal projections (Figure 10D). The table in Figure 10E summarizes additional
329 examples of the atypical morphologies of MBONs. Overall in 1241 brain hemispheres
330 examined, we found mislocalization of dendrites and axons in 3.14% and 0.97% of MB cell
331 types, respectively. If this rate of mislocalization is generalizable to other brain regions, a fly
332 brain of ~130,000 neurons (Dorkenwald et al., 2023) would have a few thousands of neurons
333 with mislocalized dendrites or axons. These examples of atypical morphology were observed
334 only once in dozens of samples, and thus can be considered as erroneous projections either
335 resulting from stochastic developmental processes, or possibly caused by ectopic expression
336 of reporter proteins on the plasma membrane at a high level.

337 In contrast to these rare, and seemingly erroneous, morphological variations, we
338 observed much more frequent and reproducible variations in the composition as well as
339 morphologies in the two MBONs (MBON08 and MBON09) labeled by MB083C, which may
340 amount to "individuality". This split-GAL4 driver line invariably labels two cells in each
341 hemisphere in 169 brain samples examined with four different reporters and in both sexes
342 (57 males and 112 females; Figure 11-figure supplement 1). In all samples, these MBONs
343 arborize dendrites in the γ3 and β′1 compartments. An obvious mistargeting of the axon was
344 observed in only one sample, suggesting highly consistent development of these MBONs
345 (Figure 11A-B). However, MCFO method visualized two distinct morphologies of these
346 MBONs: MBON08 arborizes dendrites in the γ3 compartment of both hemispheres, whereas
347 MBON09 arborize dendrites in ipsilateral γ3 and contralateral β′1 (Figure 11C-H)(Aso et al.,
348 2014a). β′1 compartment was always labeled in both hemispheres for all 169 samples,
349 suggesting that MBON09 represents at least one of the two cells in each hemisphere. The
350 second cell can be either MBON08 or MBON09. In MCFO experiments, we observed 21
351 instances of MBON08 (8 in the left and 13 in the right hemisphere) and 188 instances of
352 MBON09 (Figure 11I). Based on these observations, we expect 65% of flies contain four
353 MBON09, while the remaining 35% of flies likely have at least one MBON08 (Figure 11J). In
354 71 hemispheres, two cells were visualized in different colors of MCFO: 52 contained two
355 MBON09 and 19 contained one MBON08 and MBON09. We never observed a brain with
356 MBON08 on both hemispheres or two MBON08 in one hemisphere (Figure 11J). When
357 MBON08 and MBON09 coexist, MBON09 arborized in the lateral part of the ipsilateral γ3 and

358 MBON08 arborize in the medial part of the contralateral γ3 (Figure 11E-H). This seemingly
359 extended γ3 compartment innervated by MBON08 is not part of γ4, because it did not overlap
360 with DANs in the γ4 (Figure 11-figure supplement 2A-B).
361 Although MBON08 was not found in brain samples used for the hemibrain or FAFB
362 EM connectome (Dorkenwald et al., 2023; Scheffer et al., 2020; Zheng et al., 2018), DANs in
363 the γ3 could be subdivided to two groups that innervate the medial or lateral part of the γ3
364 (Figure 11-figure supplement 2C) (Li et al., 2020b). Therefore, subdivision of the γ3
365 compartment may exist irrespective of heterogeneity on the MBON side. In larval brains, two
366 MBONs that correspond to adult MBON08/09 exhibit identical morphology (Eichler et al.,
367 2017; Saumweber et al., 2018; Truman et al., 2023). During metamorphosis, these larval
368 MBONs may acquire distinct morphology as MBON08 at 21/209 odds. We have never
369 observed a brain with MBON08 on both hemispheres, and therefore MBON08 is likely to
370 appear in only one hemisphere, if at all (Figure 11J). This resulting asymmetry could be one
371 source of turning handedness and idiosyncratic learning performance (de Bivort et al., 2022;
372 Smith et al., 2022), given that MBON09 forms extensive connections with other MBONs and
373 fan-shaped body neurons (Hulse et al., 2021; Li et al., 2020b) and the activity of
374 MBON08/MBON09 has a strong influence on turning (Aso et al., 2023, 2014b; Matheson et
375 al., 2022).
376
377 **Conversion to split-LexA**
378 Split-GAL4 lines enable cell-type-specific manipulation, but some experiments require
379 independent manipulation of two cell types. Split-GAL4 lines can be converted into split-LexA
380 lines by replacing the GAL4 DNA binding domain with that of LexA (Ting et al., 2011). To
381 broaden the utility of the split-GAL4 lines that have been frequently used since the
382 publication in 2014 (Aso et al., 2014a), we have generated over 20 LexADBD lines to test the
383 conversions of split-GAL4 to split-LexA. The majority (22 out of 34) of the resulting split-LexA
384 lines exhibited very similar expression patterns to their corresponding original split-GAL4
385 lines (Figure 12). The main mode of failure when converting to LexA was that expression levels
386 become too weak and stochastic.
387
388 **Concluding Remarks**
389 The ability to define and manipulate a small group of neurons is crucial for studying neural
390 circuits. Here, we have generated and characterized driver lines targeting specific cell types
391 that are likely to be a part of associative learning circuits centered on the MB. We have
392 provided these driver lines with a comprehensive lookup table linking these cell types with
393 the EM hemibrain connectome (Supplementary File 1). These lines, together with preceding
394 collections of drivers (Aso et al., 2014a; Aso and Rubin, 2016; Davis et al., 2020; Dolan et al.,
395 2018; Rubin and Aso, 2023; Shuai et al., 2015; see for examples: Sterne et al., 2021; Strother
396 et al., 2017; Truman et al., 2023; Tuthill et al., 2013; Wang et al., 2021; Wolff and Rubin, 2018;
397 Wu et al., 2016), collectively constitute a powerful resource for precise functional

interrogation of associative learning in adult *Drosophila melanogaster*, and will be a foundation to reveal conserved principles of neural circuits for associative learning.

Materials and Methods

Fly strains

Drosophila melanogaster strains were reared at 22°C and 60% humidity on standard cornmeal food in 12:12 hour light:dark cycle. The genotypes of all split-GAL4 and split-LexA driver lines released here are listed in the Supplementary File 1. The new collection of split-GAL4 drivers reported here was designed based on confocal image databases (http://flweb.janelia.org) (Jenett et al., 2012; Tirian and Dickson, 2017), and screening expression patterns of p65ADZp and ZpGAL4DBD combinations was performed as described previously (Aso et al., 2014a; Pfeiffer et al., 2010). The confocal microscopy images of the splitGAL4 lines can be found at flylight database under "Aso 2021" release. Fly strains can be requested from Janelia or the Bloomington stock center. Split-LexA expression data and fly strains are also available upon request from Aso lab.

Immunohistochemistry

Brains and ventral nerve cords of 3-10 days old flies were dissected, fixed and immunolabeled and imaged with confocal microscopes (Zeiss LSM710, LSM780 or LSM880) as previously described (Aso et al., 2014a; Jenett et al., 2012; Meissner et al., 2023; Nern et al., 2015). The detailed protocols and videos are available at https://www.janelia.org/project-team/flylight/protocols.

Most samples were collected from females, though typically at least one male fly was examined for each driver line. While we noticed certain lines such as SS48900, exhibited distinct expression patterns in females and males, we did not particularly focus on sexual dimorphism, which is analyzed elsewhere (Meissner et al., 2024). Therefore, unless stated otherwise, the presented samples are of mixed gender. Detailed metadata, including gender information and the reporter used, can be found in Supplementary File 7.

Whole-body sections

For sample preparation, flies were anesthetized on ice and briefly washed with 70% ethanol. Small incisions were made in the flanks of the thorax and abdomen under 2% paraformaldehyde in PBS with 0.1% Triton X-100 (PBS-T), and the flies were fixed in this solution overnight at 4°C. After washing in PBS containing 1% Triton X-100, the samples were embedded in 7% agarose and sectioned on Leica Vibratome (VT1000s) sagittally in slices of 0.3 mm. The slices were incubated in PBS with 1% Triton X-100, 0.5% DMSO, 3% normal goat serum, Texas Red-X Phalloidin (1:50, Life Technologies #T7471) and anti-GFP rabbit polyclonal antibodies (1:1000, Thermo Fisher, #A10262) at room temperature with agitation for 24 hours. After a series of three washes in PBS-T, the sections were incubated for another 24 hours in the solution containing secondary antibodies (1:1000, goat anti-rabbit, Thermo Fisher #A32731). The samples were then washed in PBS-T and mounted in Tris-HCL (pH 8.0)-buffered 80% glycerol + 0.5% DMSO. For imaging and rendering, serial optical sections were obtained at 2 µm intervals on a Zeiss 880 confocal microscope with a pan-apochromat 10x/0.45 NA objective using 488 and 594 nm lasers. Images were processed in Fiji (http://fiji.sc/) and Photoshop (Adobe Systems Inc.).

Behavioral assays

For flies expressing CsChrimson (Klapoetke et al., 2014), the food was supplemented with retinal (0.2 mM all-trans-retinal prior to eclosion and then 0.4 mM). Two- to six-day old adult females were collected and sorted on a Peltier cold plate 2-4 days before testing in behavioral assays. Flies were starved for 40–48 hr on 1% agar before they were subjected to behavioral experiments. Olfactory conditioning and optogenetic activation experiments were performed as previously described using the modified four-field olfactory arena equipped with the 627 nm LED board and odor mixers (Aso and Rubin, 2016; Pettersson, 1970). The odors were diluted in paraffin oil: pentyl acetate (PA, 1:10000, v/v) and ethyl lactate (EL, 1:10000, v/v). Videos were taken at 30 frames per second and analyzed using Fiji and Caltech FlyTracker (Eyjolfsdottir et al., 2014).

LM-EM matching

The confocal microscopy images of different split-GAL4 lines were registered to a common template JRC2018_unisex (Bogovic et al., 2020) and organized in Janelia Workstation software (https://github.com/JaneliaSciComp/workstation). Color depth MIP mask search (Otsuna et al., 2018) was used to search through the EM neuron library (hemibrain 1.2.1) for matching candidates. The searching target was obtained by either creating a mask on the full confocal image or using neurons of interest manually segmented in VVD viewer (https://github.com/takashi310/VVD_Viewer)(Wan et al., 2012). SWC files of top-matching EM neuron candidates were loaded into VVD viewer together with the confocal microscopy images in the same standard brain coordinates. By rotating the 3d images and manually scrutinizing the branching patterns, we picked the best matching candidate. Typically, we had high confidence of LM-to-EM matching for the line that labels only one cell per hemishere. For instance, we could unambiguously match the cell in SS67721 with SMP108 in the EM hemibrain volume. Our confidence of LM-to-EM matching tended to be lower for the lines that label multiple cells, because neurons of similar morphologies could be labeled together in those lines.

Connectivity analysis

Connectivity information was retrieved from neuPrint (neuprint.janelia.org), a publicly accessible website hosting the “hemibrain” dataset (Scheffer et al., 2020). For cell types, we used cell type name assignments reported in Sheffer et al., 2020. Only connections of the cells in the right hemisphere were used due to incomplete connectivity in the left hemisphere. The 3D renderings of neurons presented were generated using the visualization tools of NeuTu (Zhao et al., 2018) or VVD viewer .

Statistics

Statistical comparisons were performed on GraphPad Prism 7.0 using one-way ANOVA followed by Dunnett's test for multiple comparisons. Sample size was not predetermined based on pilot experiments.

Data Availability

The confocal images of expression patterns are available online (http://www.janelia.org/split-gal4). The values used for figures are summarized in Source Data.

481

482 **Detailed fly genotypes used by figures**

483

Figure 1F	*w/w, 20xUAS-CsChrimson-mVenus attP18; +/split-GAL4* *w/w, 20xUAS-CsChrimson-mVenus attP18; +/P{Gr64f-GAL4.9.7}5; +/P{Gr64f-GAL4.9.7}1*
Figure 2A	*w/w, 20xUAS-CsChrimson-mVenus attP18;+/SS45245-split-GAL4*
Figure 2B	w/w, pBPhsFlp2::PEST in attP3;; pJFRC201-10XUAS-FRT>STOP>FRT-myr::smGFP-HA in VK00005, pJFRC240-10XUAS-FRT>STOP>FRT-myr::smGFP-V5-THS-10XUAS-FRT>STOP>FRT-myr::smGFP-FLAG in su(Hw)attP1/SS45245-*split-GAL4*
Figure 2C	w/w;pJFRC225-5XUAS-IVS-myr::smFLAG in VK00005, pJFRC51-3XUAS-IVS-Syt::smHA in su(Hw)attP1/SS45245-*split-GAL4*
Figure 7E-J	*w/w, 20xUAS-CsChrimson-mVenus attP18;+/SS87269-split-GAL4* *w/w, 20xUAS-CsChrimson-mVenus attP18;+/SS87272-split-GAL4* *w/w, 20xUAS-CsChrimson-mVenus attP18;+/SS88801-split-GAL4* *w/w, 20xUAS-CsChrimson-mVenus attP18;+/SS87278-split-GAL4*
Figure 7K-Q	*w/w, 20xUAS-CsChrimson-mVenus attP18;+/Gr64f-split-GAL4s* *w/w, 20xUAS-CsChrimson-mVenus attP18;+/Gr66a-GAL4*
Figure 7 - figure supplement 1	*w/w; +/ P{Gr64f-GAL4.9.7}5; 5xUAS-myr-smFLAG in VK00005/P{Gr64f-GAL4.9.7}1*
Figure 8E-F, Figure 8 - figure supplement 2	*w/w, 20xUAS-CsChrimson-mVenus attP18; +/Gr64f-split-GAL4s* *w/w, 20xUAS-CsChrimson-mVenus attP18; +/ P{Gr64f-GAL4.9.7}5; +/P{Gr64f-GAL4.9.7}1* *w/w, 20xUAS-CsChrimson-mVenus attP18; +/empty-split-GAL4*
Figure 8 - figure supplement 1A	*w/w, 20xUAS-CsChrimson-mVenus attP18; +/SS87269-split-GAL4*
Figure 8 - figure supplement 1C	*w/w, 20xUAS-CsChrimson-mVenus attP18; +/SS87269-split-GAL4* *w/w, 20xUAS-CsChrimson-mVenus attP18; +/SS87278-split-GAL4* *w/w, 20xUAS-CsChrimson-mVenus attP18; +/empty-split-GAL4*
Figure 8I	*w/w, 20xUAS-CsChrimson-mVenus attP18;+/SS87269-split-GAL4* *w/w, 20xUAS-CsChrimson-mVenus attP18;+/SS88801-split-GAL4* *w/w, 20xUAS-CsChrimson-mVenus attP18;+/empty-GAL4*
Figure 9B-D	*w/w, 20xUAS-CsChrimson-mVenus attP18;+/SS01159-split-GAL4* *w/w, 20xUAS-CsChrimson-mVenus attP18;+/empty-GAL4*
Figure 10A	*w/w;pJFRC225-5XUAS-IVS-myr::smFLAG in VK00005,* *pJFRC51-3XUAS-IVS-Syt::smHA in su(Hw)attP1/SS01336-split-GAL4*
Figure 10B	*w/w;pJFRC225-5XUAS-IVS-myr::smFLAG in VK00005,* *pJFRC51-3XUAS-IVS-Syt::smHA in su(Hw)attP1/ SS01241-split-GAL4*
Figure 10C	*w/w, pBPhsFlp2::PEST in attP3;;* *pJFRC201-10XUAS-FRT>STOP>FRT-myr::smGFP-HA in VK00005,* *pJFRC240-10XUAS-FRT>STOP>FRT-myr::smGFP-V5-THS-10XUAS-FRT>STOP>FRT-myr::smGFP-FLAG in su(Hw)attP1/MB310C-split-GAL4*
Figure 10D	*w/w, pBPhsFlp2::PEST in attP3;;* *pJFRC201-10XUAS-FRT>STOP>FRT-myr::smGFP-HA in VK00005,* *pJFRC240-10XUAS-FRT>STOP>FRT-myr::smGFP-V5-THS-10XUAS-FRT>STOP>FRT-myr::smGFP-FLAG in su(Hw)attP1/MB082C-split-GAL4*
Figure 11A-B, Figure 11 - figure supplement 1	*w/w;;pJFRC225-5XUAS-IVS-myr::smFLAG in VK00005,*

	pJFRC51-3XUAS-IVS-Syt::smHA in su(Hw)attP1/ MB083C-split-GAL4 *w/w;UAS-mCD8::GFP/MB083C-split-GAL4* *w/w, 20xUAS-CsChrimson-mVenus in attP18;;+/ MB083C-split-GAL4* *w/w, pJFRC12-10XUAS-IVS-myr::GFP in attP18/ MB083C-split-GAL4*
Figure 11 - figure supplement 2	*w, 10xUAS-IVS-myr::smGdP-HA in attP18, 13xLexAop2-IVS-myr::smGdP-V5 in su(Hw)attP8; +/R52G04-LexA (MBON08/09);+/MB312C-split-GAL4 (PAM-γ4)* *w, 10xUAS-IVS-myr::smGdP-HA in attP18, 13xLexAop2-IVS-myr::smGdP-V5 in su(Hw)attP8; +/R52G04-LexA (MBON08/09);+/MB441B-split-GAL4 (PAM-γ3)* *w/w;;VT006202-LexAp65 in attP2/pJFRC19-13XLexAop2-IVS-myr::GFP in attP2*
Figure 12	*w/w, 20xUAS-CsChrimson-mVenus attP18; +/split-GAL4s* *w/w, 13xLexAop2-CsChrimson-mVenus attp18; +/split-LexAs*

Supplemental information

Supplementary File 1 A list of released driver lines and their corresponding EM neurons.

Listed are stable split-GAL4 lines (SS, MB) and split-LexA lines (SL). Drivers are grouped by the anatomical regions where they have their primary expression. Matching to EM cell types in the hemibrain v1.2.1 dataset was performed by an algorithmic search of the morphologies of EM skeletons, followed by manual evaluation of proposed matches using 3D visualization software. The best-matching candidates are listed. Where multiple candidates seem valid, the alternatives are listed in the note column. In some cases, a matching EM BodyId can be found in the hemibrain v1.2.1 dataset but an EM cell type has not been defined; these are listed as TBD. Number of cells observed in light microscopy (LM) or electron microscopy (EM) are from one hemisphere, unless otherwise stated. A descriptive cell type column is included, which uses conventional names (if available) to facilitate searching and includes cell types with weak/stochastic expression (bracketed) or putative cell types with less matching confidence. When there are multiple drivers for the same cell type(s), one is chosen as the primary driver based on specificity, consistency, and expression strength. Abbreviations: AL, antennal lobe; ORNs, olfactory receptor neurons; AL LNs, antennal lobe local interneurons; PNs, projection neurons; MB, mushroom body; KCs, Kenyon cells; MBONs, mushroom body output neurons; DANs, dopaminergic neurons; LH, lateral horn; LHONs, lateral horn output neurons; LHLNs, lateral horn local neurons; SNP, superior neuropils; CRE, crepine; CX, central complex; LAL, lateral accessory lobe; ANs, ascending neurons; DNs, descending neurons; OANs, octopaminergic neurons; 5-HT, serotonergic neurons; OL, optic lobe; VLNP, ventrolateral neuropils; INP, inferior neuropils (other than crepine); VMNP, ventromedial neuropils; PENP, periesophageal neuropils; GNG, gnathal ganglia; VNC, ventral nerve cord; N.D., not determined.

Supplementary File 2 New transgenic flies generated in this study.

The enhancer fragments, insertion sites, and inserted chromosomes used to construct the lines are listed. For some of the transgenes, an additional version with a *p10* 3'-UTR (Pfeiffer et al., 2012) was generated to increase the expression.

Supplementary File 3 Coverage of MBON-downstream and DAN-upstream

Connection matrix between MB interneurons and DANs and MBONs. A threshold was set to exclude connections with a low number of neuron-neuron connections, specifically, 10 connections for MBON

517 to a downstream neuron and 5 connections for upstream neurons to a DAN (Li et al., 2020b).
518 Recurrent neurons are defined as cell types receiving input from MBONs and supplying output to
519 DANs. Neurotransmitter (NT) prediction data were from (Eckstein et al., 2023), and the fraction of
520 synapses predicted for the neurotransmitter was pooled from all cells of the cell type.
521
522 **Supplementary File 4 List of non-KC cell types within the MB**
523 The list came from a query in hemibrain 1.2.1 for neurons that have either >= 50 pre-synaptic
524 connections or >=250 post-synaptic connections in the MB region of interest (excluding the accessory
525 calyx) on the right hemisphere. KCs were intentionally omitted from the list. Other than PNs, MBONs
526 and DANs, the list also highlights a couple of cell types interconnecting LH and MB.
527
528 **Supplementary File 5 Updated list of driver lines for cell types within the MB excluding KCs.**
529 This includes new or improved split-GAL4 and split-LexA lines from the present study, lines from the
530 Aso 2014 collection (Aso et al., 2014a), a recent MBON collection (Rubin and Aso, 2023), MB630B (Aso
531 and Rubin, 2016), SS01308 (Aso et al., 2019), MB063B, SS23107 and SS23112 (Dolan et al., 2019),
532 SS46348 (Otto et al., 2020), and some regular Gal4 lines VT43924-Gal4.2 (Amin et al., 2020) and G0239
533 (Chiang et al., 2011). Lines listed in boldface are generally of higher quality.
534
535 **Supplementary File 6 Coverage of PN cell types**
536 A list of split-GAL4 lines and their coverage of PNs of the antennal lobe. Shading indicates expression
537 level. Many of the multi-glomerular PN (mPN) cell types cannot be easily differentiated based on light
538 microscopy images, so they are listed as a broad mPN category in the table.
539
540 **Supplementary File 7 Metadata for presented samples**
541 Detailed metadata organized by figures, including information about genotype, gender and the
542 reporter used. Similar metadata can be found on FlyLight website for deposited confocal imaging data.
543
544 **Video 1 Olfactory arena learning experiment with SS87269**
545 An exemplar video of learning of flies of the genotype SS87269/UAS-CsChrimson-mVenus attP18.
546 Movies were tracked with Caltech FlyTracker (Eyjolfsdottir et al., 2014). Trailing trajectories of
547 individual flies in the last 5 s were overlaid. Delivery of odor A and B to the quadrants along with the
548 625 nm LED activation are indicated. Experiment movie and data from the first 1x 1 m training and
549 test are presented with the gray line indicating session transition.
550
551 **Video 2 Activation phenotypes with SS87269**
552 An exemplar video of activation of flies of the genotype SS87269/UAS-CsChrimson-mVenus attP18.
553 Flies receive six consecutive 60s trials; during each trial a 10s LED activation was presented (from 10-
554 20s) as indicated. The trajectories of individual flies over the previous 5 s are shown.
555
556 **Video 3 Return phenotype of SS87269 at LED offset**
557 Behaviors of individual flies with their trajectories from LED offset up to 15 s after LED offset. Videos are
558 centered to the positions of flies at LED offset. The two white circles indicate 3 mm and 10 mm
559 boundaries from the position. Flies were sorted by the time they re-entered the 3-mm inner circle after
560 they exited the 10-mm outer circle. Flies at the bottom row did not return within the 15-s time frame.

561

562 **Video 4 Proboscis extension upon SS87269 activation for flies walking on a ball**

563 Flies were thorax-fixed by tethering to a pin and allowed to walk on an air-floated foam ball. Proboscis
564 activities were tracked with the Animal Part Tracker (https://github.com/kristinbranson/APT) (Kabra
565 et al., 2022).

566

567 **Video 5 Activation preference of SS01159 in the LED choice experiment.**

568 An exemplar video of LED choices of flies of the genotype SS01159/UAS-CsChrimson-mVenus attP18.
569 The trajectories of individual flies over the previous 5 s are shown. 625 nm LED was on from 30 s to
570 60 s and from 90 s to 120 s, and the lit quadrants are indicated.

571

572 **Appendix 1—key resources table**

Reagent type (species) or resource	Designation	Source or reference	Identifiers	Additional information
strain, strain background (*Drosophila melanogaster*)	New split-GAL4 and split-LexA lines	This paper	https://splitgal4.janelia.org/cgi-bin/splitgal4.cgi	Available from Aso lab
strain, strain background (*Drosophila melanogaster*)	20xUAS-CsChrimson-mVenus attP18	(Klapoetke et al., 2014); PMID: 24509633	N.A.	
strain, strain background (*Drosophila melanogaster*)	pJFRC200-10xUAS-IVS-myr::smGFP-HA in attP18	(Nern et al., 2015); PMID: 25964354	N.A.	
strain, strain background (*Drosophila melanogaster*)	pJFRC225-5xUAS-IVS-myr::smGFP-FLAG in VK00005	(Nern et al., 2015); PMID: 25964354	N.A.	
strain, strain background (*Drosophila melanogaster*)	pBPhsFlp2::PEST in attP3	(Nern et al., 2015); PMID: 25964354	N.A.	
strain, strain background (*Drosophila melanogaster*)	pJFRC201-10XUAS-FRT>STOP > FRT-myr::smGFP-HA in VK0005	(Nern et al., 2015); PMID: 25964354	N.A.	
strain, strain background (*Drosophila melanogaster*)	pJFRC240-10XUAS-FRT>STOP > FRT-myr::smGFP-V5-THS-10XUAS-FRT>STOP > FRT-myr::smGFP-FLAG_in_su(Hw)attP1	(Nern et al., 2015); PMID: 25964354	N.A.	

strain, strain background (*Drosophila melanogaster*)	empty-split-GAL4 (p65ADZp attP40, ZpGAL4DBD attP2)	(Hampel et al., 2015); PMID: 26344548	RRID:BDSC_79603	
strain, strain background (*Drosophila melanogaster*)	empty-Gal4 (pBDPGal4U attP2)	(Pfeiffer et al., 2008); PMID: 18621688	RRID:BDSC_68384	
strain, strain background (*Drosophila melanogaster*)	MB083C split-GAL4	(Aso et al., 2014a); PMID: 25535793	RRID:BDSC_68287	Available from Aso lab
strain, strain background (*Drosophila melanogaster*)	w*; P{Gr64f-GAL4.9.7}5/CyO; P{Gr64f-GAL4.9.7}1/TM3, Sb^1	(Haberkern et al., 2019); PMID: 31056392	RRID: BDSC_57668, BDSC_57669	
strain, strain background (*Drosophila melanogaster*)	Gr66a-Gal4	(Joseph and Heberlein, 2012); PMID: 22798487	N.A.	
antibody	anti-GFP (rabbit polyclonal)	Invitrogen	A11122 RRID:AB_221569	1:1000
antibody	anti-Brp (mouse monoclonal)	Developmental Studies Hybridoma Bank	nc82 RRID:AB_2341866	1:30
antibody	anti-HA-Tag (mouse monoclonal)	Cell Signaling Technology	C29F4; #3724 RRID:AB_10693385	1:300
antibody	anti-FLAG (rat monoclonal)	Novus Biologicals	NBP1-06712 RRID:AB_1625981	1:200
antibody	anti-V5-TAG Dylight-549 (mouse monoclonal)	Bio-Rad	MCA2894D549GA RRID:AB_10845946	1:500
antibody	anti-mouse IgG(H&L) AlexaFluor-568 (goat polyclonal)	Invitrogen	A11031 RRID:AB_144696	1:400
antibody	anti-rabbit IgG(H&L) AlexaFluor-488 (goat polyclonal)	Invitrogen	A11034 RRID:AB_2576217	1:800

antibody	anti-mouse IgG(H&L) AlexaFluor-488 conjugated (donkey polyclonal)	Jackson Immuno Research Labs	715-545-151 RRID:AB_2341099	1:400
antibody	anti-rabbit IgG(H&L) AlexaFluor-594 (donkey polyclonal)	Jackson Immuno Research Labs	711-585-152 RRID:AB_2340621	1:500
antibody	anti-rat IgG(H&L) AlexaFluor-647 (donkey polyclonal)	Jackson Immuno Research Labs	712-605-153 RRID:AB_2340694	1:300
antibody	anti-mouse IgG(H&L) ATTO 647 N (goat polyclonal)	ROCKLAND	610-156-121 RRID:AB_10894200	1:100
antibody	anti-rabbit IgG(H+L) Alexa Fluor 568 (goat polyclonal)	Invitrogen	A-11036 RRID:AB_10563566	1:1000
chemical compound, drug	Pentyl acetate	Sigma-Aldrich	109584	1:10000 in paraffin oil
chemical compound, drug	Ethyl lactate	Sigma-Aldrich	W244015	1:10000 in paraffin oil
chemical compound, drug	Paraffin oil	Sigma-Aldrich	18512	
software, algorithm	ImageJ and Fiji	NIH; (Schindelin et al., 2012)	https://imagej.nih.gov/ij/ http://fiji.sc/	
software, algorithm	MATLAB	MathWorks	https://www.mathworks.com/	
software, algorithm	Adobe Illustrator CC	Adobe Systems	https://www.adobe.com/products/illustrator.html	
software, algorithm	GraphPad Prism 9	GraphPad Software	https://www.graphpad.com/scientific-software/prism/	
software, algorithm	Python	Python Software Foundation	https://www.python.org/	

software, algorithm	Caltech FlyTracker(Eyjolfsdottir et al., 2014)	(Eyjolfsdottir et al., 2014)	https://github.com/kristinbranson/FlyTracker	
software, algorithm	Animal Part Tracker	(Kabra et al., 2022)	(https://github.com/kristinbranson/APT)	
software, algorithm	neuPrint	(Plaza et al., 2022)	https://neuprint.janelia.org/	
software, algorithm	Cytoscape	(Shannon et al., 2003)	https://cytoscape.org/	
software, algorithm	Janelia workstation	HHMI Janelia	https://doi.org/10.25378/janelia.8182256.v1	
software, algorithm	NeuTu	(Zhao et al., 2018)	https://github.com/janelia-flyem/NeuTu	
software, algorithm	VVD Viewer	(Wan et al., 2012)	https://github.com/takashi310/VVD_Viewer	
other	Grade 3 MM Chr Blotting Paper	Whatman	3030–335	Used in glass vials with paraffin-oil diluted odors
other	mass flow controller	Alicat	MCW-200SCCM-D	Mass flow controller used for the olfactory arena

Acknowledgments

We thank Toshihide Hige, Daisuke Hattori, members of the Y.A., G.M.R. and G.T. laboratories for valuable comments on the manuscript. We thank all the members of Janelia Flylight (https://www.janelia.org/project-team/flylight) and Project Technical Resources (https://www.janelia.org/support-team/project-technical-resources) for technical assistance for constructing split-GAL4 drivers and generating confocal microscopy images. During this effort, the FlyLight Project Team and Project Technical Resources included Gudrun Ihrke, Megan Atkins, Shelby Bowers, Kari Close, Gina DePasquale, Zack Dorman, Kaitlyn Forster, Jaye Anne Gallagher, Theresa Gibney, Asish Gulati, Joanna Hausenfluck, Yisheng He, Kristin Hendersen, Hsing Hsi Li, Nirmala Iyer, Jennifer Jeter, Lauren Johnson, Rebecca Johnston, Rachel Lazarus, Kelley Lee, Hua-Peng Liaw, Oz Malkesman, Geoffrey Meissner, Brian Melton, Scott Miller, Reeham Motaher, Alexandra Novak, Omatara Ogundeyi, Alyson Petruncio, Jacquelyn Price, Sophia Protopapas, Susana Tae, Athreya Tata, Jennifer Taylor, Allison Vannan, Rebecca Vorimo, Brianna Yarborough, Kevin Xiankun Zeng, and Chris Zugates, with Steering Committee of Y.A., G.M.R, Gwyneth Card, Barry Dickson, Reed George, Wyatt

Korff, and James Truman. We also thank Kelly Ashley, Pria Chang, Tam Dang, Dona Fetter, Guillermo Gonzalez, Donald Hall, Jui-Chun Kao, James McMahon, Monti Mercer, Brenda Perez, Scarlett Pitts, Danielle Ruiz, Brandi Sharp, Viruthika Vallanadu, Grace Zheng, Amanda Cavallaro, Todd Laverty of Janelia Fly facility (https://www.janelia.org/support-team/fly-facility) for husbandry of stocks, and Eric Trautman, Rob Svirskas, Hideo Otsuna, Takashi Kawase and other members of Janelia Scientific Computing (https://www.janelia.org/support-team/scientific-computing-software) for supporting organization and analysis of confocal and EM microscopy images.

Author contributions

Conceptualization, G.M.R., G.T., T.L. and Y.A.; Formal Analysis and Investigation, Y.S., M.S., G.B., K.H., C.Y., C.M., I.S., and Y.A.; Writing, Y.S., G.M.R., G.T., G.S., and Y.A.; Supervision, G.M.R., G.T., T.L., and Y.A.; Funding Acquisition, G.M.R., G.T., T.L. and Y.A.

Competing interests

The authors declare no competing interests.

References

Amin H, Apostolopoulou AA, Suárez-Grimalt R, Vrontou E, Lin AC. 2020. Localized inhibition in the Drosophila mushroom body. *Elife* **9**. doi:10.7554/eLife.56954

Aso Y, Hattori D, Yu Y, Johnston RM, Iyer NA, Ngo T-TB, Dionne H, Abbott LF, Axel R, Tanimoto H, Rubin GM. 2014a. The neuronal architecture of the mushroom body provides a logic for associative learning. *Elife* **3**:e04577.

Aso Y, Ray RP, Long X, Bushey D, Cichewicz K, Ngo T-T, Sharp B, Christoforou C, Hu A, Lemire AL, Tillberg P, Hirsh J, Litwin-Kumar A, Rubin GM. 2019. Nitric oxide acts as a cotransmitter in a subset of dopaminergic neurons to diversify memory dynamics. *Elife* **8**. doi:10.7554/eLife.49257

Aso Y, Rubin GM. 2016. Dopaminergic neurons write and update memories with cell-type-specific rules. *Elife* **5**. doi:10.7554/eLife.16135

Aso Y, Sitaraman D, Ichinose T, Kaun KR, Vogt K, Belliart-Guérin G, Plaçais P-Y, Robie AA, Yamagata N, Schnaitmann C, Rowell WJ, Johnston RM, Ngo T-TB, Chen N, Korff W, Nitabach MN, Heberlein U, Preat T, Branson KM, Tanimoto H, Rubin GM. 2014b. Mushroom body output neurons encode valence and guide memory-based action selection in Drosophila. *Elife* **3**:e04580.

Aso Y, Siwanowicz I, Bräcker L, Ito K, Kitamoto T, Tanimoto H. 2010. Specific dopaminergic neurons for the formation of labile aversive memory. *Curr Biol* **20**:1445–1451.

Aso Y, Yamada D, Bushey D, Hibbard KL, Sammons M, Otsuna H, Shuai Y, Hige T. 2023. Neural circuit mechanisms for transforming learned olfactory valences into wind-oriented movement. *Elife* **12**. doi:10.7554/eLife.85756

Awata H, Takakura M, Kimura Y, Iwata I, Masuda T, Hirano Y. 2019. The neural circuit linking mushroom body parallel circuits induces memory consolidation in. *Proc Natl Acad Sci U S A* **116**:16080–16085.

Bates AS, Schlegel P, Roberts RJV, Drummond N, Tamimi IFM, Turnbull R, Zhao X, Marin EC, Popovici PD, Dhawan S, Jamasb A, Javier A, Serratosa Capdevila L, Li F, Rubin GM, Waddell S, Bock DD, Costa M, Jefferis GSXE. 2020. Complete Connectomic Reconstruction of Olfactory Projection Neurons in the Fly Brain. *Curr Biol* **30**:3183–3199.e6.

Berry JA, Phan A, Davis RL. 2018. Dopamine Neurons Mediate Learning and Forgetting through Bidirectional Modulation of a Memory Trace. *Cell Rep* **25**:651–662.e5.

631 Bogovic JA, Otsuna H, Heinrich L, Ito M, Jeter J, Meissner G, Nern A, Colonell J, Malkesman O, Ito K,
632 Saalfeld S. 2020. An unbiased template of the Drosophila brain and ventral nerve cord. *PLoS*
633 *One* **15**:e0236495.
634 Bohra AA, Kallman BR, Reichert H, VijayRaghavan K. 2018. Identification of a Single Pair of
635 Interneurons for Bitter Taste Processing in the Drosophila Brain. *Curr Biol* **28**:847–858.e3.
636 Burke CJ, Huetteroth W, Owald D, Perisse E, Krashes MJ, Das G, Gohl D, Silies M, Certel S, Waddell S.
637 2012. Layered reward signalling through octopamine and dopamine in Drosophila. *Nature*
638 **492**:433–437.
639 Chen H-L, Motevalli D, Stern U, Yang C-H. 2022. A functional division of sweet taste neurons that is
640 value-based and task-specific. *Proc Natl Acad Sci U S A* **119**. doi:10.1073/pnas.2110158119
641 Chiang A-S, Lin C-Y, Chuang C-C, Chang H-M, Hsieh C-H, Yeh C-W, Shih C-T, Wu J-J, Wang G-T, Chen Y-
642 C, Wu C-C, Chen G-Y, Ching Y-T, Lee P-C, Lin C-Y, Lin H-H, Wu C-C, Hsu H-W, Huang Y-A, Chen J-Y,
643 Chiang H-J, Lu C-F, Ni R-F, Yeh C-Y, Hwang J-K. 2011. Three-dimensional reconstruction of brain-
644 wide wiring networks in Drosophila at single-cell resolution. *Curr Biol* **21**:1–11.
645 Claridge-Chang A, Roorda RD, Vrontou E, Sjulson L, Li H, Hirsh J, Miesenböck G. 2009. Writing
646 memories with light-addressable reinforcement circuitry. *Cell* **139**:405–415.
647 Corfas RA, Sharma T, Dickinson MH. 2019. Diverse Food-Sensing Neurons Trigger Idiothetic Local
648 Search in Drosophila. *Curr Biol* **29**:1660–1668.e4.
649 Costa M, Manton JD, Ostrovsky AD, Prohaska S, Jefferis GSXE. 2016. NBLAST: Rapid, Sensitive
650 Comparison of Neuronal Structure and Construction of Neuron Family Databases. *Neuron*
651 **91**:293–311.
652 Dahanukar A, Lei Y-T, Kwon JY, Carlson JR. 2007. Two Gr genes underlie sugar reception in
653 Drosophila. *Neuron* **56**:503–516.
654 Datta SR, Vasconcelos ML, Ruta V, Luo S, Wong A, Demir E, Flores J, Balonze K, Dickson BJ, Axel R.
655 2008. The Drosophila pheromone cVA activates a sexually dimorphic neural circuit. *Nature*
656 **452**:473–477.
657 Davis FP, Nern A, Picard S, Reiser MB, Rubin GM, Eddy SR, Henry GL. 2020. A genetic, genomic, and
658 computational resource for exploring neural circuit function. *Elife* **9**. doi:10.7554/eLife.50901
659 Davis RL. 2023. Learning and memory using Drosophila melanogaster: a focus on advances made in
660 the fifth decade of research. *Genetics*. doi:10.1093/genetics/iyad085
661 de Bivort B, Buchanan S, Skutt-Kakaria K, Gajda E, Ayroles J, O'Leary C, Reimers P, Akhund-Zade J,
662 Senft R, Maloney R, Ho S, Werkhoven Z, Smith MA-Y. 2022. Precise Quantification of Behavioral
663 Individuality From 80 Million Decisions Across 183,000 Flies. *Front Behav Neurosci* **16**:836626.
664 Deere JU, Sarkissian AA, Yang M, Uttley HA, Martinez Santana N, Nguyen L, Ravi K, Devineni AV.
665 2023. Selective integration of diverse taste inputs within a single taste modality. *Elife* **12**.
666 doi:10.7554/eLife.84856
667 Dionne H, Hibbard KL, Cavallaro A, Kao J-C, Rubin GM. 2018. Genetic Reagents for Making Split-GAL4
668 Lines in. *Genetics* **209**:31–35.
669 Dolan M-J, Belliart-Guérin G, Bates AS, Frechter S, Lampin-Saint-Amaux A, Aso Y, Roberts RJV,
670 Schlegel P, Wong A, Hammad A, Bock D, Rubin GM, Preat T, Plaçais P-Y, Jefferis GSXE. 2018.
671 Communication from Learned to Innate Olfactory Processing Centers Is Required for Memory
672 Retrieval in Drosophila. *Neuron* **100**:651–668.e8.
673 Dolan M-J, Frechter S, Bates AS, Dan C, Huoviala P, Roberts RJ, Schlegel P, Dhawan S, Tabano R,
674 Dionne H, Christoforou C, Close K, Sutcliffe B, Giuliani B, Li F, Costa M, Ihrke G, Meissner GW,
675 Bock DD, Aso Y, Rubin GM, Jefferis GS. 2019. Neurogenetic dissection of the Drosophila lateral
676 horn reveals major outputs, diverse behavioural functions, and interactions with the mushroom
677 body. *Elife* **8**. doi:10.7554/eLife.43079
678 Dorkenwald S, Matsliah A, Sterling AR, Schlegel P, Yu S-C, McKellar CE, Lin A, Costa M, Eichler K, Yin
679 Y, Silversmith W, Schneider-Mizell C, Jordan CS, Brittain D, Halageri A, Kuehner K, Ogedengbe O,
680 Morey R, Gager J, Kruk K, Perlman E, Yang R, Deutsch D, Bland D, Sorek M, Lu R, Macrina T, Lee
681 K, Bae JA, Mu S, Nehoran B, Mitchell E, Popovych S, Wu J, Jia Z, Castro M, Kemnitz N, Ih D, Bates

682 AS, Eckstein N, Funke J, Collman F, Bock DD, Jefferis GSXE, Seung HS, Murthy M, FlyWire
683 Consortium. 2023. Neuronal wiring diagram of an adult brain. *bioRxiv*.
684 doi:10.1101/2023.06.27.546656
685 Dunipace L, Meister S, McNealy C, Amrein H. 2001. Spatially restricted expression of candidate taste
686 receptors in the Drosophila gustatory system. *Curr Biol* **11**:822–835.
687 Eckstein N, Bates AS, Champion A, Du M, Yin Y, Schlegel P, Lu AK-Y, Rymer T, Finley-May S, Paterson
688 T, Parekh R, Dorkenwald S, Matsliah A, Yu S-C, McKellar C, Sterling A, Eichler K, Costa M, Seung
689 S, Murthy M, Hartenstein V, Jefferis GSX, Funke J. 2023. Neurotransmitter Classification from
690 Electron Microscopy Images at Synaptic Sites in Drosophila Melanogaster. *bioRxiv*.
691 doi:10.1101/2020.06.12.148775
692 Eichler K, Li F, Litwin-Kumar A, Park Y, Andrade I, Schneider-Mizell CM, Saumweber T, Huser A,
693 Eschbach C, Gerber B, Fetter RD, Truman JW, Priebe CE, Abbott LF, Thum AS, Zlatic M, Cardona
694 A. 2017. The complete connectome of a learning and memory centre in an insect brain. *Nature*
695 **548**:175–182.
696 Enjin A, Zaharieva EE, Frank DD, Mansourian S, Suh GSB, Gallio M, Stensmyr MC. 2016. Humidity
697 Sensing in Drosophila. *Curr Biol* **26**:1352–1358.
698 Eschbach C, Fushiki A, Winding M, Schneider-Mizell CM, Shao M, Arruda R, Eichler K, Valdes-Aleman
699 J, Ohyama T, Thum AS, Gerber B, Fetter RD, Truman JW, Litwin-Kumar A, Cardona A, Zlatic M.
700 2020. Recurrent architecture for adaptive regulation of learning in the insect brain. *Nat*
701 *Neurosci* **23**:544–555.
702 Eyjolfsdottir E, Branson S, Burgos-Artizzu XP, Hoopfer ED, Schor J, Anderson DJ, Perona P. 2014.
703 Detecting Social Actions of Fruit FliesComputer Vision – ECCV 2014. Springer International
704 Publishing. pp. 772–787.
705 Felsenberg J, Barnstedt O, Cognigni P, Lin S, Waddell S. 2017. Re-evaluation of learned information in
706 Drosophila. *Nature* **544**:240–244.
707 Felsenberg J, Jacob PF, Walker T, Barnstedt O, Edmondson-Stait AJ, Pleijzier MW, Otto N, Schlegel P,
708 Sharifi N, Perisse E, Smith CS, Lauritzen JS, Costa M, Jefferis GSXE, Bock DD, Waddell S. 2018.
709 Integration of Parallel Opposing Memories Underlies Memory Extinction. *Cell* **175**:709–722.e15.
710 Frank DD, Jouandet GC, Kearney PJ, Macpherson LJ, Gallio M. 2015. Temperature representation in
711 the Drosophila brain. *Nature* **519**:358–361.
712 Fujii S, Yavuz A, Slone J, Jagge C, Song X, Amrein H. 2015. Drosophila sugar receptors in sweet taste
713 perception, olfaction, and internal nutrient sensing. *Curr Biol* **25**:621–627.
714 Gallio M, Ofstad TA, Macpherson LJ, Wang JW, Zuker CS. 2011. The coding of temperature in the
715 Drosophila brain. *Cell* **144**:614–624.
716 Gao R, Asano SM, Upadhyayula S, Pisarev I, Milkie DE, Liu T-L, Singh V, Graves A, Huynh GH, Zhao Y,
717 Bogovic J, Colonell J, Ott CM, Zugates C, Tappan S, Rodriguez A, Mosaliganti KR, Sheu S-H,
718 Pasolli HA, Pang S, Xu CS, Megason SG, Hess H, Lippincott-Schwartz J, Hantman A, Rubin GM,
719 Kirchhausen T, Saalfeld S, Aso Y, Boyden ES, Betzig E. 2019. Cortical column and whole-brain
720 imaging with molecular contrast and nanoscale resolution. *Science* **363**.
721 doi:10.1126/science.aau8302
722 Haberkern H, Basnak MA, Ahanonu B, Schauder D, Cohen JD, Bolstad M, Bruns C, Jayaraman V. 2019.
723 Visually Guided Behavior and Optogenetically Induced Learning in Head-Fixed Flies Exploring a
724 Virtual Landscape. *Curr Biol* **29**:1647–1659.e8.
725 Hammer M. 1993. An identified neuron mediates the unconditioned stimulus in associative olfactory
726 learning in honeybees. *Nature* **366**:59–63.
727 Hampel S, Franconville R, Simpson JH, Seeds AM. 2015. A neural command circuit for grooming
728 movement control. *Elife* **4**:e08758.
729 Handler A, Graham TGW, Cohn R, Morantte I, Siliciano AF, Zeng J, Li Y, Ruta V. 2019. Distinct
730 Dopamine Receptor Pathways Underlie the Temporal Sensitivity of Associative Learning. *Cell*.
731 doi:10.1016/j.cell.2019.05.040
732 Harris DT, Kallman BR, Mullaney BC, Scott K. 2015. Representations of Taste Modality in the

Drosophila Brain. *Neuron* **86**:1449–1460.
Hattori D, Aso Y, Swartz KJ, Rubin GM, Abbott LF, Axel R. 2017. Representations of Novelty and Familiarity in a Mushroom Body Compartment. *Cell* **169**:956–969.e17.
Heisenberg M. 2003. Mushroom body memoir: from maps to models. *Nat Rev Neurosci* **4**:266–275.
Hige T, Aso Y, Modi MN, Rubin GM, Turner GC. 2015a. Heterosynaptic Plasticity Underlies Aversive Olfactory Learning in Drosophila. *Neuron* **88**:985–998.
Hige T, Aso Y, Rubin GM, Turner GC. 2015b. Plasticity-driven individualization of olfactory coding in mushroom body output neurons. *Nature* **526**:258–262.
Hiroi M, Marion-Poll F, Tanimura T. 2002. Differentiated Response to Sugars among Labellar Chemosensilla in Drosophila. *jzoo* **19**:1009–1018.
Honegger KS, Campbell RAA, Turner GC. 2011. Cellular-resolution population imaging reveals robust sparse coding in the Drosophila mushroom body. *J Neurosci* **31**:11772–11785.
Huetteroth W, Perisse E, Lin S, Klappenbach M, Burke C, Waddell S. 2015. Sweet taste and nutrient value subdivide rewarding dopaminergic neurons in Drosophila. *Curr Biol* **25**:751–758.
Hulse BK, Haberkern H, Franconville R, Turner-Evans D, Takemura S-Y, Wolff T, Noorman M, Dreher M, Dan C, Parekh R, Hermundstad AM, Rubin GM, Jayaraman V. 2021. A connectome of the Drosophila central complex reveals network motifs suitable for flexible navigation and context-dependent action selection. *Elife* **10**. doi:10.7554/eLife.66039
Hwang RY, Zhong L, Xu Y, Johnson T, Zhang F, Deisseroth K, Tracey WD. 2007. Nociceptive Neurons Protect Drosophila Larvae from Parasitoid Wasps. *Curr Biol* **17**:2105–2116.
Ichinose T, Aso Y, Yamagata N, Abe A, Rubin GM, Tanimoto H. 2015. Reward signal in a recurrent circuit drives appetitive long-term memory formation. *Elife* **4**:e10719.
Jenett A, Rubin GM, Ngo T-TB, Shepherd D, Murphy C, Dionne H, Pfeiffer BD, Cavallaro A, Hall D, Jeter J, Iyer N, Fetter D, Hausenfluck JH, Peng H, Trautman ET, Svirskas RR, Myers EW, Iwinski ZR, Aso Y, DePasquale GM, Enos A, Hulamm P, Lam SCB, Li H-H, Laverty TR, Long F, Qu L, Murphy SD, Rokicki K, Safford T, Shaw K, Simpson JH, Sowell A, Tae S, Yu Y, Zugates CT. 2012. A GAL4-driver line resource for Drosophila neurobiology. *Cell Rep* **2**:991–1001.
Jiang L, Litwin-Kumar A. 2021. Models of heterogeneous dopamine signaling in an insect learning and memory center. *PLoS Comput Biol* **17**:e1009205.
Joseph RM, Heberlein U. 2012. Tissue-specific activation of a single gustatory receptor produces opposing behavioral responses in Drosophila. *Genetics* **192**:521–532.
Kabra M, Lee A, Robie A, Egnor R, Huston S, Rodriguez IF, Edwards A, Branson K. 2022. APT: Animal Part Tracker v0.3.4. Zenodo. doi:10.5281/ZENODO.6366082
Kanzaki R, Ikeda A, Shibuya T. 1994. [引用] Morphology and physiology of pheromone-triggered flip-flop descending interneurons of the male silkworm moth, Bombyx mori. *J Comp Physiol A*.
Kim H, Kirkhart C, Scott K. 2017. Long-range projection neurons in the taste circuit of Drosophila. *Elife* **6**. doi:10.7554/eLife.23386
Kirkhart C, Scott K. 2015. Gustatory learning and processing in the Drosophila mushroom bodies. *J Neurosci* **35**:5950–5958.
Klapoetke NC, Murata Y, Kim SS, Pulver SR, Birdsey-Benson A, Cho YK, Morimoto TK, Chuong AS, Carpenter EJ, Tian Z, Wang J, Xie Y, Yan Z, Zhang Y, Chow BY, Surek B, Melkonian M, Jayaraman V, Constantine-Paton M, Wong GK-S, Boyden ES. 2014. Independent optical excitation of distinct neural populations. *Nat Methods* **11**:338–346.
König C, Khalili A, Niewalda T, Gao S, Gerber B. 2019. An optogenetic analogue of second-order reinforcement in Drosophila. *Biol Lett* **15**:20190084.
Li F, Lindsey JW, Marin EC, Otto N, Dreher M, Dempsey G, Stark I, Bates AS, Pleijzier MW, Schlegel P, Nern A, Takemura S-Y, Eckstein N, Yang T, Francis A, Braun A, Parekh R, Costa M, Scheffer LK, Aso Y, Jefferis GS, Abbott LF, Litwin-Kumar A, Waddell S, Rubin GM. 2020a. The connectome of the adult Drosophila mushroom body provides insights into function. *Elife* **9**. doi:10.7554/eLife.62576
Li F, Lindsey JW, Marin EC, Otto N, Dreher M, Dempsey G, Stark I, Bates AS, Pleijzier MW, Schlegel P,

Nern A, Takemura S-Y, Eckstein N, Yang T, Francis A, Braun A, Parekh R, Costa M, Scheffer LK, Aso Y, Jefferis GS, Abbott LF, Litwin-Kumar A, Waddell S, Rubin GM. 2020b. The connectome of the adult Drosophila mushroom body provides insights into function. *Elife* **9**. doi:10.7554/eLife.62576

Lin H-H, Chu L-A, Fu T-F, Dickson BJ, Chiang A-S. 2013. Parallel neural pathways mediate CO2 avoidance responses in Drosophila. *Science* **340**:1338–1341.

Lin H-H, Lai JS-Y, Chin A-L, Chen Y-C, Chiang A-S. 2007. A Map of Olfactory Representation in the Drosophila Mushroom Body. *Cell* **128**:1205–1217.

Liu C, Plaçais P-Y, Yamagata N, Pfeiffer BD, Aso Y, Friedrich AB, Siwanowicz I, Rubin GM, Preat T, Tanimoto H. 2012. A subset of dopamine neurons signals reward for odour memory in Drosophila. *Nature*. doi:10.1038/nature11304

Liu WW, Mazor O, Wilson RI. 2015. Thermosensory processing in the Drosophila brain. *Nature* **519**:353–357.

Luan H, Diao F, Scott RL, White BH. 2020. The Drosophila Split Gal4 System for Neural Circuit Mapping. *Frontiers in Neural Circuits*. doi:10.3389/fncir.2020.603397

Luan H, Peabody NC, Vinson CR, White BH. 2006. Refined spatial manipulation of neuronal function by combinatorial restriction of transgene expression. *Neuron* **52**:425–436.

Mao Z, Davis RL. 2009. Eight different types of dopaminergic neurons innervate the Drosophila mushroom body neuropil: anatomical and physiological heterogeneity. *Front Neural Circuits* **3**:612.

Marin EC, Büld L, Theiss M, Sarkissian T, Roberts RJV, Turnbull R, Tamimi IFM, Pleijzier MW, Laursen WJ, Drummond N, Schlegel P, Bates AS, Li F, Landgraf M, Costa M, Bock DD, Garrity PA, Jefferis GSXE. 2020. Connectomics Analysis Reveals First-, Second-, and Third-Order Thermosensory and Hygrosensory Neurons in the Adult Drosophila Brain. *Curr Biol* **30**:3167–3182.e4.

Martinez-Cervantes J, Shah P, Phan A, Cervantes-Sandoval I. 2022. Higher-order unimodal olfactory sensory preconditioning in. *Elife* **11**. doi:10.7554/eLife.79107

Masek P, Worden K, Aso Y, Rubin GM, Keene AC. 2015. A dopamine-modulated neural circuit regulating aversive taste memory in Drosophila. *Curr Biol* **25**:1535–1541.

Masse NY, Cachero S, Ostrovsky AD, Jefferis GSXE. 2012. A mutual information approach to automate identification of neuronal clusters in Drosophila brain images. *Front Neuroinform* **6**:21.

Matheson AMM, Lanz AJ, Medina AM, Licata AM, Currier TA, Syed MH, Nagel KI. 2022. A neural circuit for wind-guided olfactory navigation. *Nat Commun* **13**:1–21.

McCurdy LY, Sareen P, Davoudian PA, Nitabach MN. 2021. Dopaminergic mechanism underlying reward-encoding of punishment omission during reversal learning in Drosophila. *Nat Commun* **12**:1115.

McKellar CE, Siwanowicz I, Dickson BJ, Simpson JH. 2020. Controlling motor neurons of every muscle for fly proboscis reaching. *Elife* **9**:e54978.

Meissner GW, Nern A, Dorman Z, DePasquale GM, Forster K, Gibney T, Hausenfluck JH, He Y, Iyer NA, Jeter J, Johnson L, Johnston RM, Lee K, Melton B, Yarbrough B, Zugates CT, Clements J, Goina C, Otsuna H, Rokicki K, Svirskas RR, Aso Y, Card GM, Dickson BJ, Ehrhardt E, Goldammer J, Ito M, Kainmueller D, Korff W, Mais L, Minegishi R, Namiki S, Rubin GM, Sterne GR, Wolff T, Malkesman O. 2023. A searchable image resource of Drosophila GAL4 driver expression patterns with single neuron resolution. doi:10.7554/eLife.80660

Meissner GW, Vannan A, Jeter J, Close K, DePasquale GM, Dorman Z, Forster K, Beringer JA, Gibney TV, Hausenfluck JH, He Y, Henderson K, Johnson L, Johnston RM, Ihrke G, Iyer N, Lazarus R, Lee K, Li H-H, Liaw H-P, Melton B, Miller S, Motaher R, Novak A, Ogundeyi O, Petruncio A, Price J, Protopapas S, Tae S, Taylor J, Vorimo R, Yarbrough B, Zeng KX, Zugates CT, Dionne H, Angstadt C, Ashley K, Cavallaro A, Dang T, Gonzalez GA, Hibbard KL, Huang C, Kao J-C, Laverty T, Mercer M, Perez B, Pitts S, Ruiz D, Vallanadu V, Zheng GZ, Goina C, Otsuna H, Rokicki K, Svirskas RR, Cheong HSJ, Dolan M-J, Ehrhardt E, Feng K, El Galfi B, Goldammer J, Huston SJ, Hu N, Ito M,

McKellar C, Minegishi R, Namiki S, Nern A, Schretter CE, Sterne GR, Venkatasubramanian L, Wang K, Wolff T, Wu M, George R, Malkesman O, Aso Y, Card GM, Dickson BJ, Korff W, Ito K, Truman JW, Zlatic M, Rubin GM. 2024. A split-GAL4 driver line resource for Drosophila CNS cell types. *bioRxiv*. doi:10.1101/2024.01.09.574419

Miyamoto T, Slone J, Song X, Amrein H. 2012. A fructose receptor functions as a nutrient sensor in the Drosophila brain. *Cell* **151**:1113–1125.

Miyazaki T, Lin T-Y, Ito K, Lee C-H, Stopfer M. 2015. A gustatory second-order neuron that connects sucrose-sensitive primary neurons and a distinct region of the gnathal ganglion in the Drosophila brain. *J Neurogenet* **29**:144–155.

Modi MN, Shuai Y, Turner GC. 2020. The Drosophila Mushroom Body: From Architecture to Algorithm in a Learning Circuit. *Annu Rev Neurosci* **43**:465–484.

Namiki S, Dickinson MH, Wong AM, Korff W, Card GM. 2018. The functional organization of descending sensory-motor pathways in Drosophila. doi:10.7554/eLife.34272

Nern A, Loesche F, Takemura S-Y, Burnett LE, Dreher M, Gruntman E, Hoeller J, Huang GB, Januszewski M, Klapoetke NC, Koskela S, Longden KD, Lu Z, Preibisch S, Qiu W, Rogers EM, Seenivasan P, Zhao A, Bogovic J, Canino BS, Clements J, Cook M, Finley-May S, Flynn MA, Hameed I, Fragniere AM, Hayworth KJ, Hopkins GP, Hubbard PM, Katz WT, Kovalyak J, Lauchie SA, Leonard M, Lohff A, Maldonado CA, Mooney C, Okeoma N, Olbris DJ, Ordish C, Paterson T, Phillips EM, Pietzsch T, Salinas JR, Rivlin PK, Schlegel P, Scott AL, Scuderi LA, Takemura S, Talebi I, Thomson A, Trautman ET, Umayam L, Walsh C, Walsh JJ, Xu CS, Yakal EA, Yang T, Zhao T, Funke J, George R, Hess HF, Jefferis GS, Knecht C, Korff W, Plaza SM, Romani S, Saalfeld S, Scheffer LK, Berg S, Rubin GM, Reiser MB. 2024. Connectome-driven neural inventory of a complete visual system. *bioRxiv*. doi:10.1101/2024.04.16.589741

Nern A, Pfeiffer BD, Rubin GM. 2015. Optimized tools for multicolor stochastic labeling reveal diverse stereotyped cell arrangements in the fly visual system. *Proc Natl Acad Sci U S A* **112**:E2967–76.

Ohyama T, Schneider-Mizell CM, Fetter RD, Aleman JV, Franconville R, Rivera-Alba M, Mensh BD, Branson KM, Simpson JH, Truman JW, Cardona A, Zlatic M. 2015. A multilevel multimodal circuit enhances action selection in Drosophila. *Nature* **520**:633–639.

Otsuna H, Ito M, Kawase T. 2018. Color depth MIP mask search: a new tool to expedite Split-GAL4 creation. *bioRxiv*. doi:10.1101/318006

Otto N, Pleijzier MW, Morgan IC, Edmondson-Stait AJ, Heinz KJ, Stark I, Dempsey G, Ito M, Kapoor I, Hsu J, Schlegel PM, Bates AS, Feng L, Costa M, Ito K, Bock DD, Rubin GM, Jefferis GSXE, Waddell S. 2020. Input Connectivity Reveals Additional Heterogeneity of Dopaminergic Reinforcement in Drosophila. *Curr Biol* **30**:3200–3211.e8.

Owald D, Felsenberg J, Talbot CB, Das G, Perisse E, Huetteroth W, Waddell S. 2015. Activity of defined mushroom body output neurons underlies learned olfactory behavior in Drosophila. *Neuron* **86**:417–427.

Owald D, Waddell S. 2015. Olfactory learning skews mushroom body output pathways to steer behavioral choice in Drosophila. *Curr Opin Neurobiol* **35**:178–184.

Pai T-P, Chen C-C, Lin H-H, Chin A-L, Lai JS-Y, Lee P-T, Tully T, Chiang A-S. 2013. Drosophila ORB protein in two mushroom body output neurons is necessary for long-term memory formation. *Proc Natl Acad Sci U S A* **110**:7898–7903.

Park J-H, Kwon JY. 2011. A systematic analysis of Drosophila gustatory receptor gene expression in abdominal neurons which project to the central nervous system. *Mol Cells* **32**:375–381.

Pavlowsky A, Schor J, Plaçais P-Y, Preat T. 2018. A GABAergic Feedback Shapes Dopaminergic Input on the Drosophila Mushroom Body to Promote Appetitive Long-Term Memory. *Curr Biol* **28**:1783–1793.e4.

Perez-Orive J, Mazor O, Turner GC, Cassenaer S, Wilson RI, Laurent G. 2002. Oscillations and sparsening of odor representations in the mushroom body. *Science* **297**:359–365.

Pettersson J. 1970. An Aphid Sex Attractant. *Insect Syst Evol* **1**:63–73.

Pfeiffer BD, Jenett A, Hammonds AS, Ngo T-TB, Misra S, Murphy C, Scully A, Carlson JW, Wan KH, Laverty TR, Mungall C, Svirskas R, Kadonaga JT, Doe CQ, Eisen MB, Celniker SE, Rubin GM. 2008. Tools for neuroanatomy and neurogenetics in Drosophila. *Proc Natl Acad Sci U S A* **105**:9715–9720.

Pfeiffer BD, Ngo T-TB, Hibbard KL, Murphy C, Jenett A, Truman JW, Rubin GM. 2010. Refinement of tools for targeted gene expression in Drosophila. *Genetics* **186**:735–755.

Pfeiffer BD, Truman JW, Rubin GM. 2012. Using translational enhancers to increase transgene expression in Drosophila. *Proc Natl Acad Sci U S A* **109**:6626–6631.

Plaçais P-Y, de Tredern É, Scheunemann L, Trannoy S, Goguel V, Han K-A, Isabel G, Preat T. 2017. Upregulated energy metabolism in the Drosophila mushroom body is the trigger for long-term memory. *Nat Commun* **8**:15510.

Plaçais P-Y, Trannoy S, Friedrich AB, Tanimoto H, Preat T. 2013. Two pairs of mushroom body efferent neurons are required for appetitive long-term memory retrieval in Drosophila. *Cell Rep* **5**:769–780.

Plaza SM, Clements J, Dolafi T, Umayam L, Neubarth NN, Scheffer LK, Berg S. 2022. neuPrint: An open access tool for EM connectomics. *Front Neuroinform* **16**:896292.

Rajagopalan AE, Darshan R, Fitzgerald JE, Turner GC. 2022. Expectation-based learning rules underlie dynamic foraging in Drosophila. *bioRxiv*. doi:10.1101/2022.05.24.493252

Rodrigues V, Siddiqi O. 1978. Genetic analysis of chemosensory pathway. *Proceedings / Indian Academy of Sciences* **87**:147–160.

Rubin GM, Aso Y. 2024. New genetic tools for mushroom body output neurons in. *Elife* **12**. doi:10.7554/eLife.90523

Rubin GM, Aso Y. 2023. New genetic tools for mushroom body output neurons in Drosophila. *bioRxiv*. doi:10.1101/2023.06.23.546330

Rybak J, Menzel R. 2017. Mushroom Body of the Honeybee. Oxford University Press.

Saumweber T, Rohwedder A, Schleyer M, Eichler K, Chen Y-C, Aso Y, Cardona A, Eschbach C, Kobler O, Voigt A, Durairaja A, Mancini N, Zlatic M, Truman JW, Thum AS, Gerber B. 2018. Functional architecture of reward learning in mushroom body extrinsic neurons of larval Drosophila. *Nat Commun* **9**:1104.

Sayin S, De Backer J-F, Siju KP, Wosniack ME, Lewis LP, Frisch L-M, Gansen B, Schlegel P, Edmondson-Stait A, Sharifi N, Fisher CB, Calle-Schuler SA, Lauritzen JS, Bock DD, Costa M, Jefferis GSXE, Gjorgjieva J, Grunwald Kadow IC. 2019. A Neural Circuit Arbitrates between Persistence and Withdrawal in Hungry Drosophila. *Neuron* **104**:544–558.e6.

Scaplen KM, Talay M, Fisher JD, Cohn R, Sorkaç A, Aso Y, Barnea G, Kaun KR. 2021. Transsynaptic mapping of Drosophila mushroom body output neurons. *Elife* **10**. doi:10.7554/eLife.63379

Scheffer LK, Xu CS, Januszewski M, Lu Z, Takemura S-Y, Hayworth KJ, Huang GB, Shinomiya K, Maitlin-Shepard J, Berg S, Clements J, Hubbard PM, Katz WT, Umayam L, Zhao T, Ackerman D, Blakely T, Bogovic J, Dolafi T, Kainmueller D, Kawase T, Khairy KA, Leavitt L, Li PH, Lindsey L, Neubarth N, Olbris DJ, Otsuna H, Trautman ET, Ito M, Bates AS, Goldammer J, Wolff T, Svirskas R, Schlegel P, Neace E, Knecht CJ, Alvarado CX, Bailey DA, Ballinger S, Borycz JA, Canino BS, Cheatham N, Cook M, Dreher M, Duclos O, Eubanks B, Fairbanks K, Finley S, Forknall N, Francis A, Hopkins GP, Joyce EM, Kim S, Kirk NA, Kovalyak J, Lauchie SA, Lohff A, Maldonado C, Manley EA, McLin S, Mooney C, Ndama M, Ogundeyi O, Okeoma N, Ordish C, Padilla N, Patrick CM, Paterson T, Phillips EE, Phillips EM, Rampally N, Ribeiro C, Robertson MK, Rymer JT, Ryan SM, Sammons M, Scott AK, Scott AL, Shinomiya A, Smith C, Smith K, Smith NL, Sobeski MA, Suleiman A, Swift J, Takemura S, Talebi I, Tarnogorska D, Tenshaw E, Tokhi T, Walsh JJ, Yang T, Horne JA, Li F, Parekh R, Rivlin PK, Jayaraman V, Costa M, Jefferis GS, Ito K, Saalfeld S, George R, Meinertzhagen IA, Rubin GM, Hess HF, Jain V, Plaza SM. 2020. A connectome and analysis of the adult central brain. *Elife* **9**. doi:10.7554/eLife.57443

Schindelin J, Arganda-Carreras I, Frise E, Kaynig V, Longair M, Pietzsch T, Preibisch S, Rueden C, Saalfeld S, Schmid B, Tinevez J-Y, White DJ, Hartenstein V, Eliceiri K, Tomancak P, Cardona A.

2012. Fiji: an open-source platform for biological-image analysis. *Nat Methods* **9**:676–682.
Schretter CE, Aso Y, Robie AA, Dreher M, Dolan M-J, Chen N, Ito M, Yang T, Parekh R, Branson KM, Rubin GM. 2020. Cell types and neuronal circuitry underlying female aggression in Drosophila. *eLife*. doi:10.7554/elife.58942
Schroll C, Riemensperger T, Bucher D, Ehmer J, Völler T, Erbguth K, Gerber B, Hendel T, Nagel G, Buchner E, Fiala A. 2006. Light-induced activation of distinct modulatory neurons triggers appetitive or aversive learning in Drosophila larvae. *Curr Biol* **16**:1741–1747.
Schwaerzel M, Monastirioti M, Scholz H, Friggi-Grelin F, Birman S, Heisenberg M. 2003. Dopamine and octopamine differentiate between aversive and appetitive olfactory memories in Drosophila. *J Neurosci* **23**:10495–10502.
Séjourné J, Plaçais P-Y, Aso Y, Siwanowicz I, Trannoy S, Thoma V, Tedjakumala SR, Rubin GM, Tchénio P, Ito K, Isabel G, Tanimoto H, Preat T. 2011. Mushroom body efferent neurons responsible for aversive olfactory memory retrieval in Drosophila. *Nat Neurosci* **14**:903–910.
Shannon P, Markiel A, Ozier O, Baliga NS, Wang JT, Ramage D, Amin N, Schwikowski B, Ideker T. 2003. Cytoscape: a software environment for integrated models of biomolecular interaction networks. *Genome Res* **13**:2498–2504.
Shimono K, Fujimoto A, Tsuyama T, Yamamoto-Kochi M, Sato M, Hattori Y, Sugimura K, Usui T, Kimura K-I, Uemura T. 2009. Multidendritic sensory neurons in the adult Drosophila abdomen: origins, dendritic morphology, and segment- and age-dependent programmed cell death. *Neural Dev* **4**:37.
Shuai Y, Hirokawa A, Ai Y, Zhang M, Li W, Zhong Y. 2015. Dissecting neural pathways for forgetting in Drosophila olfactory aversive memory. *Proc Natl Acad Sci U S A* **112**:E6663–72.
Shyu W-H, Chiu T-H, Chiang M-H, Cheng Y-C, Tsai Y-L, Fu T-F, Wu T, Wu C-L. 2017. Neural circuits for long-term water-reward memory processing in thirsty Drosophila. *Nat Commun* **8**:15230.
Smith MA-Y, Honegger KS, Turner G, de Bivort B. 2022. Idiosyncratic learning performance in flies. *Biol Lett* **18**:20210424.
Sterne GR, Otsuna H, Dickson BJ, Scott K. 2021. Classification and genetic targeting of cell types in the primary taste and premotor center of the adult brain. *Elife* **10**. doi:10.7554/eLife.71679
Stocker RF, Lienhard MC, Borst A, Fischbach KF. 1990. Neuronal architecture of the antennal lobe in Drosophila melanogaster. *Cell Tissue Res* **262**:9–34.
Strother JA, Wu S-T, Wong AM, Nern A, Rogers EM, Le JQ, Rubin GM, Reiser MB. 2017. The Emergence of Directional Selectivity in the Visual Motion Pathway of Drosophila. *Neuron* **94**:168–182.e10.
Suh GSB, Wong AM, Hergarden AC, Wang JW, Simon AF, Benzer S, Axel R, Anderson DJ. 2004. A single population of olfactory sensory neurons mediates an innate avoidance behaviour in Drosophila. *Nature* **431**:854–859.
Takagi S, Cocanougher BT, Niki S, Miyamoto D, Kohsaka H, Kazama H, Fetter RD, Truman JW, Zlatic M, Cardona A, Nose A. 2017. Divergent Connectivity of Homologous Command-like Neurons Mediates Segment-Specific Touch Responses in Drosophila. *Neuron* **96**:1373–1387.e6.
Tanaka NK, Awasaki T, Shimada T, Ito K. 2004. Integration of chemosensory pathways in the Drosophila second-order olfactory centers. *Curr Biol* **14**:449–457.
Tanaka NK, Endo K, Ito K. 2012. Organization of antennal lobe-associated neurons in adult Drosophila melanogaster brain. *J Comp Neurol* **520**:4067–4130.
Tanaka NK, Tanimoto H, Ito K. 2008. Neuronal assemblies of the Drosophila mushroom body. *J Comp Neurol* **508**:711–755.
Thoma V, Knapek S, Arai S, Hartl M, Kohsaka H, Sirigrivatanawong P, Abe A, Hashimoto K, Tanimoto H. 2016. Functional dissociation in sweet taste receptor neurons between and within taste organs of Drosophila. *Nat Commun* **7**:10678.
Ting C-Y, Gu S, Guttikonda S, Lin T-Y, White BH, Lee C-H. 2011. Focusing transgene expression in Drosophila by coupling Gal4 with a novel split-LexA expression system. *Genetics* **188**:229–233.
Tirian L, Dickson BJ. 2017. The VT GAL4, LexA, and split-GAL4 driver line collections for targeted

expression in the Drosophila nervous system. *bioRxiv*. doi:10.1101/198648
Truman JW, Price J, Miyares RL, Lee T. 2023. Metamorphosis of memory circuits in Drosophila reveals a strategy for evolving a larval brain. doi:10.7554/eLife.80594
Tsao C-H, Chen C-C, Lin C-H, Yang H-Y, Lin S. 2018. mushroom bodies integrate hunger and satiety signals to control innate food-seeking behavior. *Elife* **7**. doi:10.7554/eLife.35264
Turner GC, Bazhenov M, Laurent G. 2008. Olfactory Representations by Drosophila Mushroom Body Neurons. *J Neurophysiol*. doi:10.1152/jn.01283.2007
Tuthill JC, Nern A, Holtz SL, Rubin GM, Reiser MB. 2013. Contributions of the 12 neuron classes in the fly lamina to motion vision. *Neuron* **79**:128–140.
Vogt K, Aso Y, Hige T, Knapek S, Ichinose T, Friedrich AB, Turner GC, Rubin GM, Tanimoto H. 2016. Direct neural pathways convey distinct visual information to Drosophila mushroom bodies. *Elife* **5**. doi:10.7554/eLife.14009
Wang K, Wang F, Forknall N, Yang T, Patrick C, Parekh R, Dickson BJ. 2021. Neural circuit mechanisms of sexual receptivity in Drosophila females. *Nature* **589**:577–581.
Wang Z, Singhvi A, Kong P, Scott K. 2004. Taste representations in the Drosophila brain. *Cell* **117**:981–991.
Wan Y, Otsuna H, Chien C-B, Hansen C. 2012. FluoRender: An Application of 2D Image Space Methods for 3D and 4D Confocal Microscopy Data Visualization in Neurobiology Research. *IEEE Pac Vis Symp* 201–208.
Winding M, Pedigo BD, Barnes CL, Patsolic HG, Park Y, Kazimiers T, Fushiki A, Andrade IV, Khandelwal A, Valdes-Aleman J, Li F, Randel N, Barsotti E, Correia A, Fetter RD, Hartenstein V, Priebe CE, Vogelstein JT, Cardona A, Zlatic M. 2023. The connectome of an insect brain. *Science* **379**:eadd9330.
Wolff T, Rubin GM. 2018. Neuroarchitecture of the Drosophila central complex: A catalog of nodulus and asymmetrical body neurons and a revision of the protocerebral bridge catalog. *J Comp Neurol* **526**:2585–2611.
Wu J-K, Tai C-Y, Feng K-L, Chen S-L, Chen C-C, Chiang A-S. 2017. Long-term memory requires sequential protein synthesis in three subsets of mushroom body output neurons in Drosophila. *Sci Rep* **7**:7112.
Wu M, Nern A, Williamson WR, Morimoto MM, Reiser MB, Card GM, Rubin GM. 2016. Visual projection neurons in the lobula link feature detection to distinct behavioral programs. *Elife* **5**. doi:10.7554/eLife.21022
Xie Q, Brbic M, Horns F, Kolluru SS, Jones RC, Li J, Reddy AR, Xie A, Kohani S, Li Z, McLaughlin CN, Li T, Xu C, Vacek D, Luginbuhl DJ, Leskovec J, Quake SR, Luo L, Li H. 2021. Temporal evolution of single-cell transcriptomes of olfactory projection neurons. *Elife* **10**. doi:10.7554/eLife.63450
Yamada D, Bushey D, Li F, Hibbard KL, Sammons M, Funke J, Litwin-Kumar A, Hige T, Aso Y. 2023. Hierarchical architecture of dopaminergic circuits enables second-order conditioning in Drosophila. *Elife* **12**. doi:10.7554/eLife.79042
Yamagata N, Ichinose T, Aso Y, Plaçais P-Y, Friedrich AB, Sima RJ, Preat T, Rubin GM, Tanimoto H. 2015. Distinct dopamine neurons mediate reward signals for short- and long-term memories. *Proc Natl Acad Sci U S A* **112**:578–583.
Yavuz A, Jagge C, Slone J, Amrein H. 2014. A genetic tool kit for cellular and behavioral analyses of insect sugar receptors. *Fly* **8**:189–196.
Zhang X, Noyes NC, Zeng J, Li Y, Davis RL. 2019. Aversive Training Induces Both Presynaptic and Postsynaptic Suppression in. *J Neurosci* **39**:9164–9172.
Zheng Z, Lauritzen JS, Perlman E, Robinson CG, Nichols M, Milkie D, Torrens O, Price J, Fisher CB, Sharifi N, Calle-Schuler SA, Kmecova L, Ali IJ, Karsh B, Trautman ET, Bogovic JA, Hanslovsky P, Jefferis GSXE, Kazhdan M, Khairy K, Saalfeld S, Fetter RD, Bock DD. 2018. A Complete Electron Microscopy Volume of the Brain of Adult Drosophila melanogaster. *Cell* **174**:730–743.e22.
Zheng Z, Li F, Fisher C, Ali IJ, Sharifi N, Calle-Schuler S, Hsu J, Masoodpanah N, Kmecova L, Kazimiers T, Perlman E, Nichols M, Li PH, Jain V, Bock DD. 2022. Structured sampling of olfactory input by

1039 the fly mushroom body. *Curr Biol* **32**:3334–3349.e6.

1040

1041 **Figures and figure legends**
1042
1043 **Figure 1 Generation and annotation of split-GAL4 lines**
1044 (A) In associative learning, flies adjust their behavioral responses to conditioned stimuli (CS), such as
1045 odors and colors, based on the contingency with innately rewarding or punishing unconditioned
1046 stimuli (US), such as sugar, bitter, shock and heat. A schematic of *Drosophila* melanogaster is from
1047 (Namiki et al., 2018).
1048 (B) An image of a standard fly brain with a rendering of the mushroom bodies (MB) and the antennal
1049 lobes (AL). Projection neurons (PN) convey information from the AL to the calyx of the MB and the
1050 lateral horn (LH).
1051 (C) A simplified diagram of the mushroom body circuit. The identity of sensory stimuli is represented
1052 by sparse activity patterns of Kenyon cells (KCs). A subset of dopaminergic neurons (DANs) respond
1053 to punishment/reward. Dopamine modulates weights of synapses between KCs and MB output
1054 neurons (MBONs) depending on the activity status of KCs. The skewed activity patterns of MBONs
1055 across compartments in response to the learned stimulus drive memory-based actions and feedback
1056 pathways to DANs.
1057 (D) A summary of the workflow to generate split-GAL4 lines.
1058 (E) Coverage of the collection. The crepine (CRE), the superior medial protocerebrum (SMP), the
1059 superior intermediate protocerebrum (SIP) and the superior lateral protocerebrum (SLP) are MB
1060 adjacent brain areas where MBONs and DANs most often have arborizations. CX, central complex.
1061 LAL, lateral accessory lobes.
1062 (F) Examples of cell types covered by the collection. Expression patterns of CsChrimson-mVenus
1063 (green) are shown with neuropil counterstaining of Bruchpilot (Brp) with nc82 antibody (magenta).
1064 The whole body image of Gr64f-Gal4 line at the left middle panel is shown with muscle
1065 counterstaining (magenta). Light gray labels indicate EM-identified neurons labeled by each line (see
1066 Supplementary File 1 for details). Putative cell types are bracketed.
1067
1068 **Figure 1-figure supplement 1 Examples of cell types covered by the split-GAL4 lines in this collection**
1069 Additional examples of cell types covered by the collection. Expression patterns of CsChrimson-
1070 mVenus (green) are shown with neuropil counterstaining of Brp (magenta). Only one brain
1071 hemisphere is shown. Light gray labels indicate EM-identified neurons labeled by each line (see
1072 Supplementary File 1 for details).
1073
1074 **Figure 2 LM-EM Match of the CRE011-specific driver SS45245**
1075 (A) Expression pattern of SS45245-split-GAL4 in the brain.
1076 (B) MCFO image of SS45245 showing individual labeled neurons.
1077 (C) Frontal (top) and ventral (bottom) views of segmented light microscopy (LM) images of an
1078 exemplary split-Gal4 line (SS45245) visualized with a membrane reporter (myr-smGFP-FLAG) that was
1079 aligned to the JRC2018 standard brain. Projections are shown with outline of relevant neuropils.
1080 (D) The skeleton reconstructed from electron microscopy (EM) data of the matched cell type CRE011
1081 in the hemibrain connectome. The CRE011 cell on the right hemisphere is shown.
1082 (E) Synaptic connectivity of CRE011 with MBONs and DANs in the MB derived from the hemibrain
1083 connectome.

1084
1085 **Figure 2-figure supplement 1 LM-EM match of SS00460**
1086 (A) Frontal and ventral views of segmented light microscopy (LM) images of SS00460 in the JRC2018
1087 standard brain. Projections are shown with the outline of relevant neuropils. A' (ventral) is a rotated
1088 view of A (frontal) with the reference axis indicated.
1089 (B) The skeleton reconstructed from electron microscopy (EM) data in the hemibrain volume of the
1090 matched cell type v2LN44.
1091 (C) EM images of neurons with the most input connections (upstream) to v2LN44 in the hemibrain
1092 connectome. The number after "#" indicates the number of connections between the matched cell
1093 type (i.e. v2LN44) and its synaptic partners. The color code and EM BodyId for each EM-reconstructed
1094 neuron are also listed.
1095 (D) EM images of neurons with the most output connections (downstream) from v2LN44 in the
1096 hemibrain connectome. In Figure 2-figure supplement 1-20, sensory neurons and KCs are not
1097 displayed as top upstream or downstream neurons.
1098
1099 **Figure 2-figure supplement 2 LM-EM match of SS34963**
1100 **Figure 2-figure supplement 3 LM-EM match of SS33915**
1101 **Figure 2-figure supplement 4 LM-EM match of SS35020**
1102 **Figure 2-figure supplement 5 LM-EM match of SS34979**
1103 **Figure 2-figure supplement 6 LM-EM match of SS34947**
1104 **Figure 2-figure supplement 7 LM-EM match of SS00486**
1105 **Figure 2-figure supplement 8 LM-EM match of SS49308**
1106 **Figure 2-figure supplement 9 LM-EM match of SS49361**
1107 **Figure 2-figure supplement 10 LM-EM match of SS49868**
1108 **Figure 2-figure supplement 11 LM-EM match of SS49352**
1109 **Figure 2-figure supplement 12 LM-EM match of SS32228**
1110 **Figure 2-figure supplement 13 LM-EM match of SS32219**
1111 **Figure 2-figure supplement 14 LM-EM match of SS48890**
1112 **Figure 2-figure supplement 15 LM-EM match of SS48799**
1113 **Figure 2-figure supplement 16 LM-EM match of SS32259**
1114 **Figure 2-figure supplement 17 LM-EM match of SS48341**
1115 **Figure 2-figure supplement 18 LM-EM match of SS35040**
1116 **Figure 2-figure supplement 19 LM-EM match of SS33905**
1117 **Figure 2-figure supplement 20 LM-EM match of SS39538**
1118
1119 **Figure 3 Drivers for MBON downstream and DAN upstream neurons.**
1120 (A) Examples of confocal microscopy images of split-GAL4 lines (bottom) and their matching cell types
1121 in the hemibrain connectome (top). CsChrimson-mVenus (green); Brp (magenta).
1122 (B) The number of cell types that receive synaptic output from MBONs and supply synaptic input to
1123 DANs. Only cell types with connection (conn) over the indicated thresholds (i.e., more than 4 synapses
1124 for DAN upstream and more than 9 synapses for MBON downstream) were considered. The number
1125 of covered cell types are indicated in the brackets.
1126 (C) A scatter plot of MB interneuron cell types connected with DANs and MBONs. Cell types covered
1127 by Split-GAL4 lines are highlighted in red.
1128

1129 **Figure 3-figure supplement 1 New or improved drivers for MB cell types**
1130 (A) Confocal images and matched EM cell types. CsChrimson-mVenus (green); Brp (magenta).
1131 (B) Summary of within-MB split-GAL4 coverage. See Supplementary File 5 for details.
1132
1133 **Figure 4 Driver lines for uni-glomerular projection neurons**
1134 (A) Examples of covered uni-glomerular PN (uPN) cell types.
1135 (B) Coverage of the 51 antennal lobe glomeruli. The new collection of split-GAL4 covers uPN in the
1136 colored glomeruli.
1137 (C) Split-GAL4 coverage summary.
1138
1139 **Figure 5 Driver lines for multi-glomerular projection neurons**
1140 Examples of multi-glomerular projection neurons (mPN) types. M_l2PN3t18 [VC5++ l2PN1],
1141 M_lPNm11A [VP4++ lPN], and M_smPNm1 [VP3+ smPN] are predicted to receive majority non-
1142 olfactory input (Marin et al., 2020).
1143
1144 **Figure 6 Driver lines for non-olfactory projection neurons and sensory neurons**
1145 Examples of thermo-/hygro-sensory PN types (A) and sensory neurons (B) covered by this collection.
1146 Other than thermo-/hygro-sensory receptor neurons (TRNs and HRNs), SS00560 and MB408B also
1147 label olfactory receptor neurons (ORNs): ORN_VL2p and ORN_VC5 for SS00560, ORN_VL1 and
1148 ORN_VC5 for MB408B.
1149
1150 **Figure 7 Driver lines for gustatory sensory neurons**
1151 (A) A summary of new transgenic lines generated by this study. In addition to Gr64f promoters,
1152 LexADBD lines were generated with Gr64f, Gr43a, Gr66a, Gr28b promoters and other GMR or VT
1153 promoters. The six Gr64f-LexADBD lines are with different insertion sites, and with the presence or
1154 absence of the p10 translational enhancer (see Supplementary File 2 for details).
1155 (B) Schematic of the screening strategy used here to subdivide the Gr64f-DBD pattern by intersecting
1156 it with GMR and VT AD lines.
1157 (C) A schematic of the sensory neuron projection types that compose the Gr64f-DBD pattern.
1158 (D) A summary of expression patterns of 6 of the Gr64f split-GAL4 lines derived from the screening
1159 strategy in (B), using the anatomical notation described in (C).
1160 (E) Expression pattern of SS87269 in the brain and VNC. The arrow indicates an ascending projection
1161 of atGRN.
1162 (F) Expression of SS87269 in the labellum.
1163 (G) Expression of SS87269 in tarsi of fore (f), middle (m) and hind (h) legs.
1164 (H) Expression of SS87272 in the labral sense organ (LSO).
1165 (I) Expression of SS88801 in tarsi.
1166 (J) Expression of SS87278 in the abdominal body wall.
1167 (K-Q) Expression patterns of designated driver lines in the Gnathal Ganglia (GNG) and VNC. The arrow
1168 in K indicates the absence of ascending projections from stGRN.
1169 Magenta in F-J indicates muscle counterstaining with phalloidin (actin filaments); magenta in other
1170 panels indicates neuropil counterstaining of Brp. All scale bars are 50µm.
1171

1172 **Figure 7-figure supplement 1 Expression pattern of Gr64f-Gal4**
1173 Expression pattern of Gr64f-GAL4 driving 5xUAS-myr-smFLAG in VK0005 in the brain and VNC (green)
1174 with neuropil counterstaining of Brp (magenta). The line used contains two copies of Gr64f-Gal4, with
1175 one copy on the second and one copy on the third chromosome. The insert on the left shows a
1176 magnified view of each cell type in different colors. The insert on the right shows a sagittal view of
1177 the VNC.
1178
1179 **Figure 7-figure supplement 2 Expression pattern of Split-LexA lines from Gr43a and Gr66a**
1180 (A) Split-LexA line derived from sugar-sensory Gr43a-LexADBD. SL99997 labels internal fructose
1181 sensory neurons (Miyamoto et al., 2012). The labeling of T1 neurons in SL99998 presumably comes
1182 from ectopic expression of Gr43a-LexADBD.
1183 (B) Split-LexA line derived from Gr66a-LexADBD labels different subsets of bitter-sensory neurons.
1184
1185 **Figure 7-figure supplement 3 Examples of covered SEZ neurons.**
1186 (Top two rows) New or improved split-GAL4 drivers for cell types already covered by the SEZ Split-
1187 GAL4 Collection (Sterne et al., 2021). (Bottom row) Split-GAL4 drivers for cell types not included in the
1188 SEZ Split-GAL4 Collection. Cell types are from Hemibrain 1.2.1, Sterne 2021 or mn2V (McKellar et al.,
1189 2020).
1190
1191 **Figure 8 Behaviors with Gr64f-split-GAL4 lines**
1192 (A) In the optogenetic olfactory arena, odors are delivered from the periphery and sucked out from
1193 the central vacuum port to deliver odors only to defined quadrants. Red LEDs (627nm peak) enable
1194 programmed optogenetic activation of neurons expressing CsChrimson.
1195 (B) Training and testing protocol for experiments shown in (E). The training protocol consisted of 3 x
1196 20s optogenetic activation training followed by the first preference test, 1x 1 min training followed
1197 by the 2nd test, and additional 2x 1 min training followed by the last test. Odors delivered to the two
1198 zones and odor durations in each period are indicated. LED intensities were 4.3 $\mu W/mm^2$ in early 20s
1199 training and 34.9 $\mu W/mm^2$ in later training. Activation LED was applied with 1s ON and 1s OFF during
1200 pairing with odor A. Odors were trained reciprocally. Pentyl acetate and Ethyl lactate were used as
1201 odor A and B, respectively, in one half of the experiments and the two odors were swapped in the
1202 other half of experiments.
1203 (C) Protocol to characterize Gr64f split-GAL4 activation phenotypes in the absence of an odor. During
1204 each trial, flies were illuminated with a red LED light continuously for 10 seconds.
1205 (D) Summary diagram of the expression patterns of the original Gr64f-GAL4 (far left) and 6 Gr64f-
1206 split-GAL4s. The expression of the original Gr64f-GAL4 in olfactory sensory neurons is not depicted
1207 here.
1208 (E) Associative memory scores after the training protocol in (B). Mean, standard error of the mean
1209 (SEM), and the number of groups are shown.
1210 (F) The kinematic parameters of trajectories measured with Caltech FlyTracker during split-GAL4
1211 activation in the absence of odor as shown in (C). Return behavior was assessed within a 15-second
1212 time window. The probability of return (P return) is the number of flies that made an excursion (>10
1213 mm) and then returned to within 3 mm of their initial position divided by the total number of flies.
1214 Curvature is the ratio of angular velocity to walking speed. Each group of flies received 6 activation
1215 trials. Summarization was based on the trial average of each group. The number of groups is indicated.

1216 The thick lines and shadows are mean and SEM. Gray lines are Empty-split-GAL4 control. Dashed lines
1217 are time bins for data summary in Figure 8-figure supplement 2.
1218 (G) Average walking speed in each of 6 trials.
1219 (H) An image of a tethered fly on a floating ball. Flies were tracked for proboscis extension (PE) activity
1220 with the Animal Part Tracker (Kabra et al., 2022). The annotated points, in the order of numbers,
1221 consisted of the tip of the abdomen (1), the highest point on the thorax (2), the midpoint between
1222 the root of the antennae (3), the base of the proboscis (4) and the tip of the proboscis (5). PE activity
1223 was quantified as the change of proboscis length, i.e., the distance from the tip to the base of the
1224 proboscis, or the distance between points 4 and 5.
1225 (I) SS87269 and SS88801 activation and proboscis extension. Each fly was recorded over 6 activation
1226 trials in which the 624 nm LED was turned on for 1 second. LED intensity for SS87269 and SS88801,
1227 11 $\mu W/mm^2$; for empty Gal4 (pBDPGal4), 50 $\mu W/mm^2$. Less saturated traces indicate behavior during
1228 LED off trials, while more saturated traces indicate behavior during LED on trials.
1229
1230 **Figure 8-figure supplement 1 Olfactory arena learning experiment, fly tracking and data analysis**
1231 (A) To test associative learning in the olfactory circular arena, two different odors (A and B) were
1232 delivered to interleaved quadrants, defined as Zone 1 and Zone 2. The trajectory of an example fly
1233 during the odor choice period after automatic tracking of the experiment movies is shown.
1234 (B) Experiment protocol for learning as in Figure 8B. Odors (green-A, purple-B) and LED delivered to
1235 the two zones are indicated. The transition between sessions that were not video-recorded are
1236 masked by gray. In the example data, the odor ethyl lactate (EL) served as CS+ and was paired with
1237 CsChrimson-activation of SS87269, while the other odor pentyl acetate (PA) served as CS- and was
1238 unpaired. The full data set included an additional reciprocal group with PA as CS+ and EL as CS-.
1239 (C) Upwind displacement towards CS+ and CS- during the experiment was quantified by a change in
1240 the mean distance-to-wall for all flies (airflow came from the periphery of the arena and was drawn
1241 out in the center). In addition to the three testing periods (0-20 second after odor onset), the mean
1242 distance-to-wall during training in the odor periods before LED onset (0-10 second after odor onset)
1243 were also quantified. “CS+” and “CS-” groups were compared with a multi-comparison t-test with
1244 Bonferroni-Dunn’s correction. *, $P<0.05$; ***, $P<0.001$.
1245
1246 **Figure 8-figure supplement 2 Summary data of Gr64f-split-Gal4 activation phenotypes**
1247 The data points during the time bin shown in Figure 8F.
1248 (A) Probability of return during the post-activation period.
1249 (B) Change of walking speed during the onset of activation period.
1250 (C) Change of curvature during the onset of activation period.
1251 (D) Change of curvature during the post-activation period.
1252 One-way ANOVA followed by Dunnett’s multiple comparisons test. ***, $P<0.001$. Individual data
1253 points are shown with minimum, maximum, median, and interquartile ranges.
1254
1255 **Figure 8-figure supplement 3 Consistency of Gr64f-split-GAL4 phenotypes over repeated activations**
1256 Flies expressing the CsChrimson-mVenus were repeatedly exposed to 10-s red LED as in Figure 8F but
1257 with lower intensity (4.3 $\mu W/mm^2$) and more repetitions. N=8.
1258 (A) The averaged time course of probability of return binned over 10 trials. LED was turned on at 10 s
1259 and lasted for 10 s.
1260 (B) The mean probability of return in the 10-s period after the LED is turned off.

1261 (C) The walking speed in the 5-s period before LED onset. Averages of 10-trial bins are displayed,
1262 except for the trial zero. Gradual increase of walking speed was observed in the Empty-split-GAL4
1263 control, likely because of dehydration caused by constant exposure to the airflow.
1264 (D) Change of walking speed during the activation onset period.
1265
1266 **Figure 9 Examples of covered ascending neurons**
1267 (A) Activation preference screen of 581 split-GAL4 lines (342 lines from this study). SS01159 (blue
1268 arrow) is one of the lines that flies showed strong avoidance at optogenetic activation.
1269 (B) Time course of flies' preference to quadrants with red LED light by SS01159>CsChrimson (blue) or
1270 empty-GAL4>CsChrimson (gray). A preference score to red LED quadrants was quantified from the
1271 distribution during the last 5s of two 30s activation periods. n = 8 groups for SS01159, n = 15 for empty
1272 Gal4. Mean (thick lines) and SEM (shadow) are plotted.
1273 (C) The mean normalized movement speed at the LED onset for flies in the LED quadrants. The 3-s
1274 period before LED onset was used as the baseline for normalization.
1275 (D) The mean cumulative turning angles in 5 movie frames (total elapsed time of 167 ms) when flies
1276 encountered the LED boundary. The boundary was defined as a 4-mm zone in between the LED and
1277 dark quadrants. Trajectories too close to the center (< 0.2*radius) or the wall (> 0.6*radius) of the
1278 arena were not analyzed.
1279 (E) Examples of split-GAL4 lines for ascending neurons. SS35227 and SS35256 shared a split half
1280 (R41C05-AD) with SS01159. SS32217 matched with TPN1 (Kim et al., 2017). No cell types (or only EM
1281 BodyIds) were assigned to the other lines shown due to missing information in the hemibrain volume.
1282
1283 **Figure 10 Stereotypy and erroneous projections**
1284 (A) V_l2PN from both hemispheres send axonal projections to the right hemisphere in an atypical case
1285 (arrowhead).
1286 (B) In this atypical case, there are two MB-DPM neurons in one hemisphere (arrowhead) and the
1287 arborizations extend beyond the pedunculus into the calyx.
1288 (C) MBON-α1 occasionally has additional arborizations in the ellipsoid body (arrowhead)
1289 (D) The localization of MBON-α3 soma widely varied along the dorso-ventral axis. It occasionally had
1290 an additional axonal branch (arrowhead).
1291 (E) A table to summarize normal and erroneous projections of MBONs and MB-DPM. In all the cases
1292 except for the DPM, "different number of cells" was likely due to stochastic expression of the drivers
1293 (i.e., lack of labeling) rather than biological difference. We defined "mislocalization" when axons or
1294 dendrites projected to outside of the normally targeted brain regions. For instance, dendrites of
1295 typical MBON07 are usually confined inside the α1, but were extended to outside the MB lobes in
1296 22.9% of samples. Variable branching patterns inside the normally targeted brain regions were not
1297 counted as mislocalization here. In some MB310C-split-GAL4 samples, we observed a third soma
1298 attached to MBON-α1 but they lacked any neurites. We did not observe obvious mislocalization of
1299 dendrites or axons for MBON03, 5, 6, 12, 18 and 19. See Figure 11 for variability of MBON08/09 in
1300 MB083C.
1301
1302 **Figure 11 Individuality and asymmetry of MBON08 and MBON09**
1303 (A) A typical image of two MBONs in MB083C-split-GAL4 driver.
1304 (B) Abnormal axonal projection of MBON08/09 observed in one of 169 samples.

1305 (C-D) MCFO images of MB083C driver from different flies show that the two cells can either be both
1306 MBON09-γ3β'1 (C) or one MBON09-γ3β'1 and one MBON08-γ3 (D).
1307 (E-G) An example of MCFO image of MB083C, which visualized one MBON08 and two MBON09 in the
1308 same brain. The projection (E) and image sections at the γ3 (F) or β'1 (G) are shown.
1309 (H) Diagrams of the three MBONs shown in E-G.
1310 (I) A summary table for observation of MBON08 and MBON09 in male and female brains.
1311 (J) All possible variations of 4 MBONs in MB083C driver, and estimated probability for each case based
1312 on the observations summarized in I.
1313 Panel (A) and (C) were adapted from Figure 8 of (Aso et al., 2014a).
1314
1315 **Figure 11-figure supplement 1 MB083C invariantly label two MBONs**
1316 Maximum intensity projection images of individual samples are shown. Note that two somas in each
1317 hemisphere are labeled in all samples. Reporters used are indicated in each panel.
1318
1319 **Figure 11-figure supplement 2 Subdivisions of medial and lateral γ3 compartments**
1320 (A) Overlay between the dendrites of MBON08/09 and axons of PAM-γ4 DANs.
1321 (B) Overlay between the dendrites of MBON08/09 and axons of PAM-γ3 DANs.
1322 (C) A subset of PAM-γ3 arborizes in the medial part of the γ3 compartment. Asterisk indicates the
1323 position of the lateral γ3 that is not labeled in this line.
1324
1325 **Figure 12 Examples of split-LexA conversion**
1326 Split-LexA shares the same enhancers with split-GAL4 but with the Gal4DBD replaced by LexADBD.
1327 Among 34 conversions tested, 22 were successful, with the split-LexA showing identical or similar
1328 expression patterns as the split-GAL4. The remaining 12 had weak/no expression or showed
1329 unintended intersectional patterns. See Supplementary File 2 for the hemidriver lines with p10
1330 translational enhancers to enhance expression level.

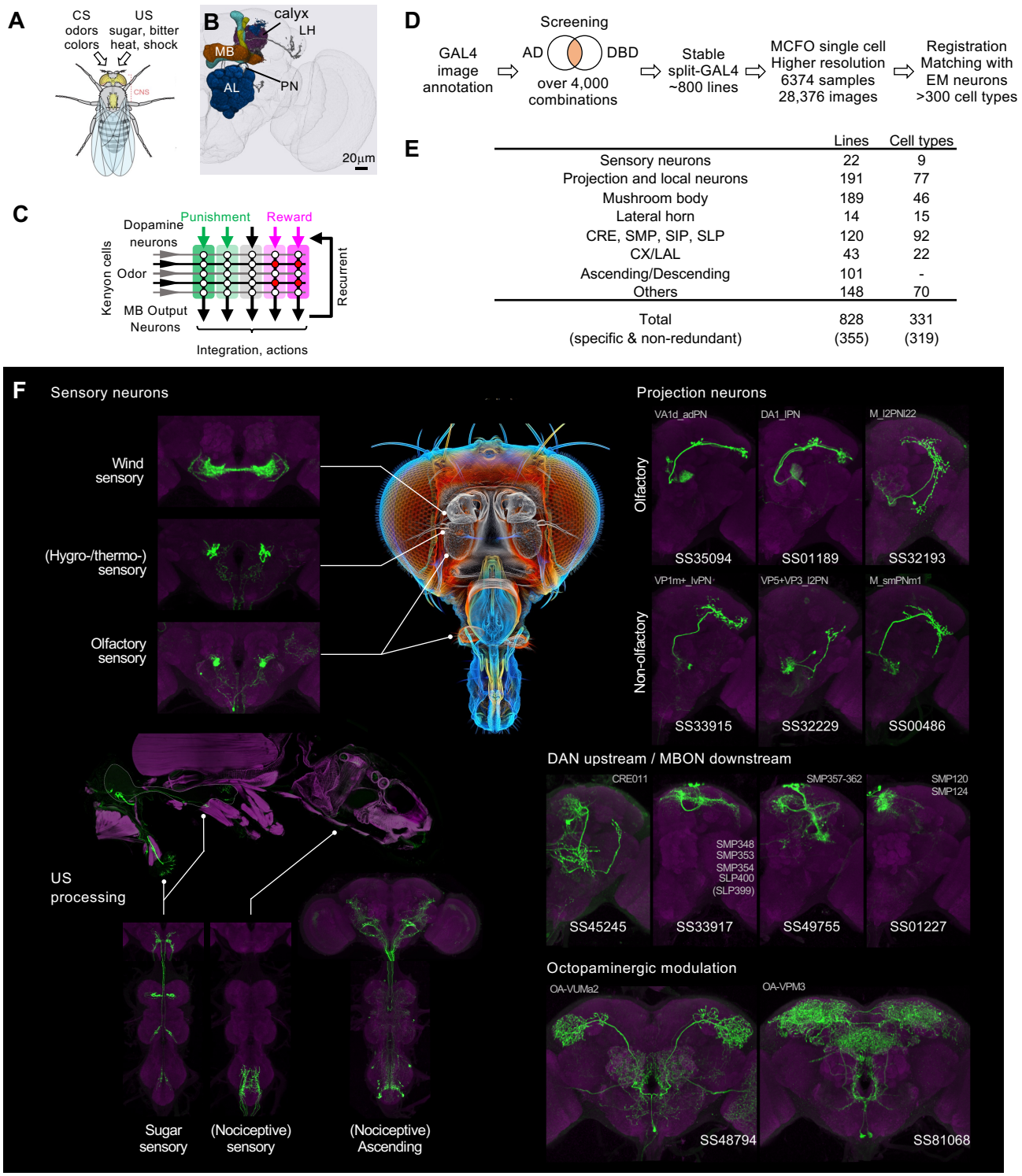

	Lines	Cell types
Sensory neurons	22	9
Projection and local neurons	191	77
Mushroom body	189	46
Lateral horn	14	15
CRE, SMP, SIP, SLP	120	92
CX/LAL	43	22
Ascending/Descending	101	-
Others	148	70
Total	828	331
(specific & non-redundant)	(355)	(319)

Figure 1 Generation and annotation of split-GAL4 lines

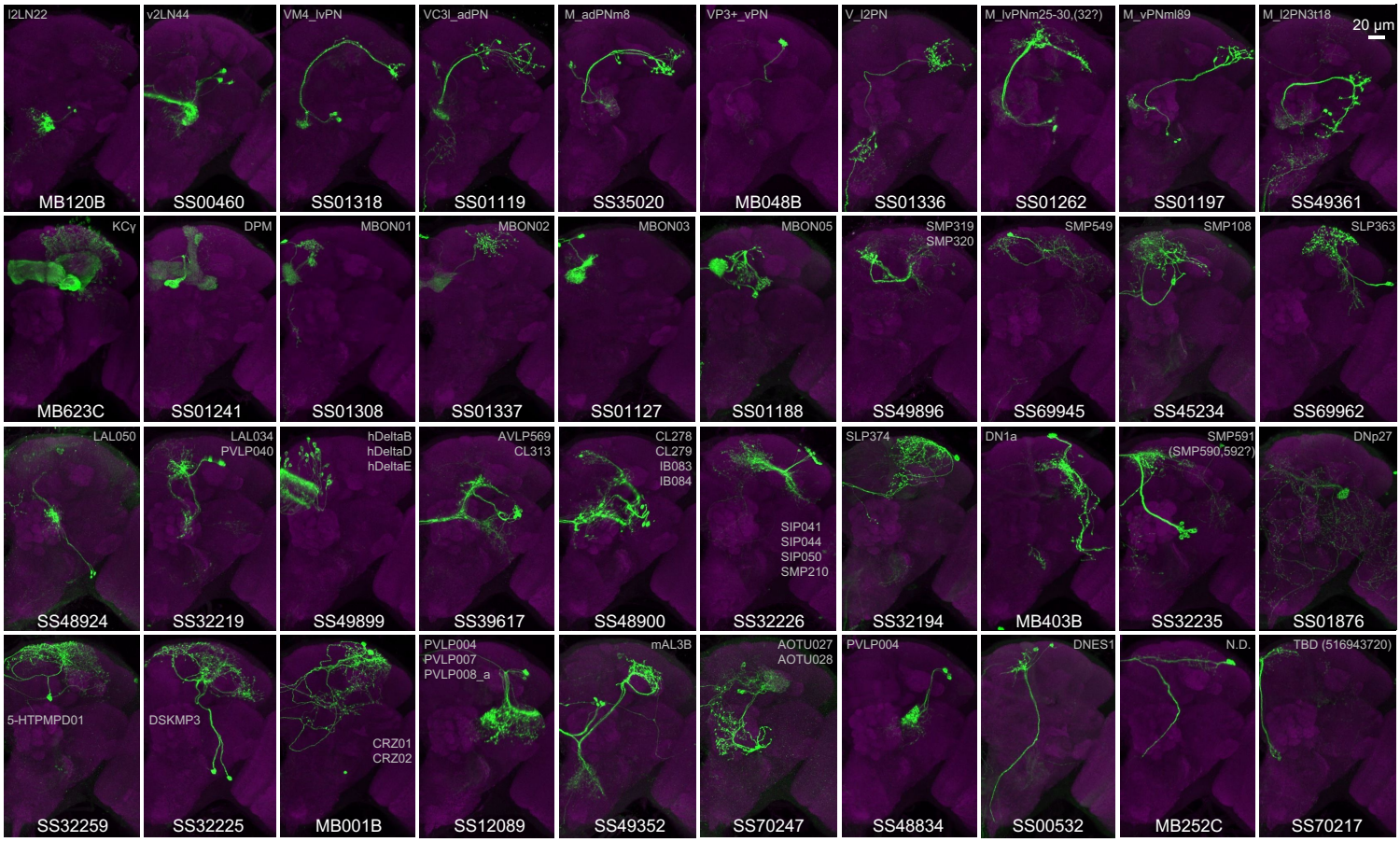

Figure 1-figure supplement 1 Examples of cell types covered by the split-GAL4 lines in this collection

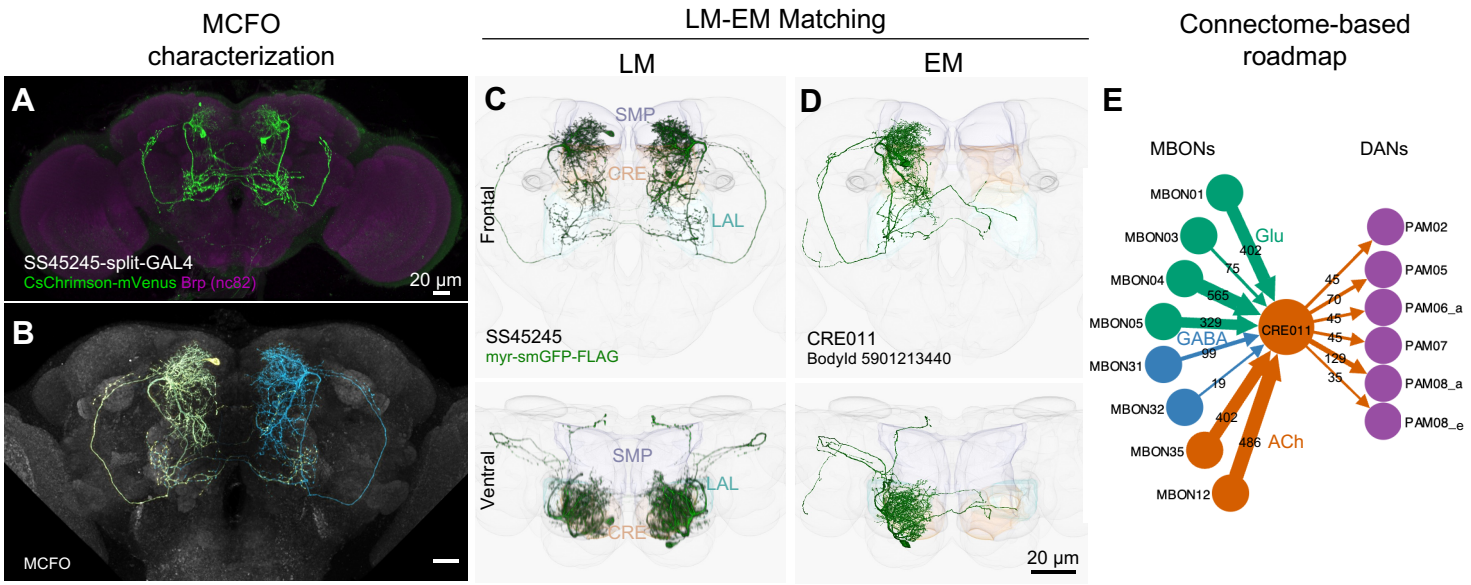

Figure 2 LM-EM Match of the CRE011-specific driver SS45245

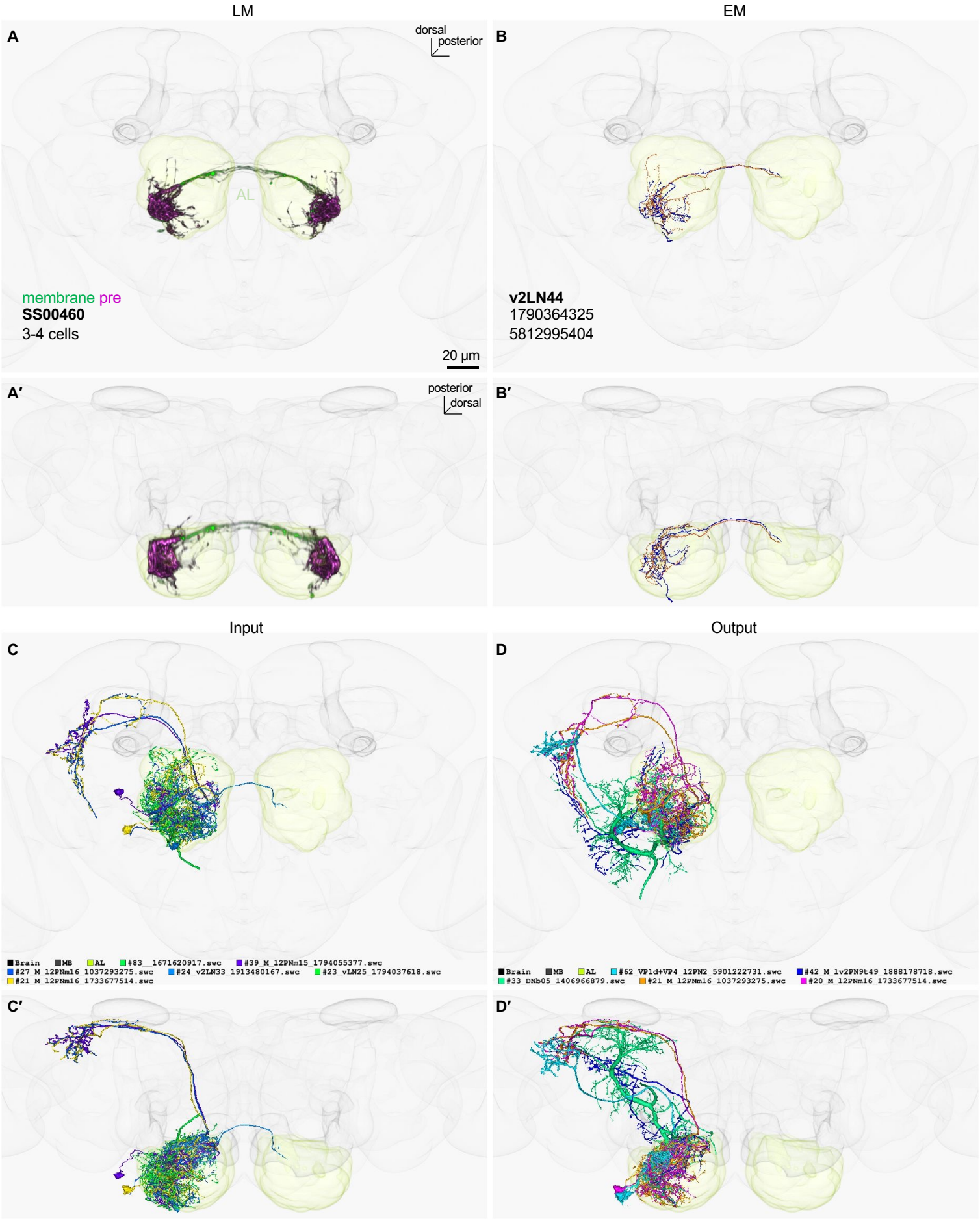

Figure 2 – figure supplement 1

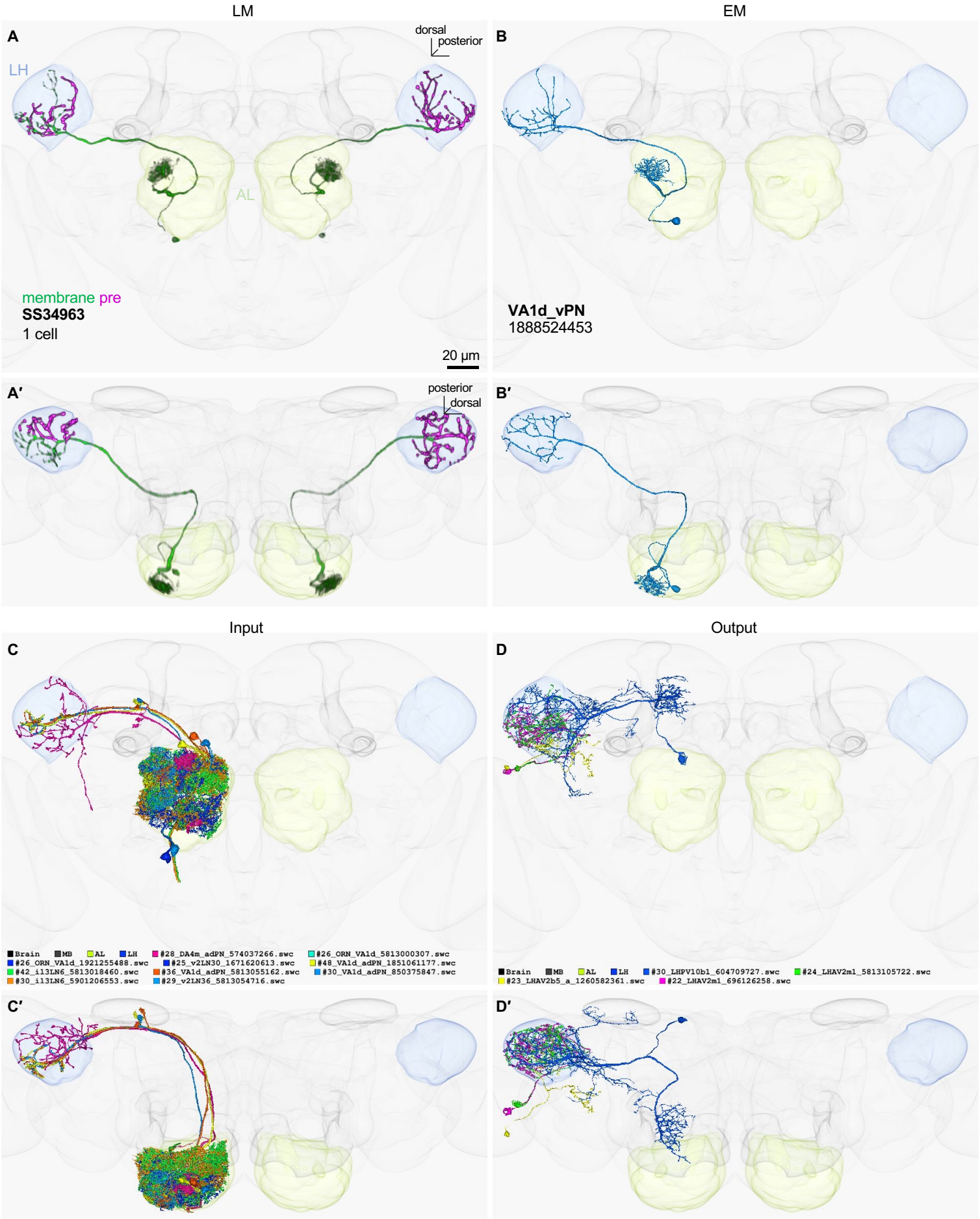

Figure 2 – figure supplement 2

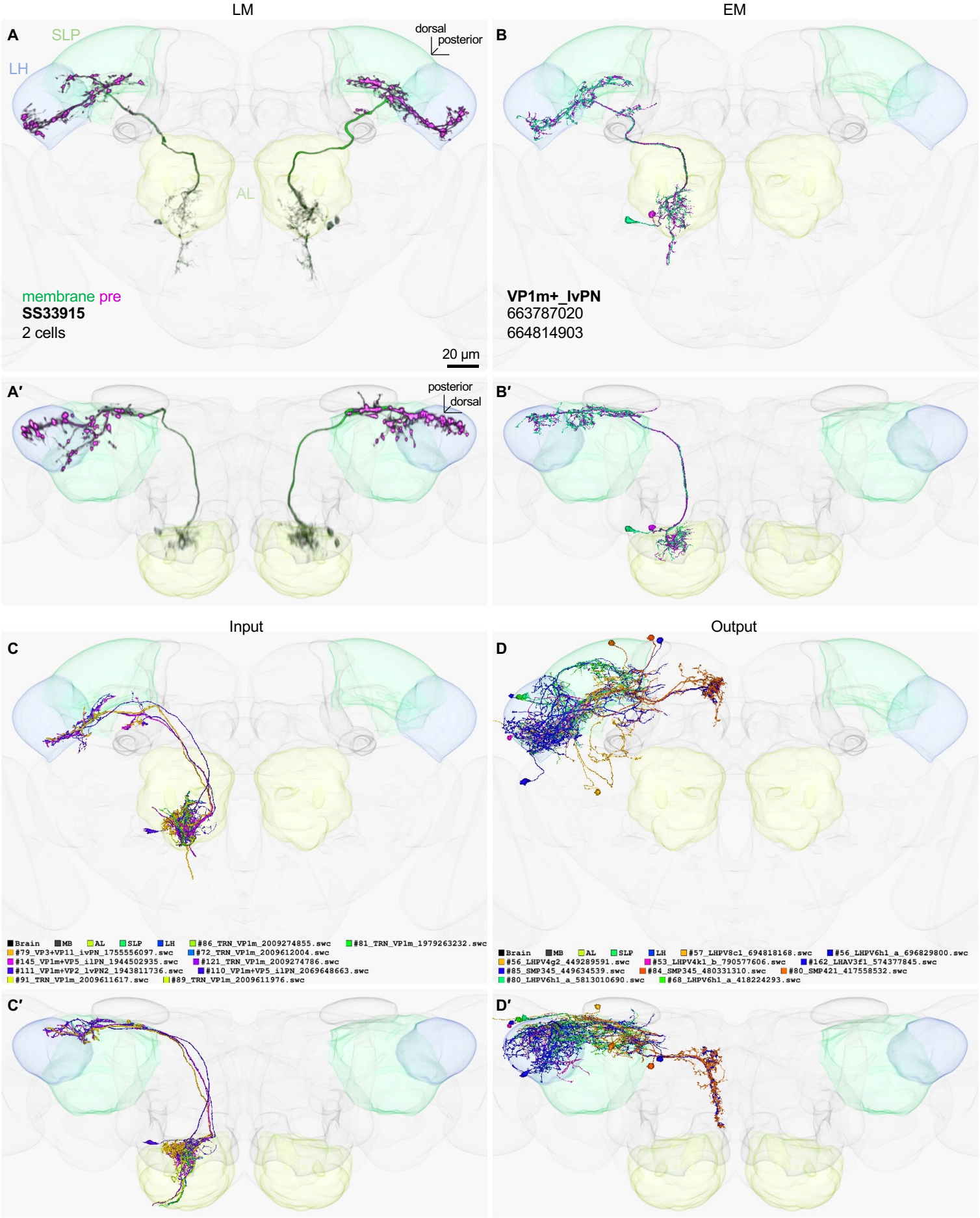

Figure 2 – figure supplement 3

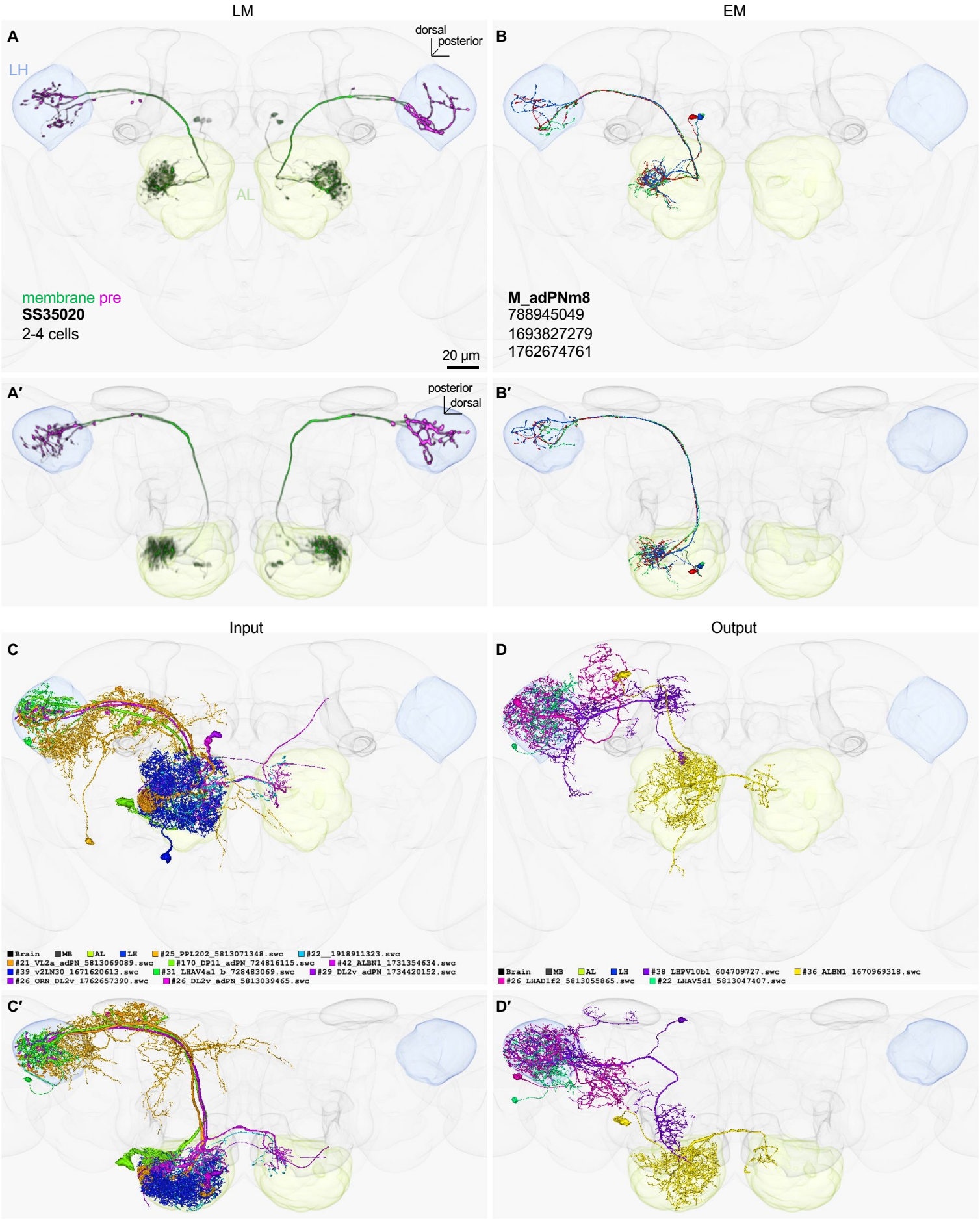

Figure 2 – figure supplement 4

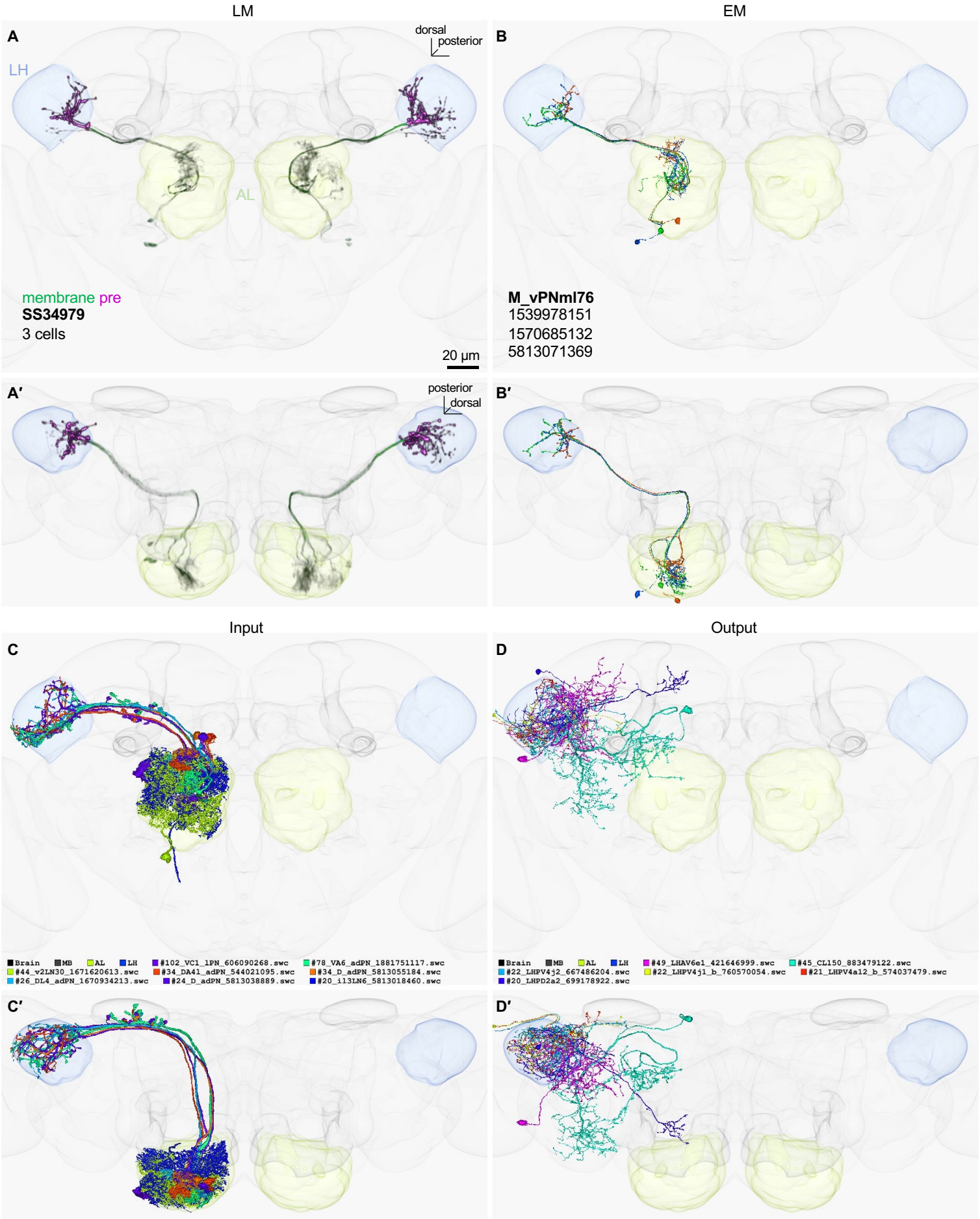

Figure 2 – figure supplement 5

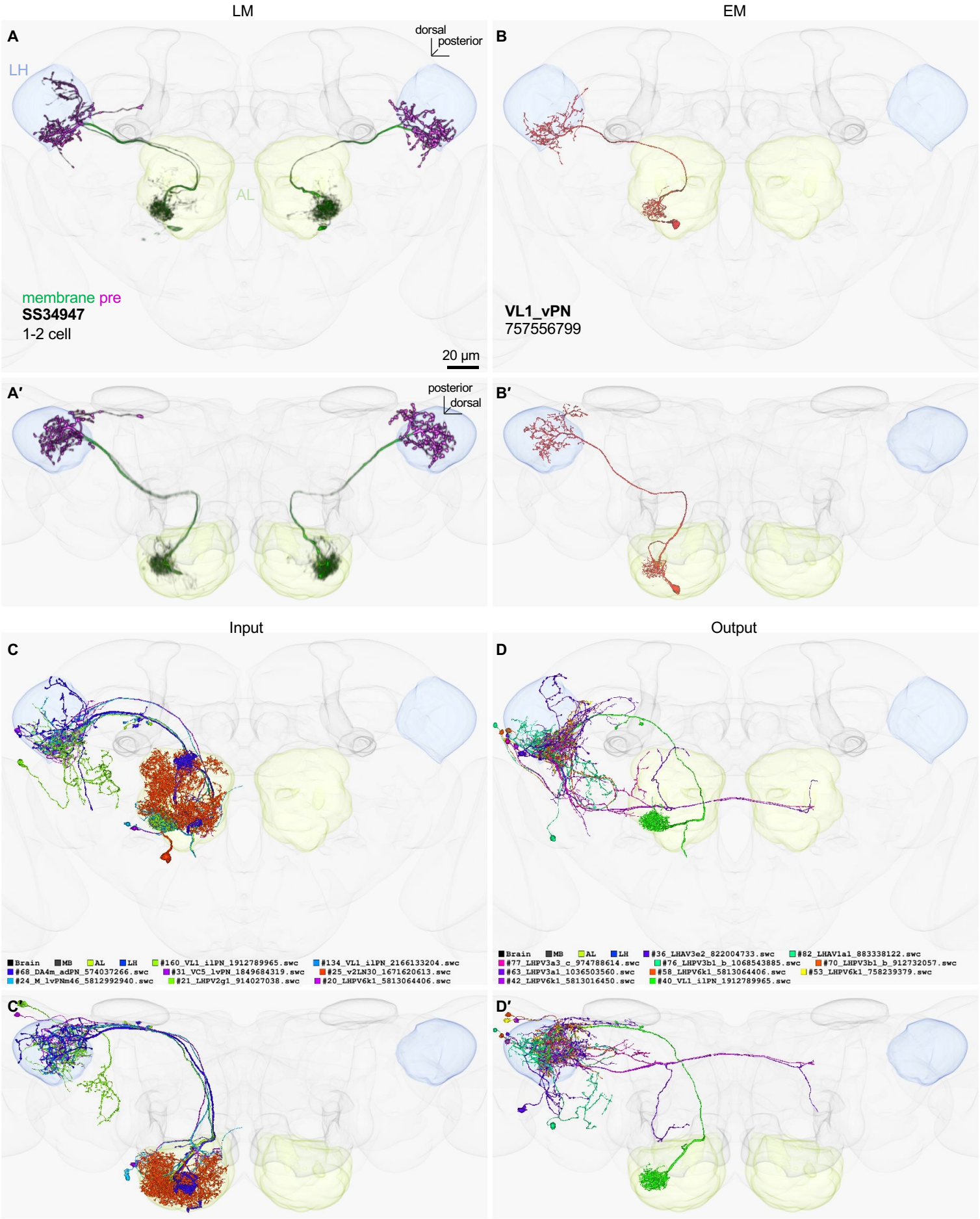

Figure 2 – figure supplement 6

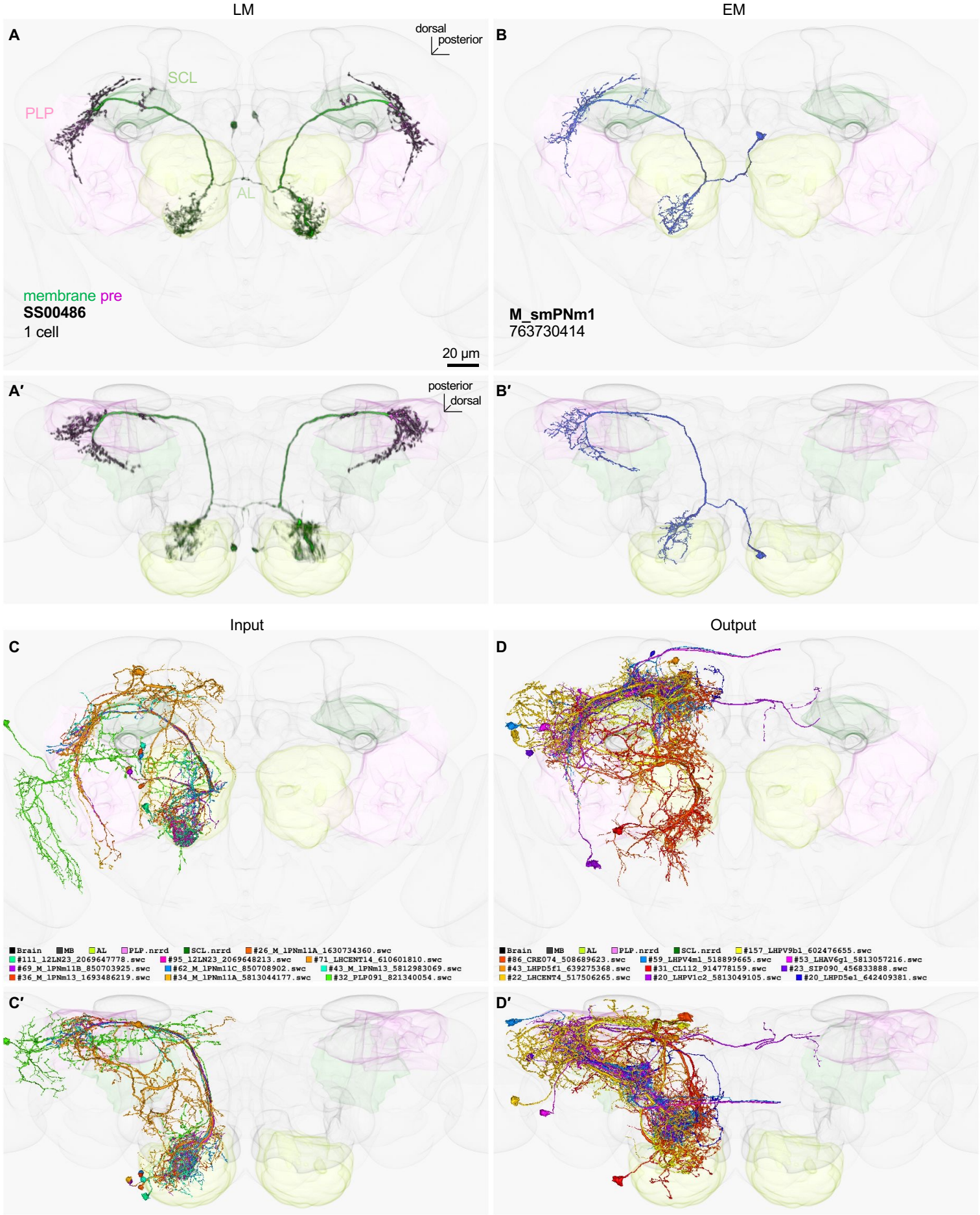

Figure 2 – figure supplement 7

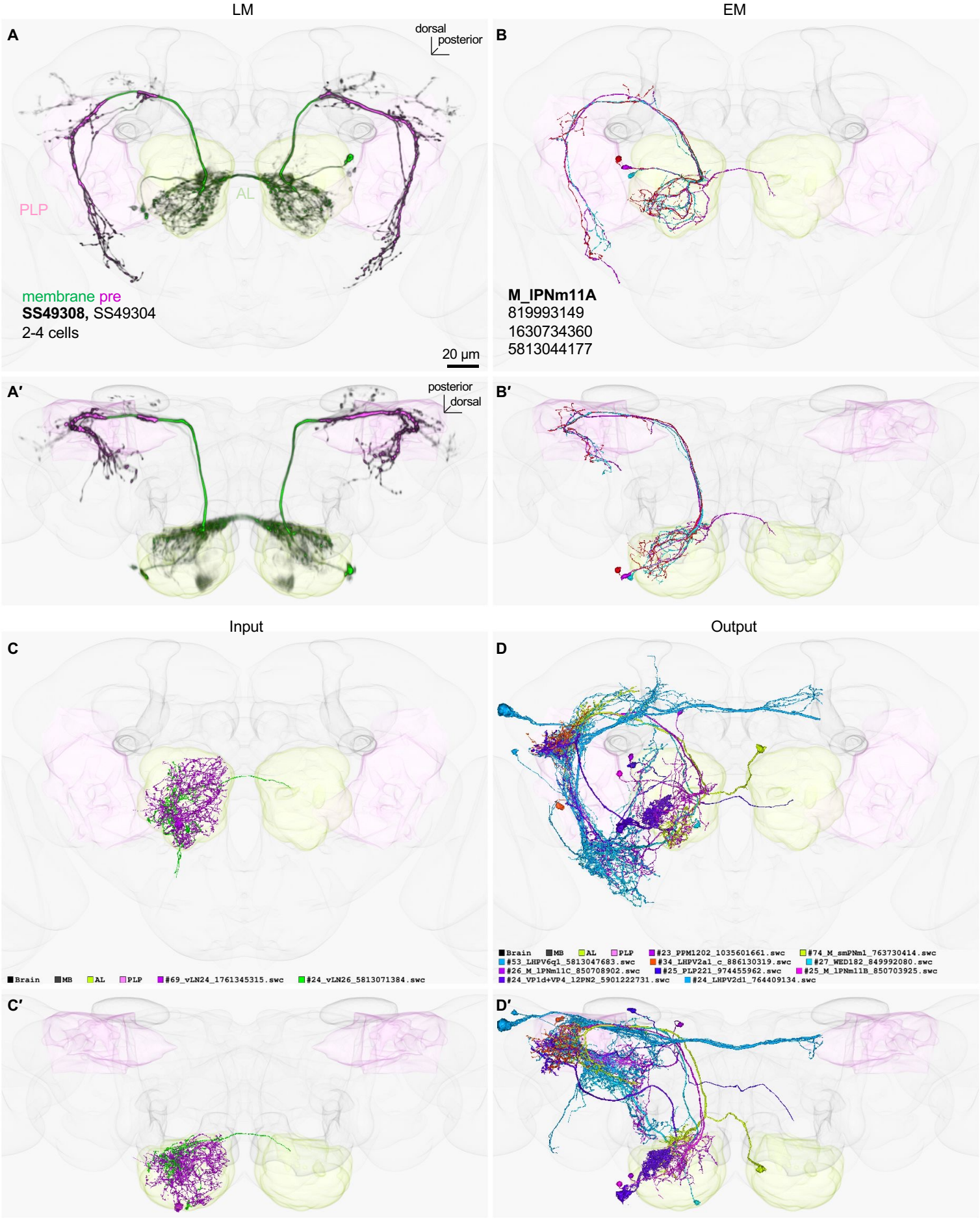

Figure 2 – figure supplement 8

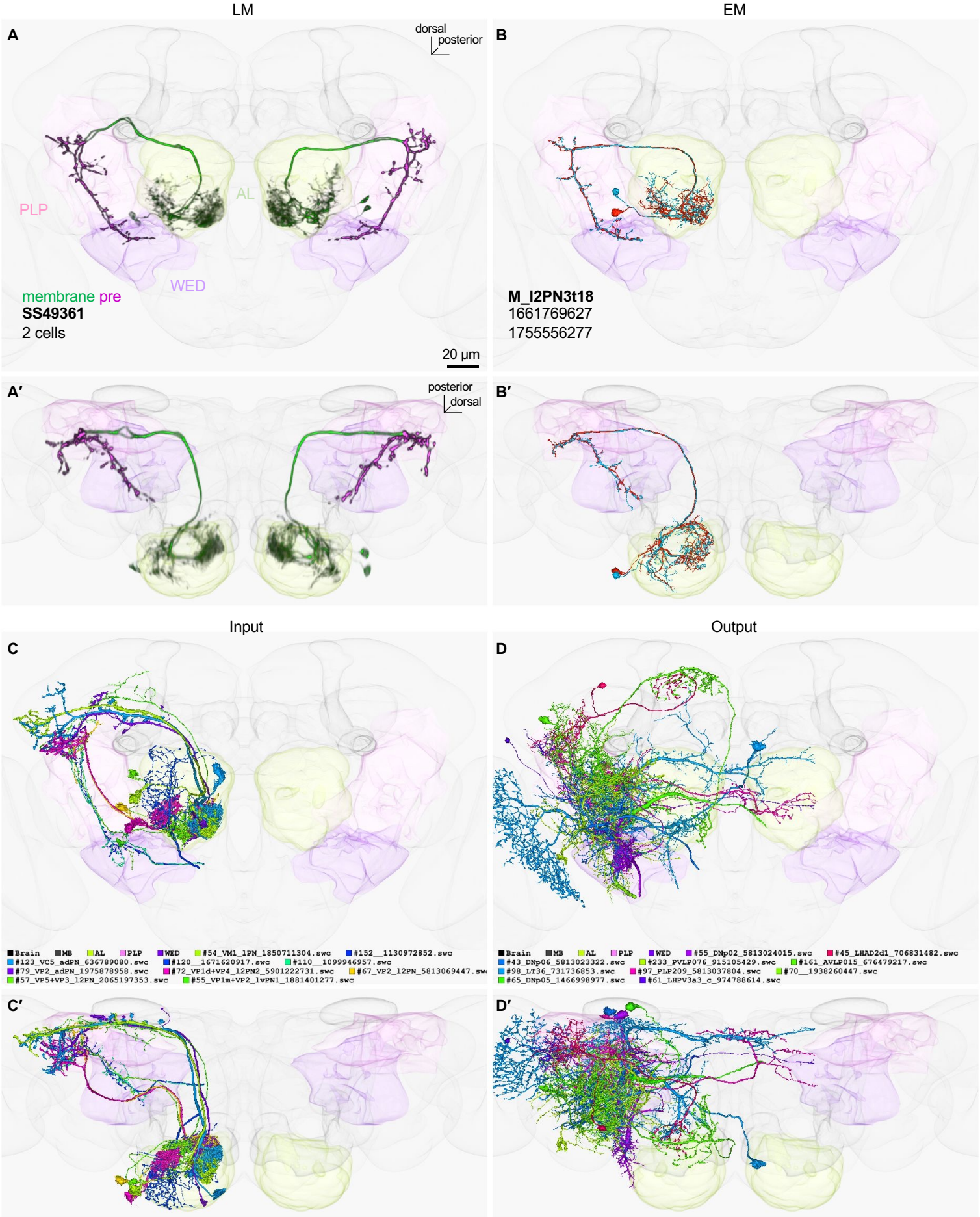

Figure 2 – figure supplement 9

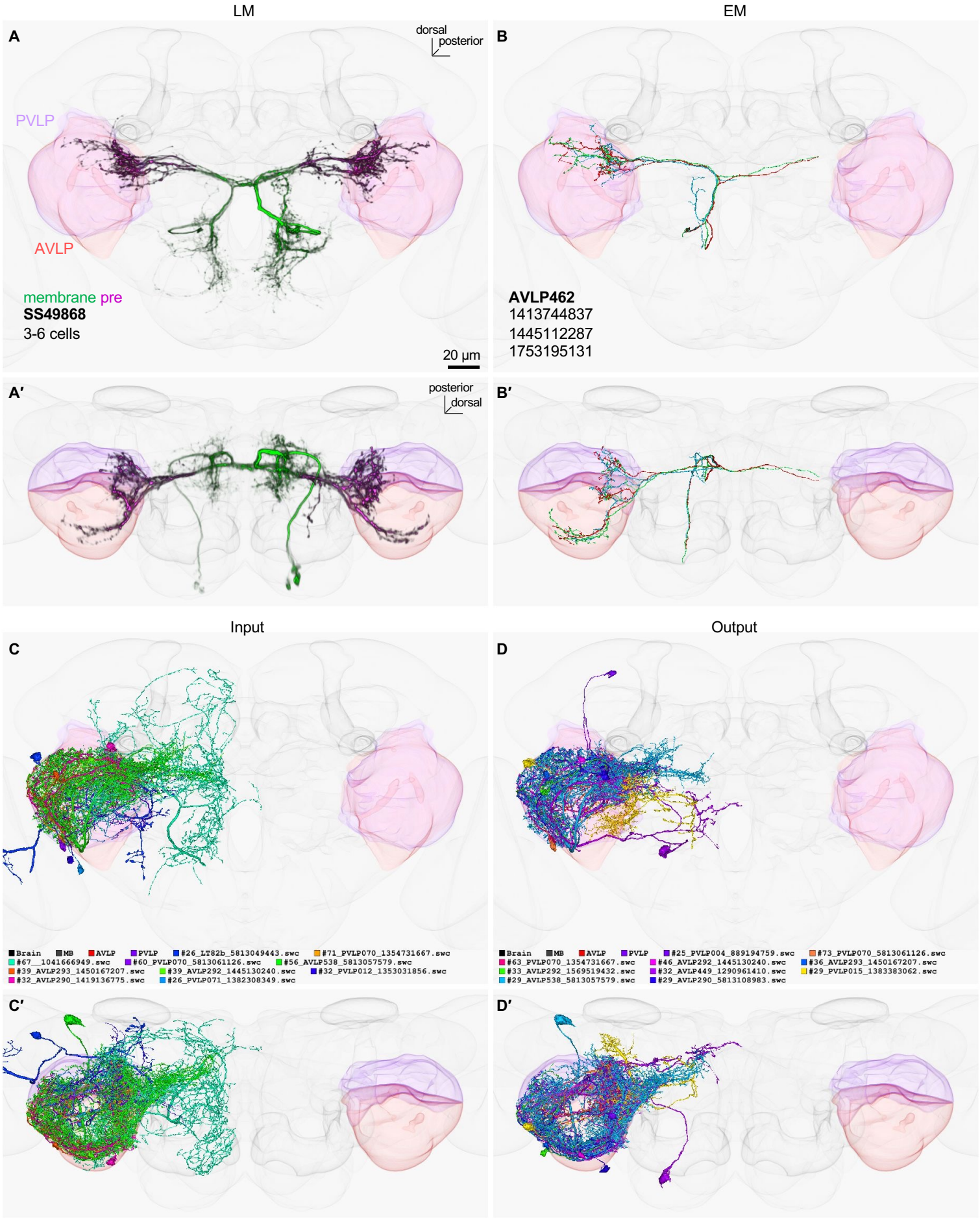

Figure 2 – figure supplement 10

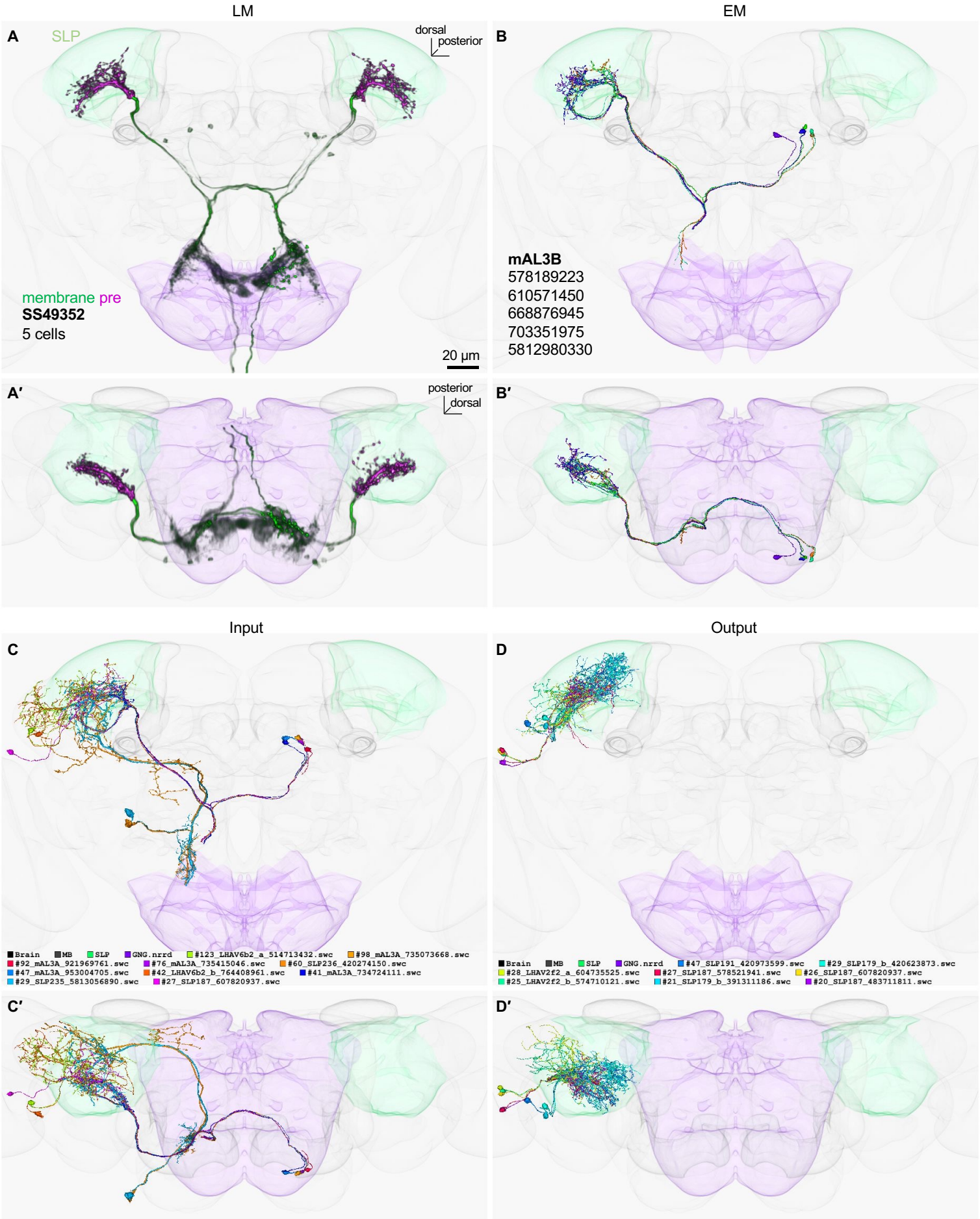

Figure 2 – figure supplement 11

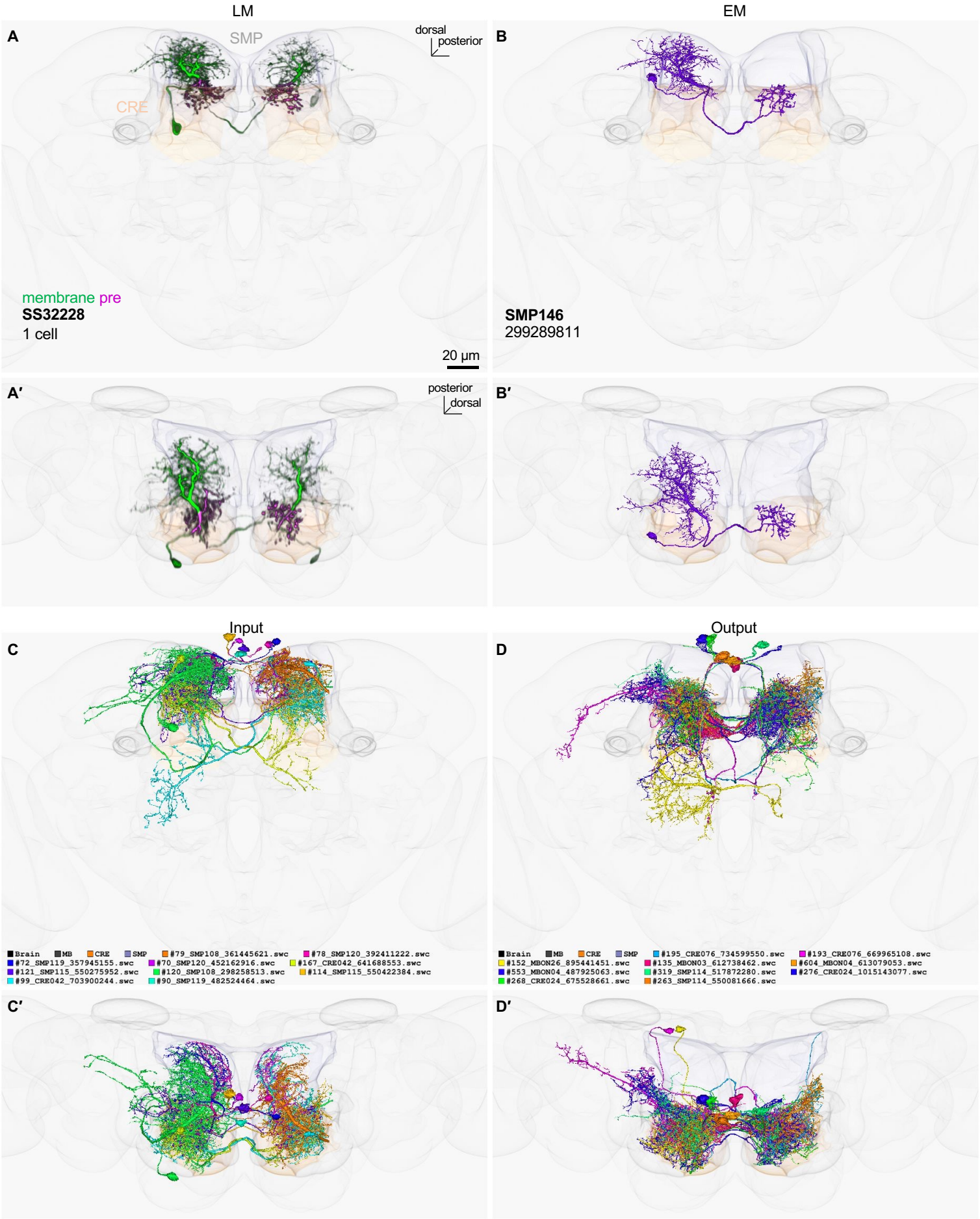

Figure 2 – figure supplement 12

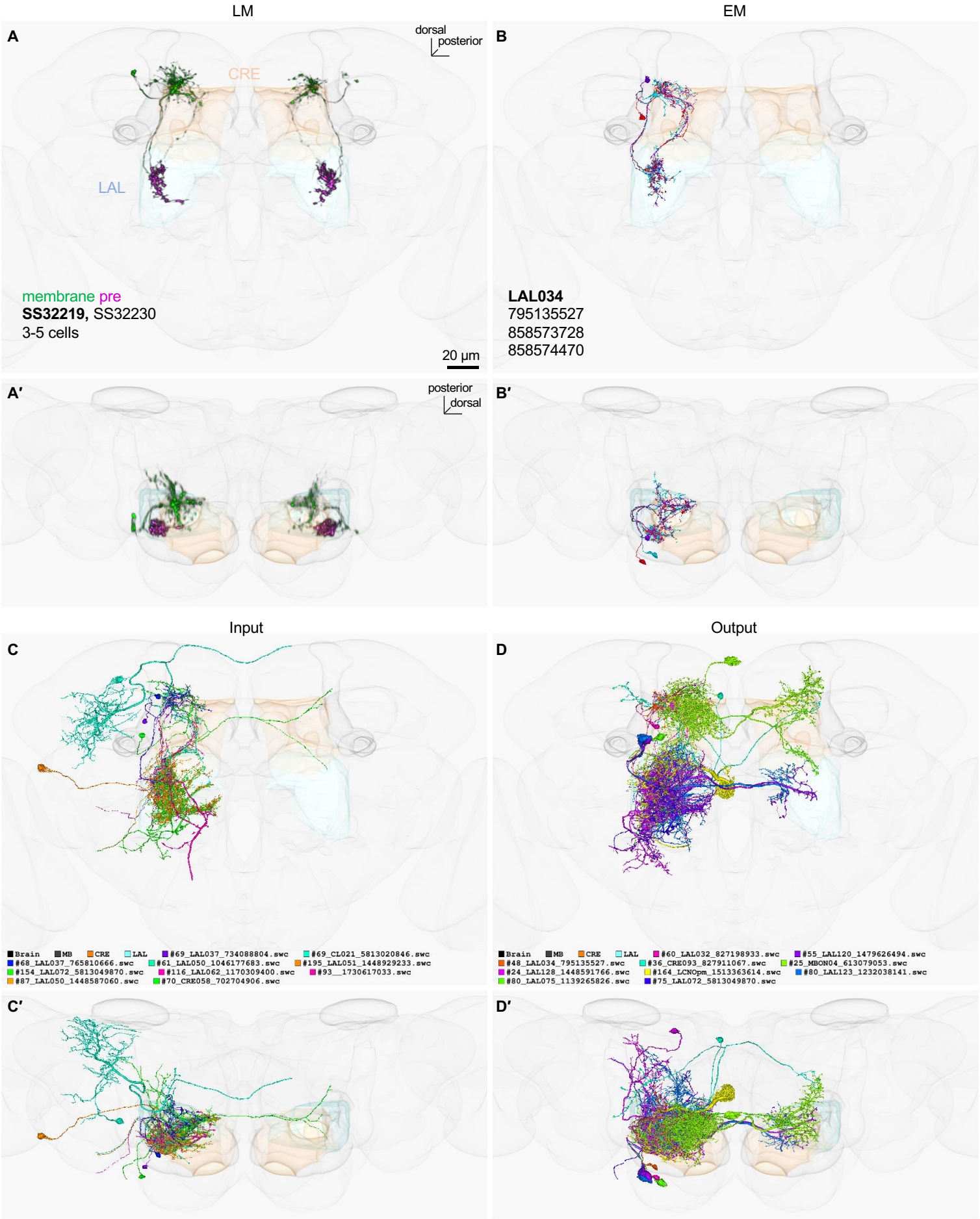

Figure 2 – figure supplement 13

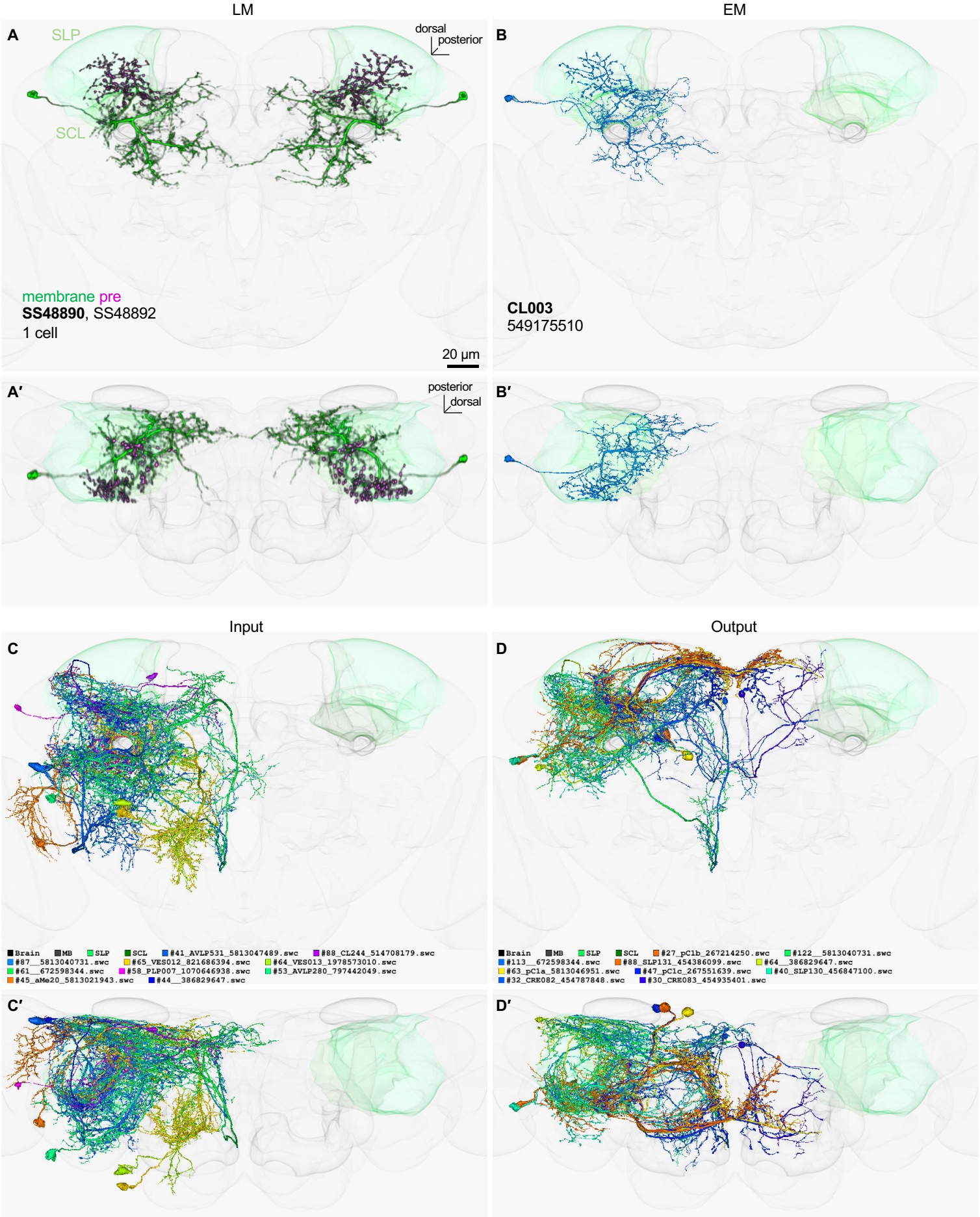

Figure 2 – figure supplement 14

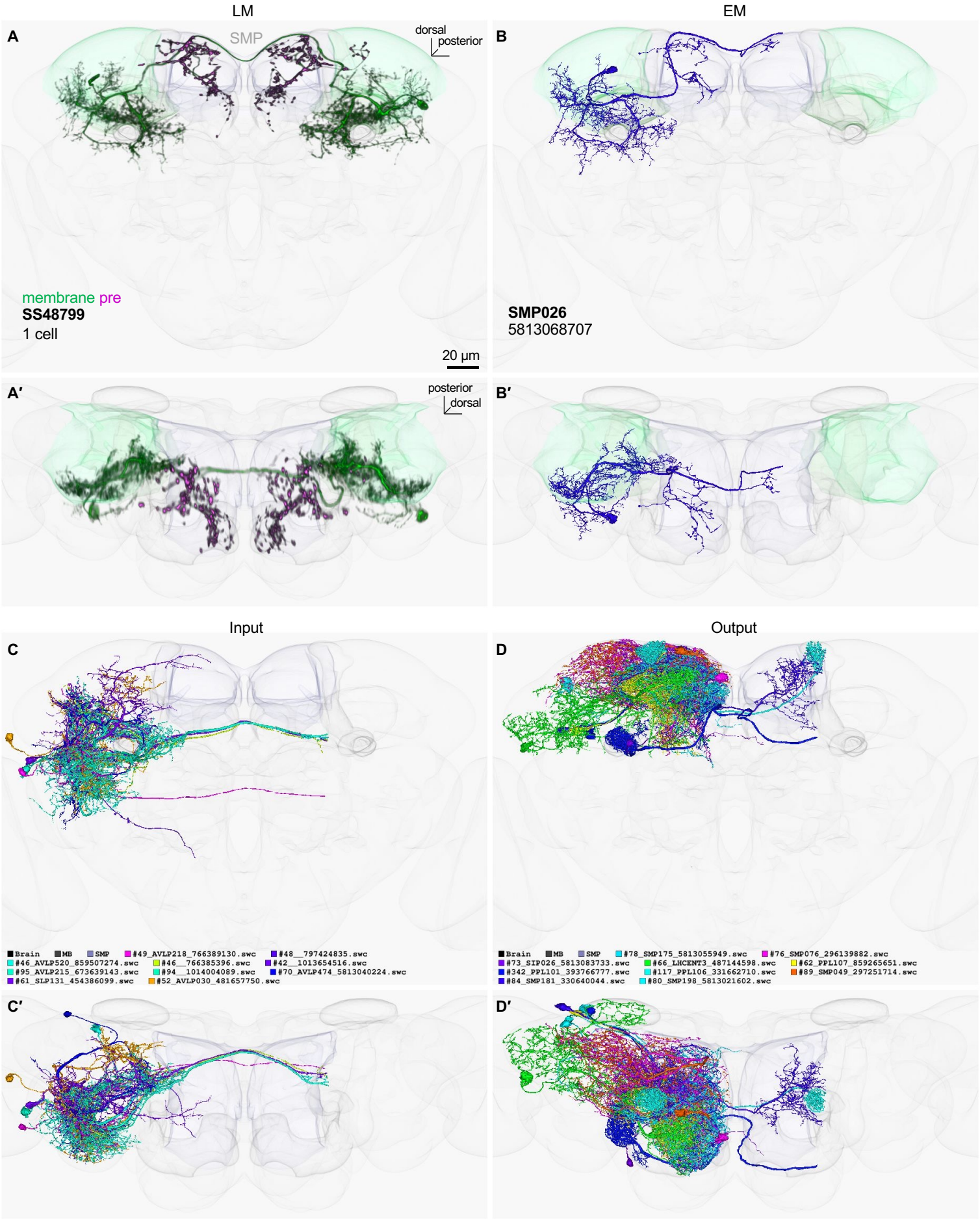

Figure 2 – figure supplement 15

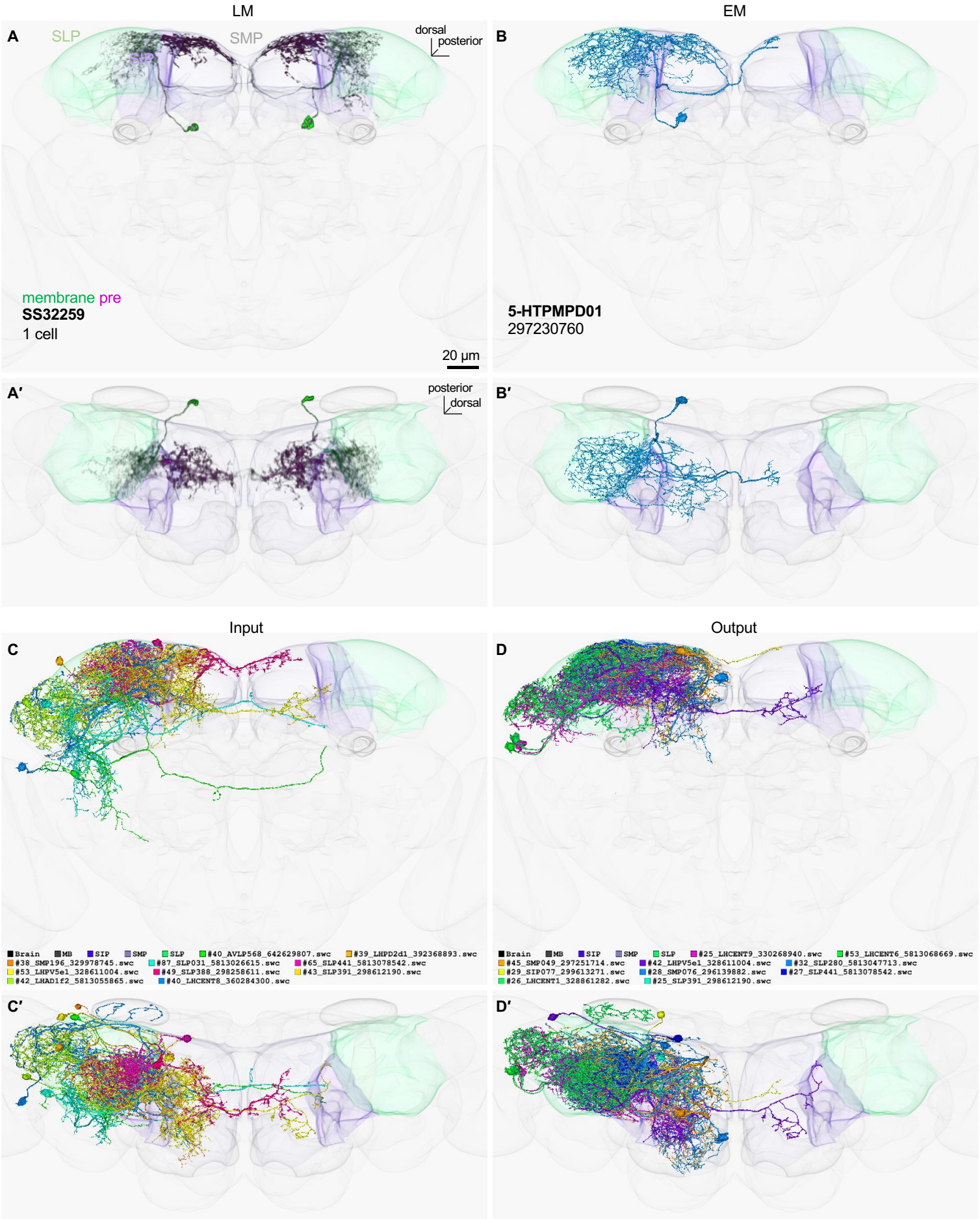

Figure 2 – figure supplement 16

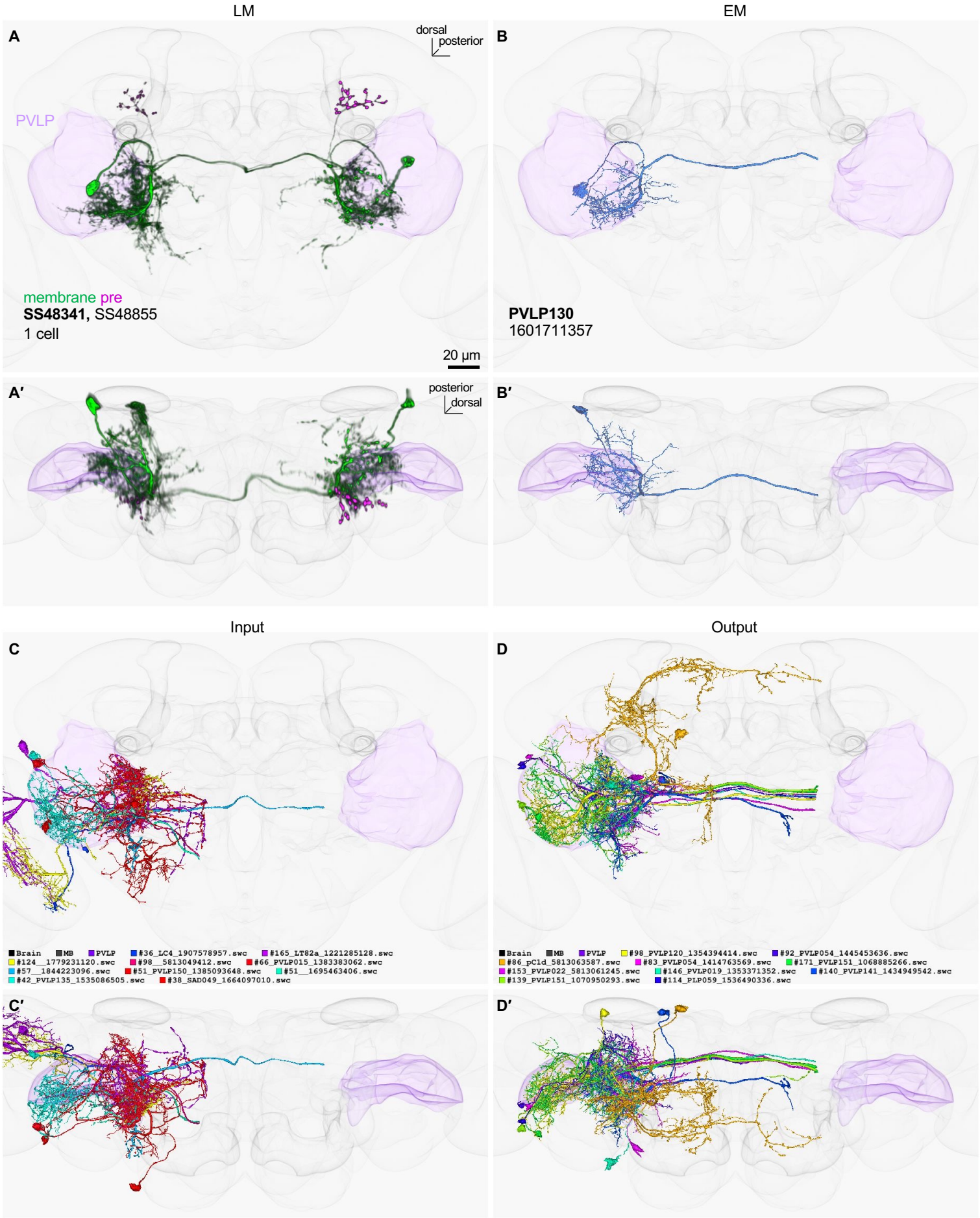

Figure 2 – figure supplement 17

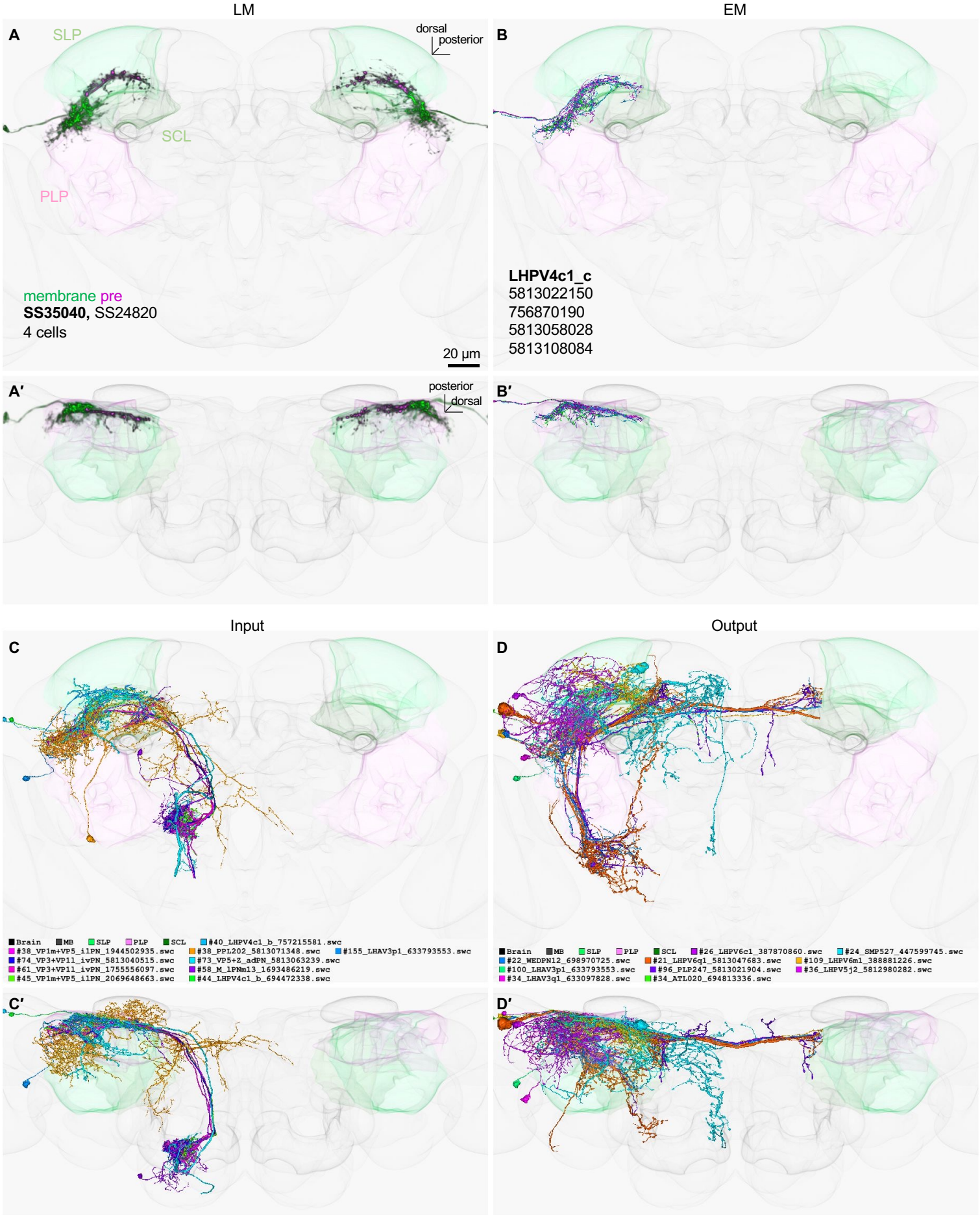

Figure 2 – figure supplement 18

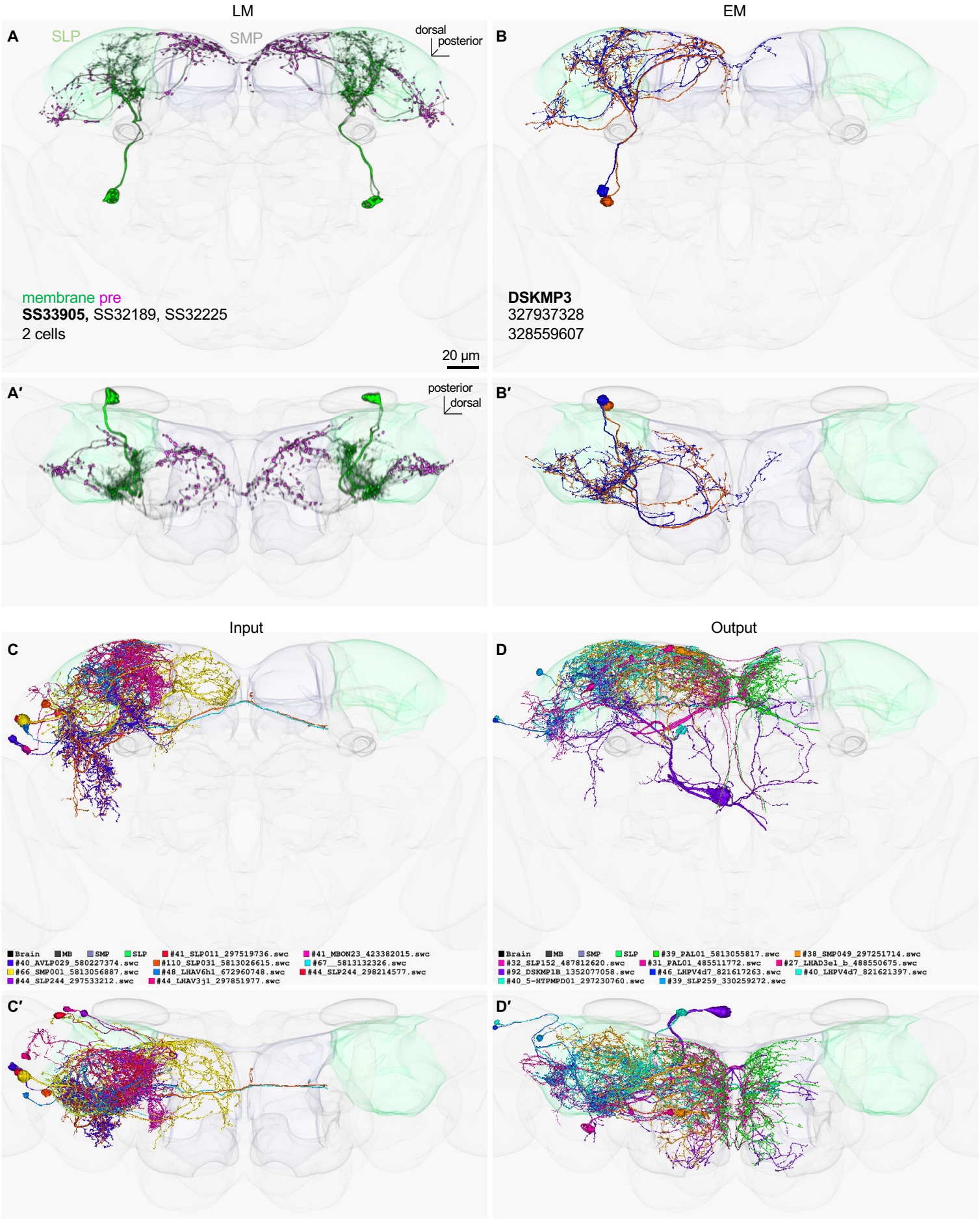

Figure 2 – figure supplement 19

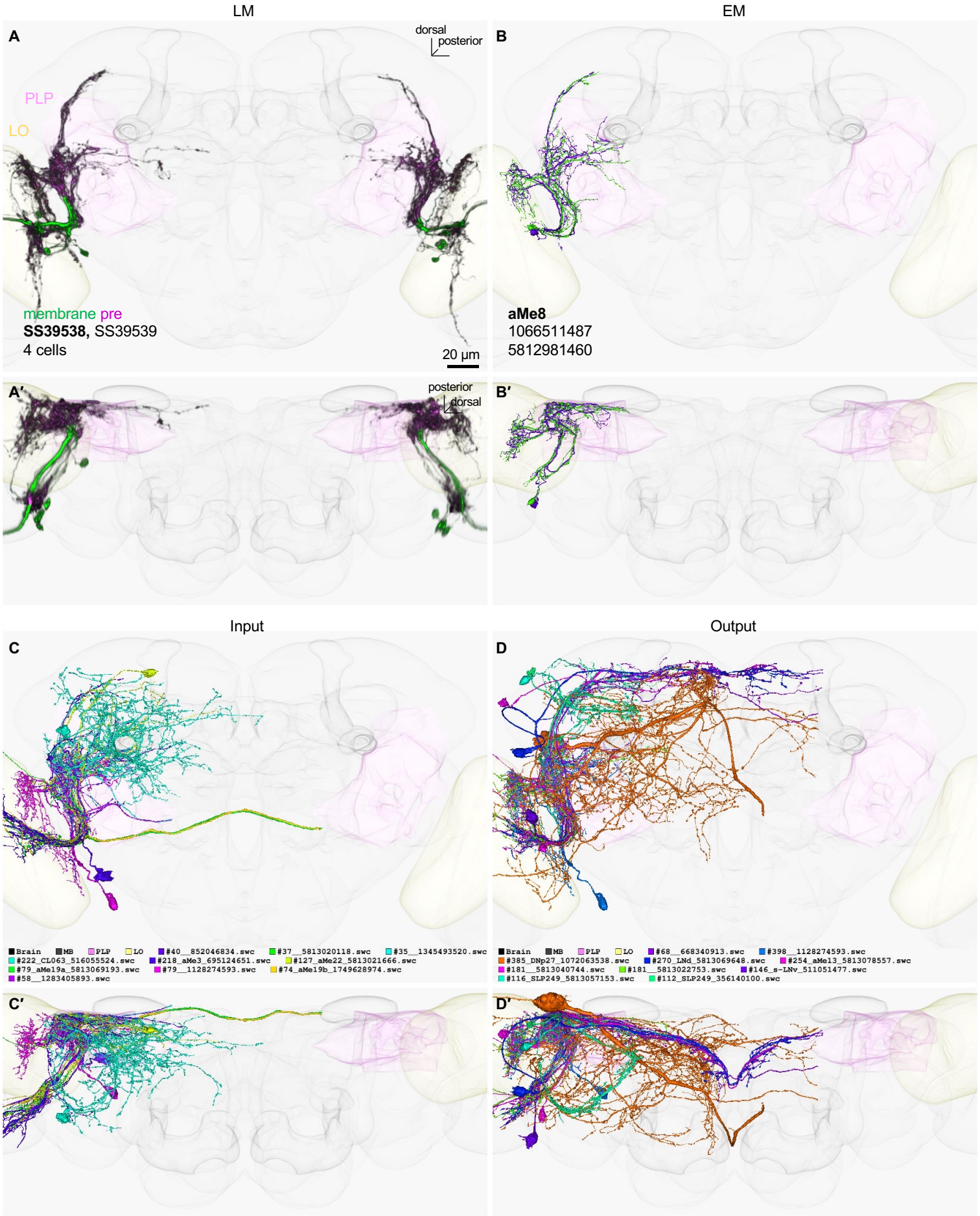

Figure 2 – figure supplement 20

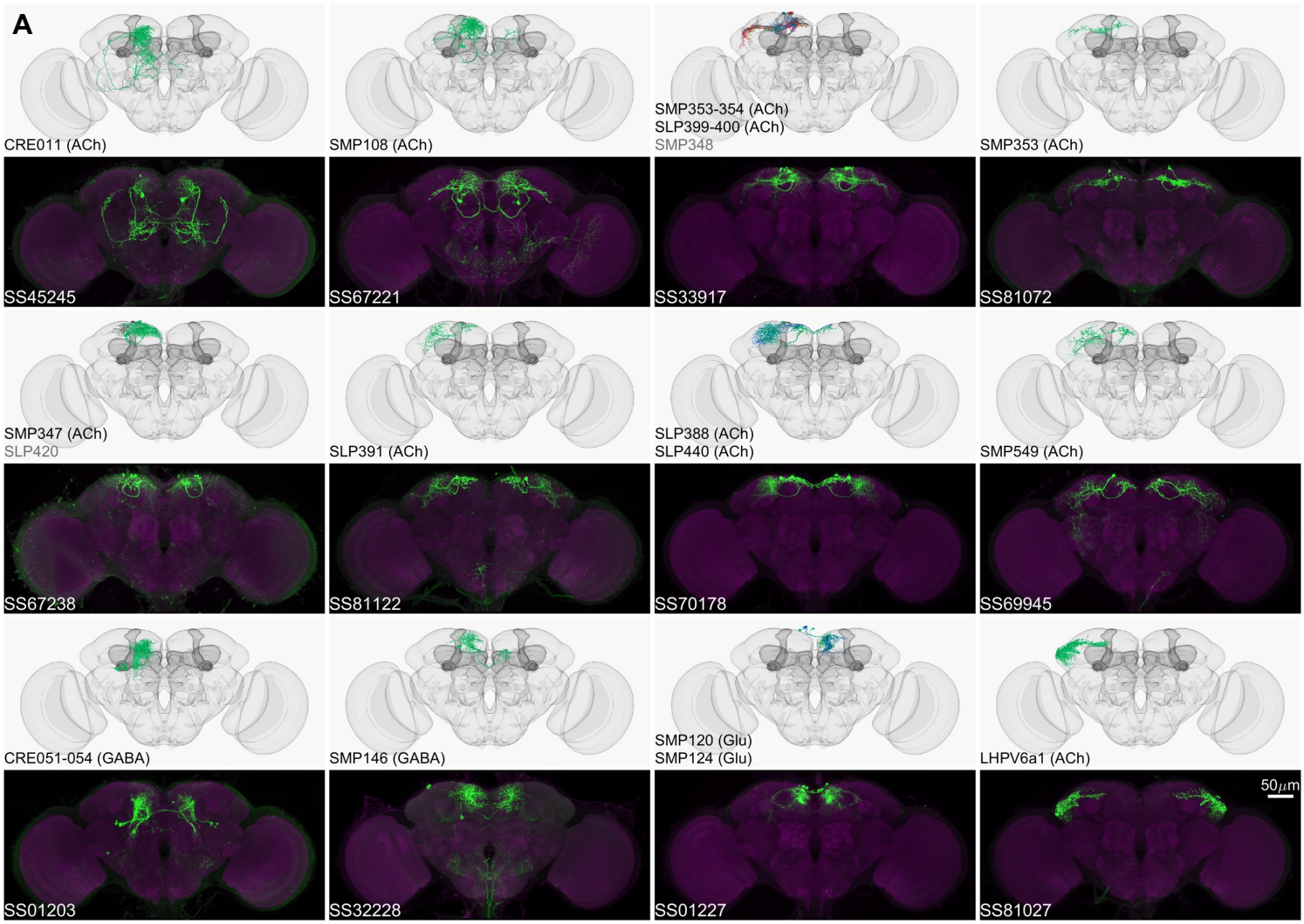

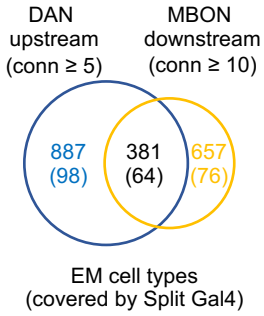

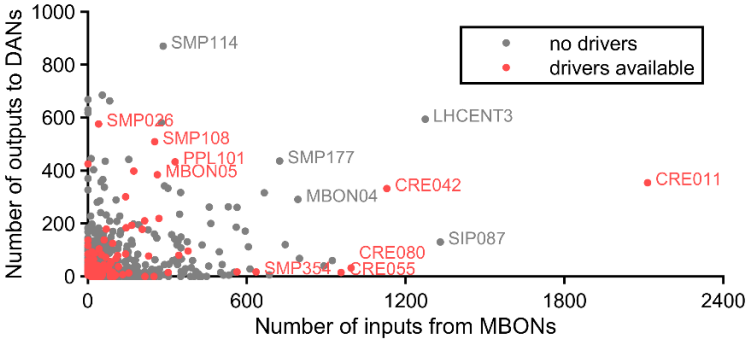

Figure 3 Drivers for MBON downstream and DAN upstream neurons.

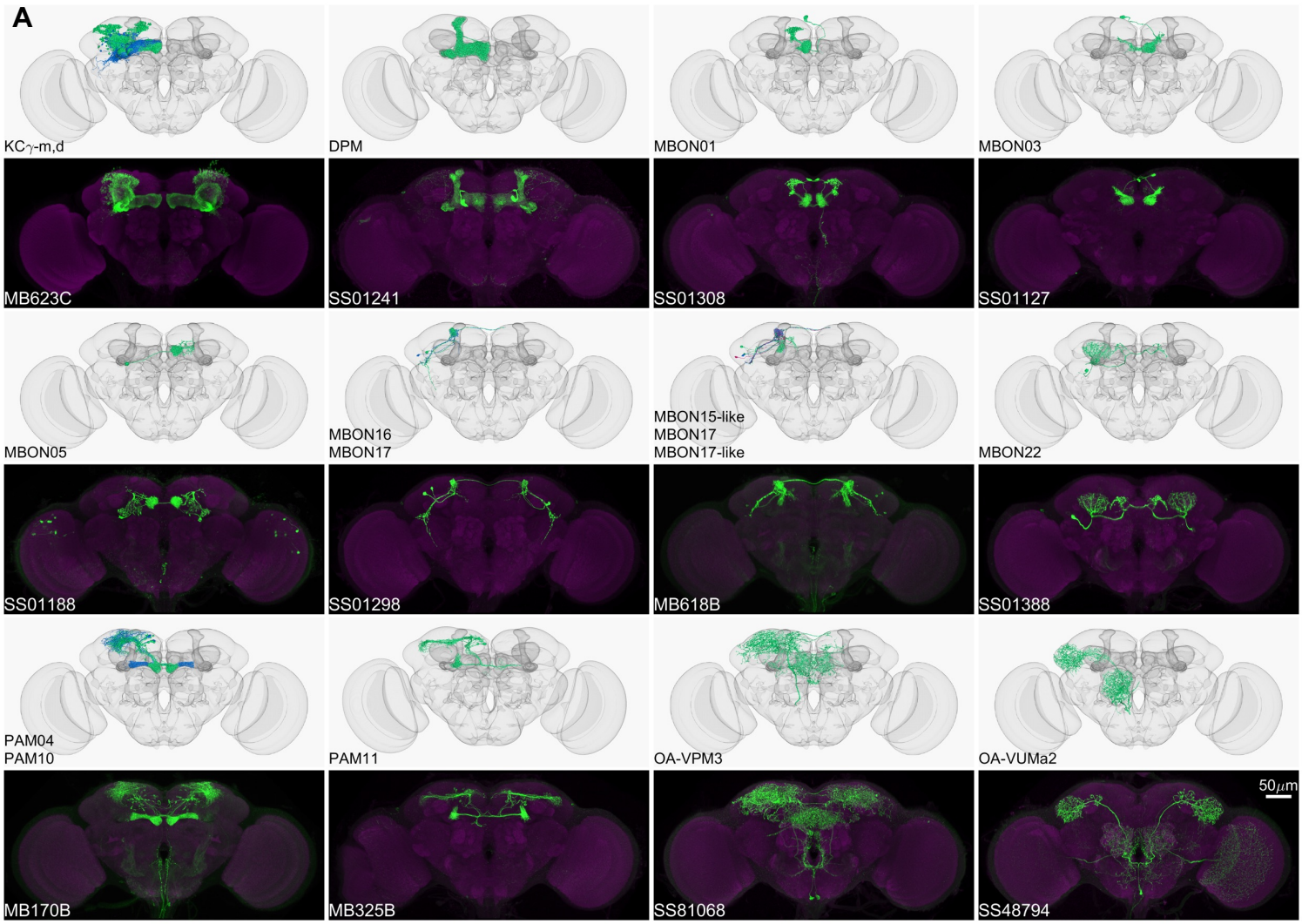

B

MB cell types	Covered cell types	Total cell types	Notable missed cell types
Intrinsic neurons (excluding KCs)	1	2	APL
MBONs	33	37	MBON24-25, 27, 34
DANs	18	23	PPL102, 201-202, PAM09,15
Modulatory (non-DANs)	6	6	
Others	4	19	
Total	62	87	

Figure 3-supplemental figure 1 New or improved drivers for MB cell types

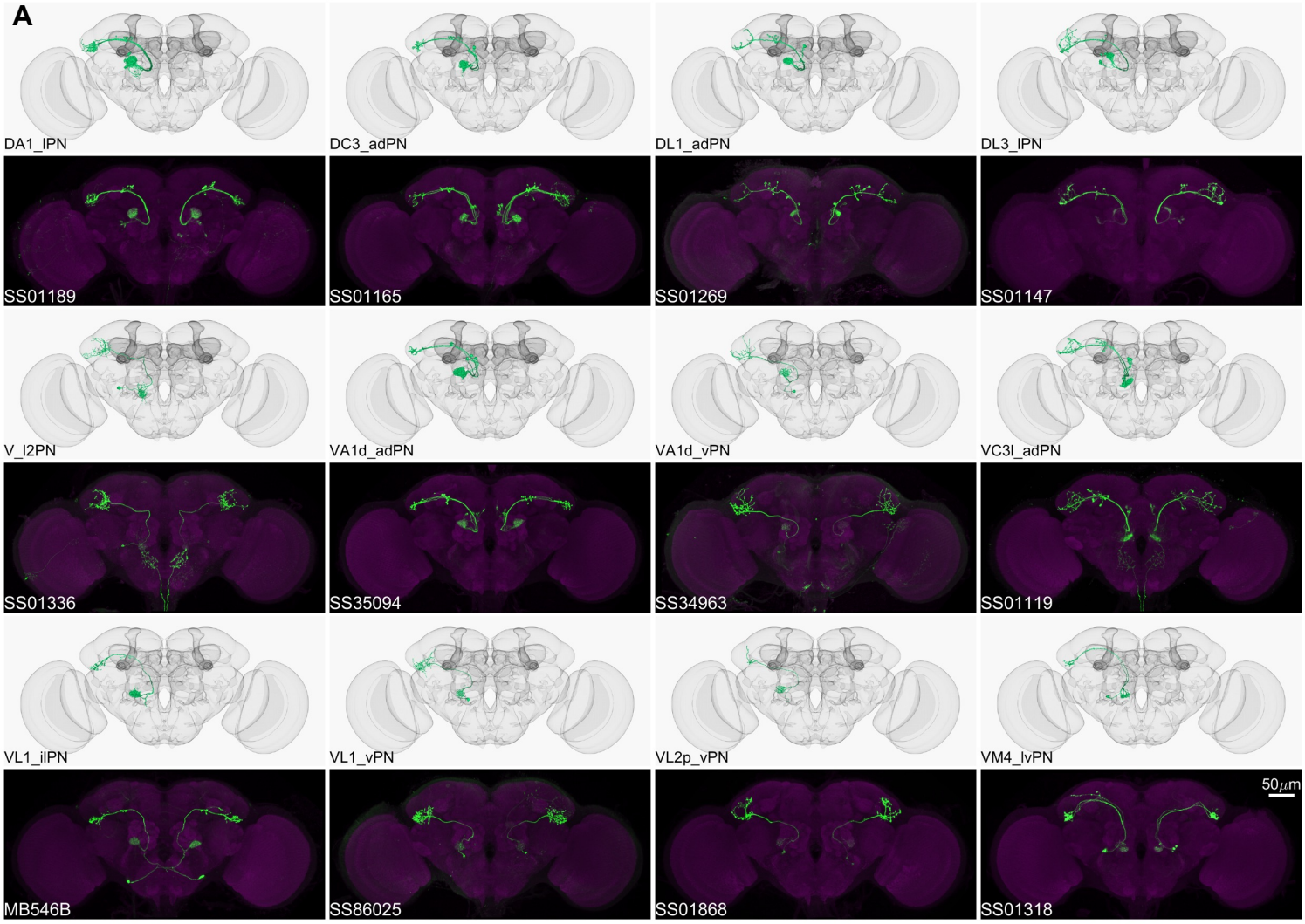

B

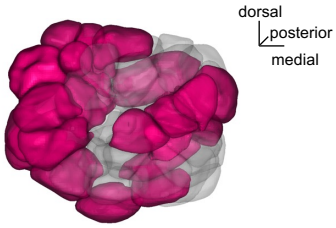

C

PN types	Covered cell types	Total cell types
Olfactory uni-glomerular PNs	26	~80
Multi-glomerular PNs and non-olfactory PNs	> 22	~110
Total	> 48	~190

Figure 4 Driver lines for uni-glomerular projection neurons

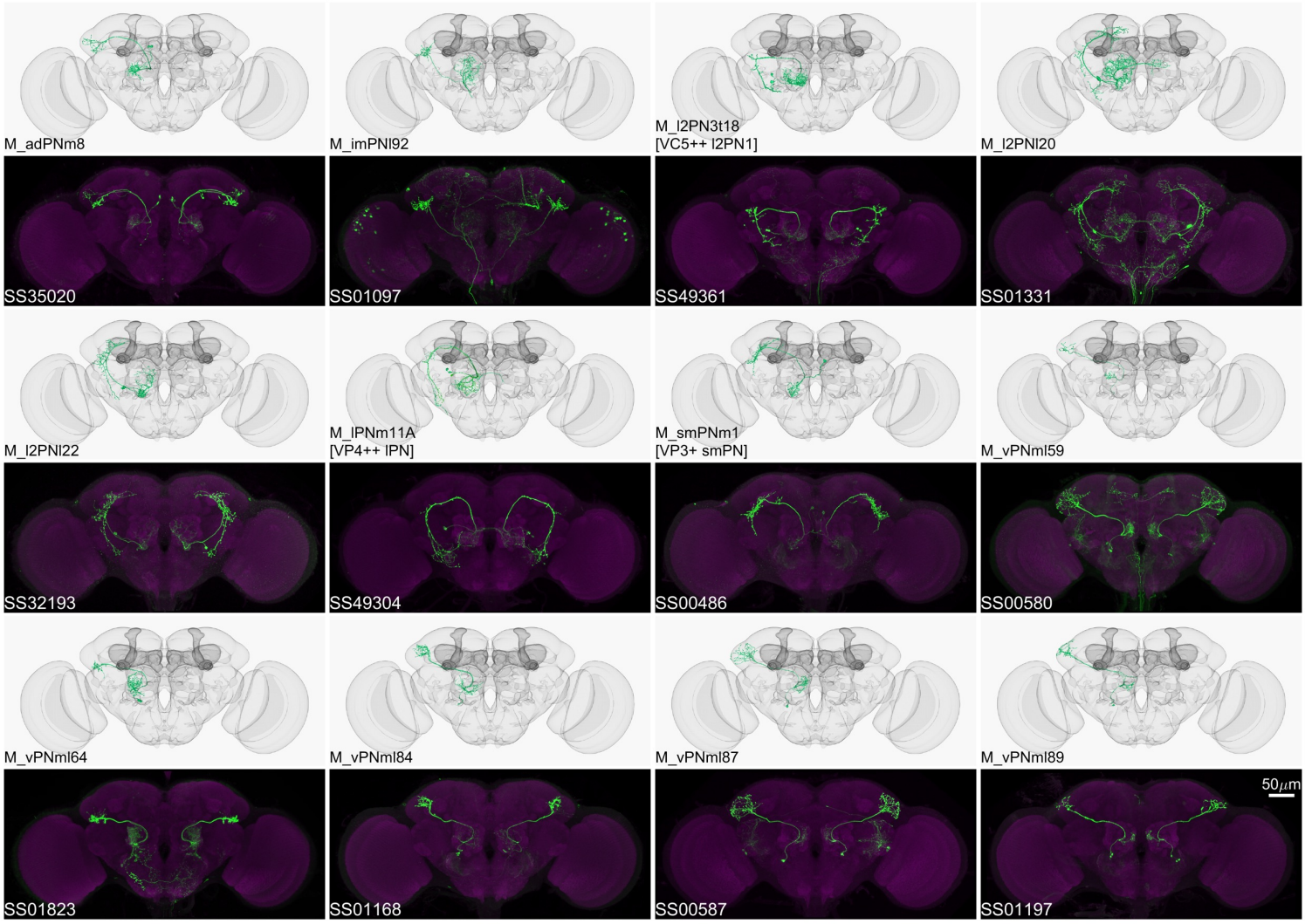

Figure 5 Driver lines for multi-glomerular projection neurons

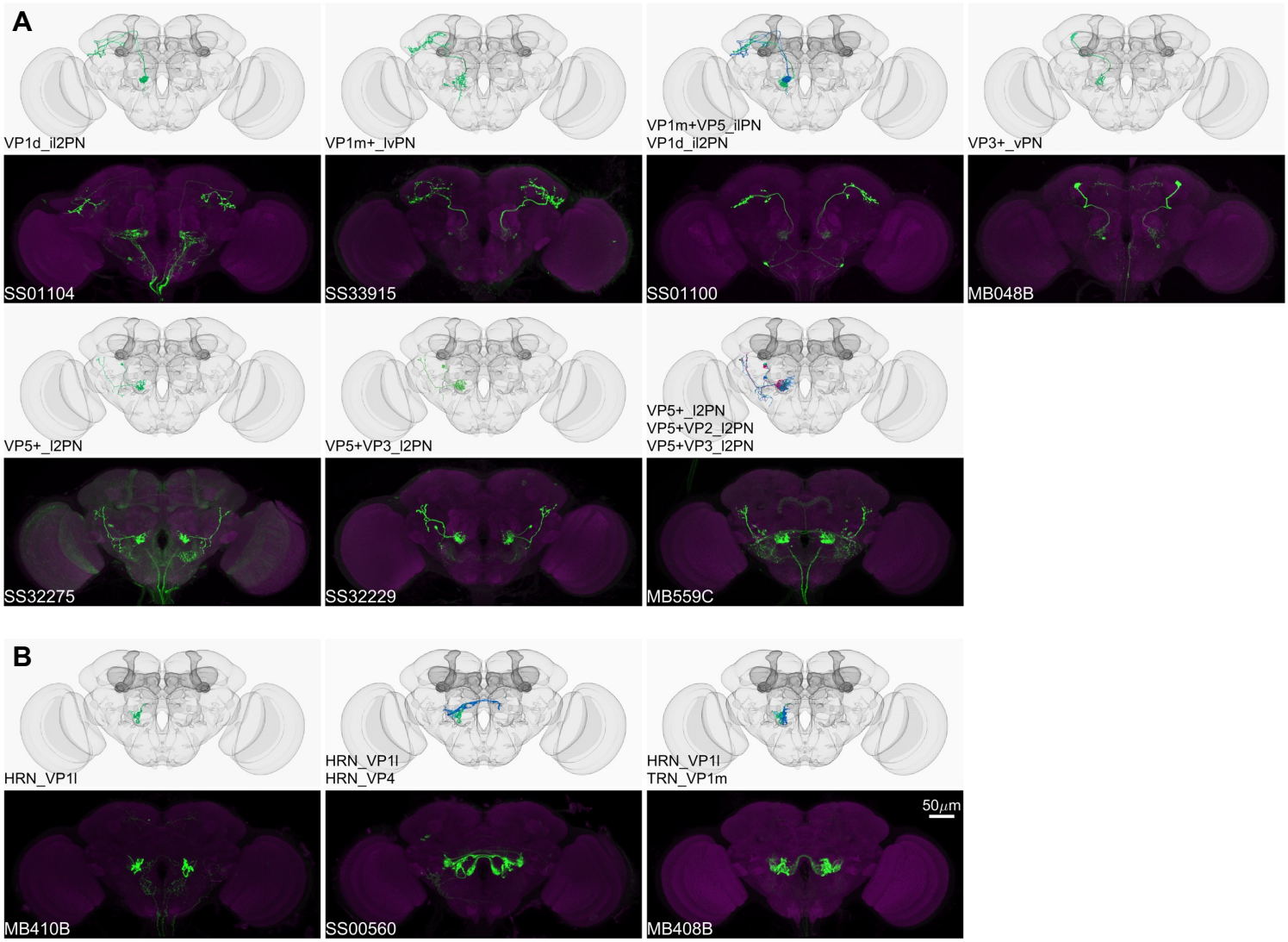

Figure 6 Driver lines for non-olfactory projection neurons and sensory neurons

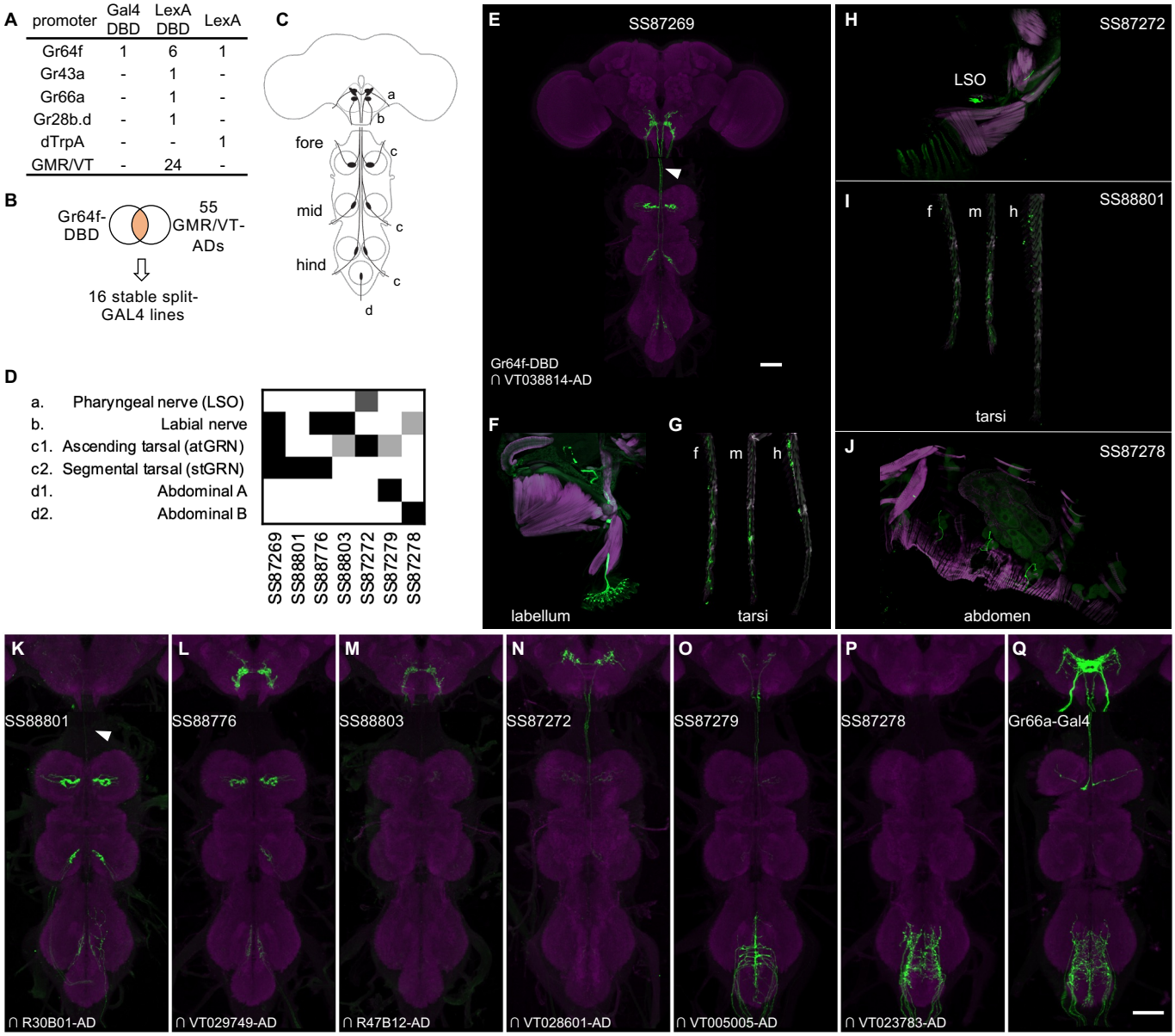

Figure 7 Driver lines for gustatory sensory neurons

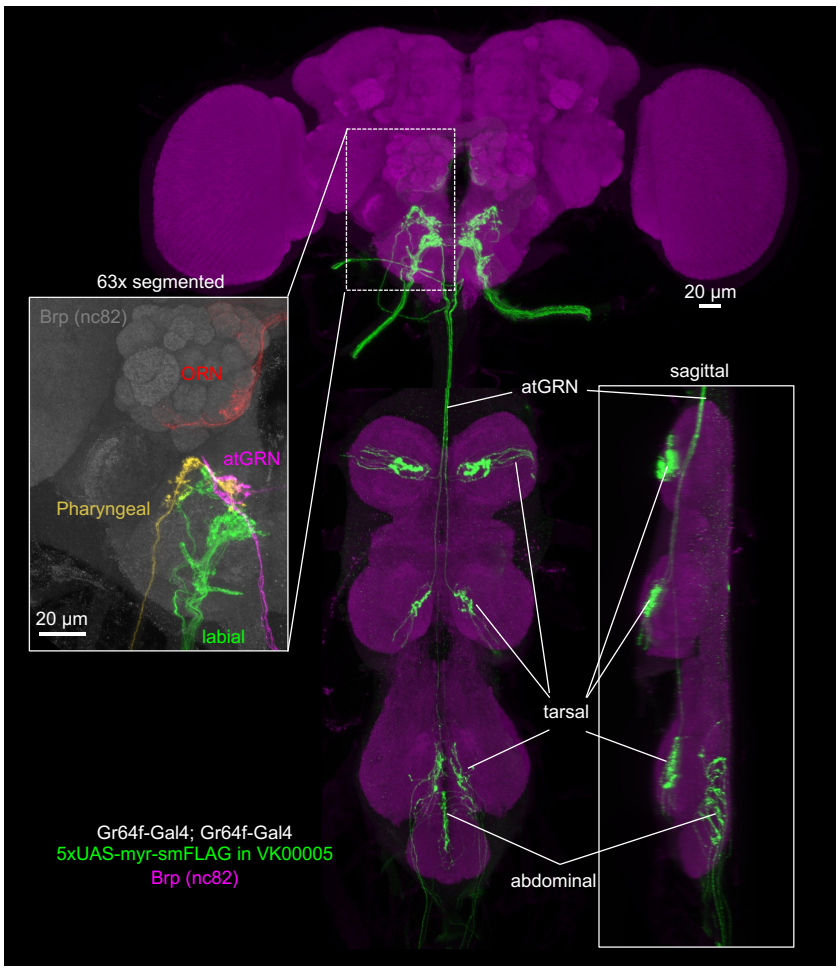

Figure 7-figure supplement 1 Expression pattern of Gr64f-Gal4

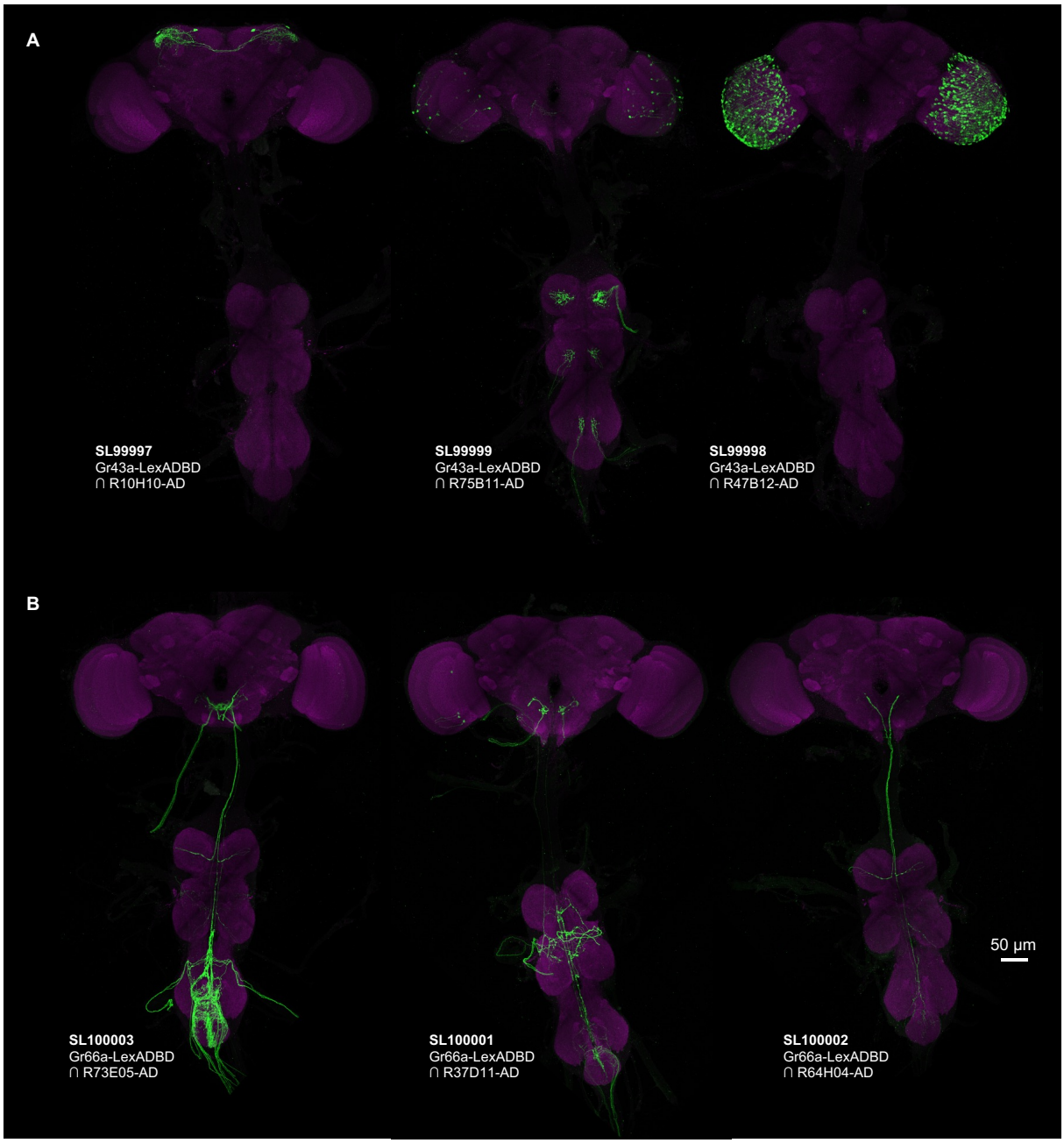

Figure 7-figure supplement 2 Expression patterns of split-LexA lines from Gr43a and Gr66a

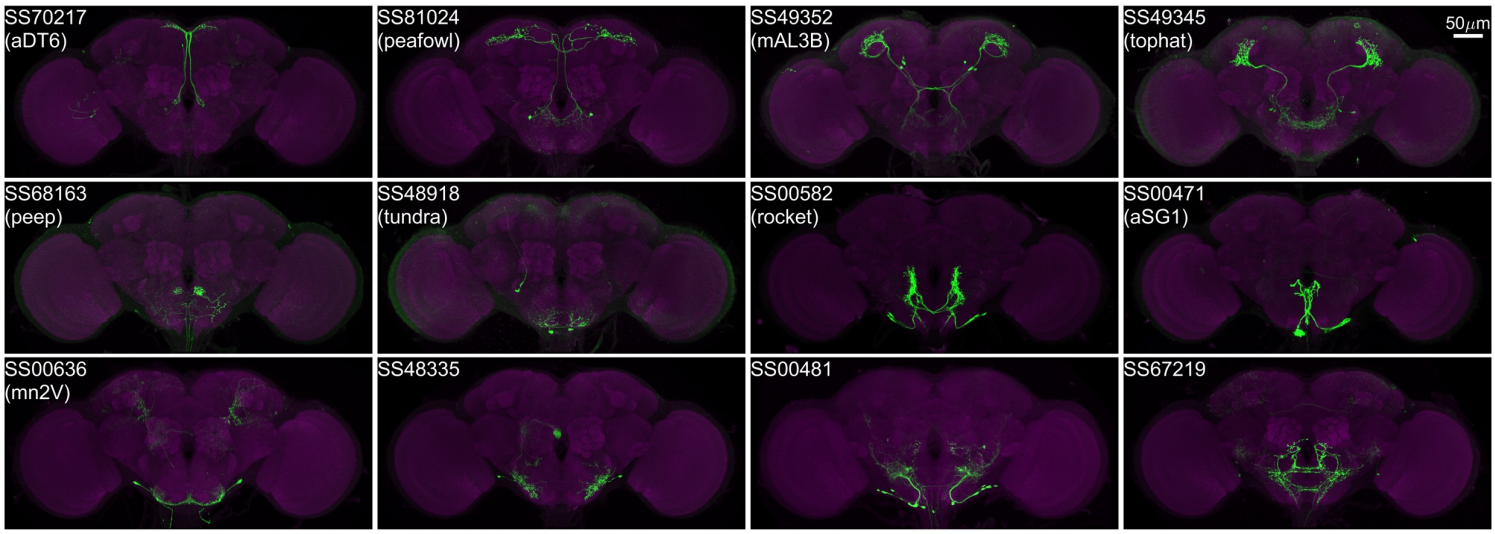

Figure 7-figure supplement 3 Examples of covered SEZ neurons

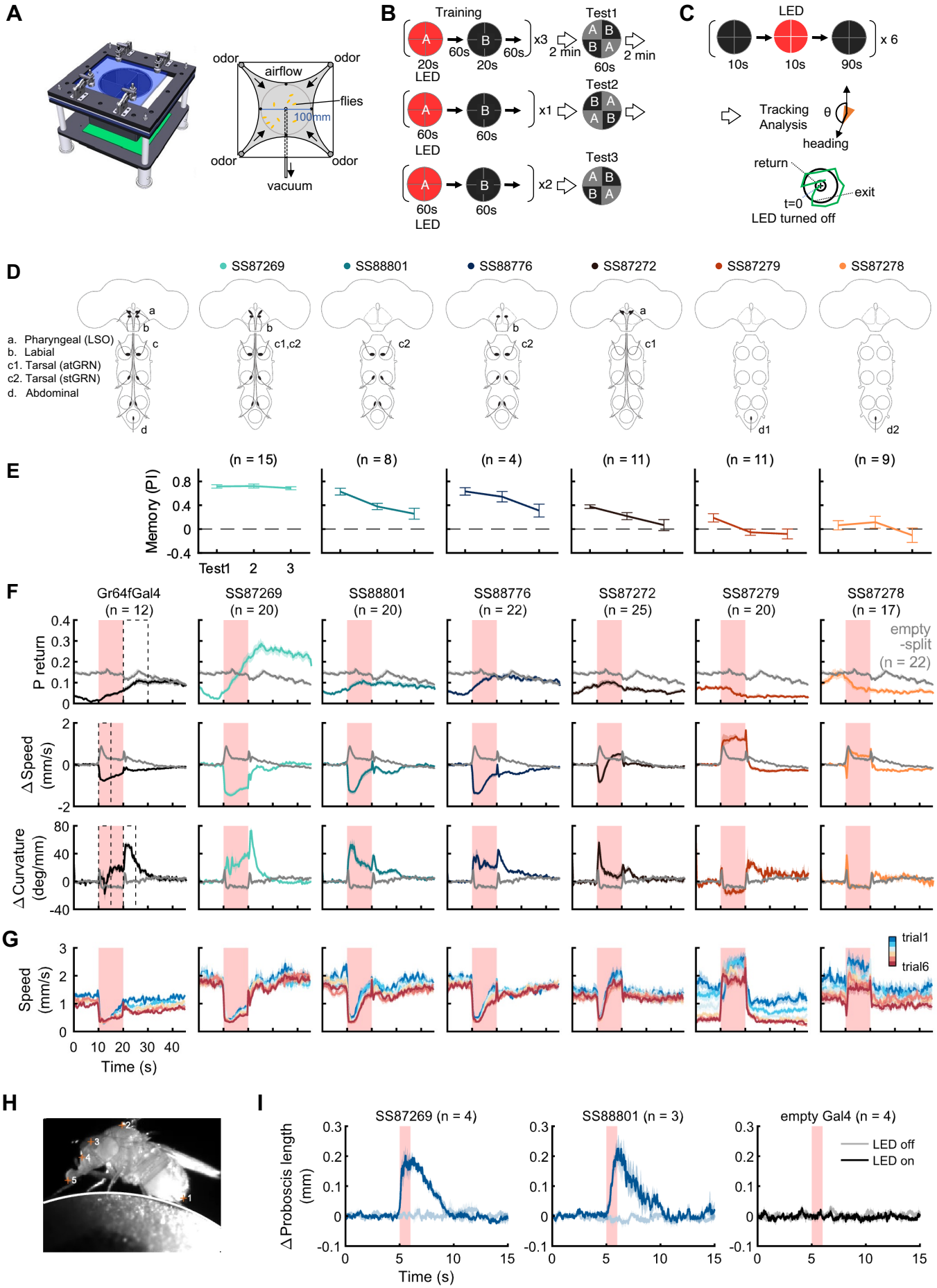

Figure 8 Behaviors with Gr64f-split-GAL4 lines

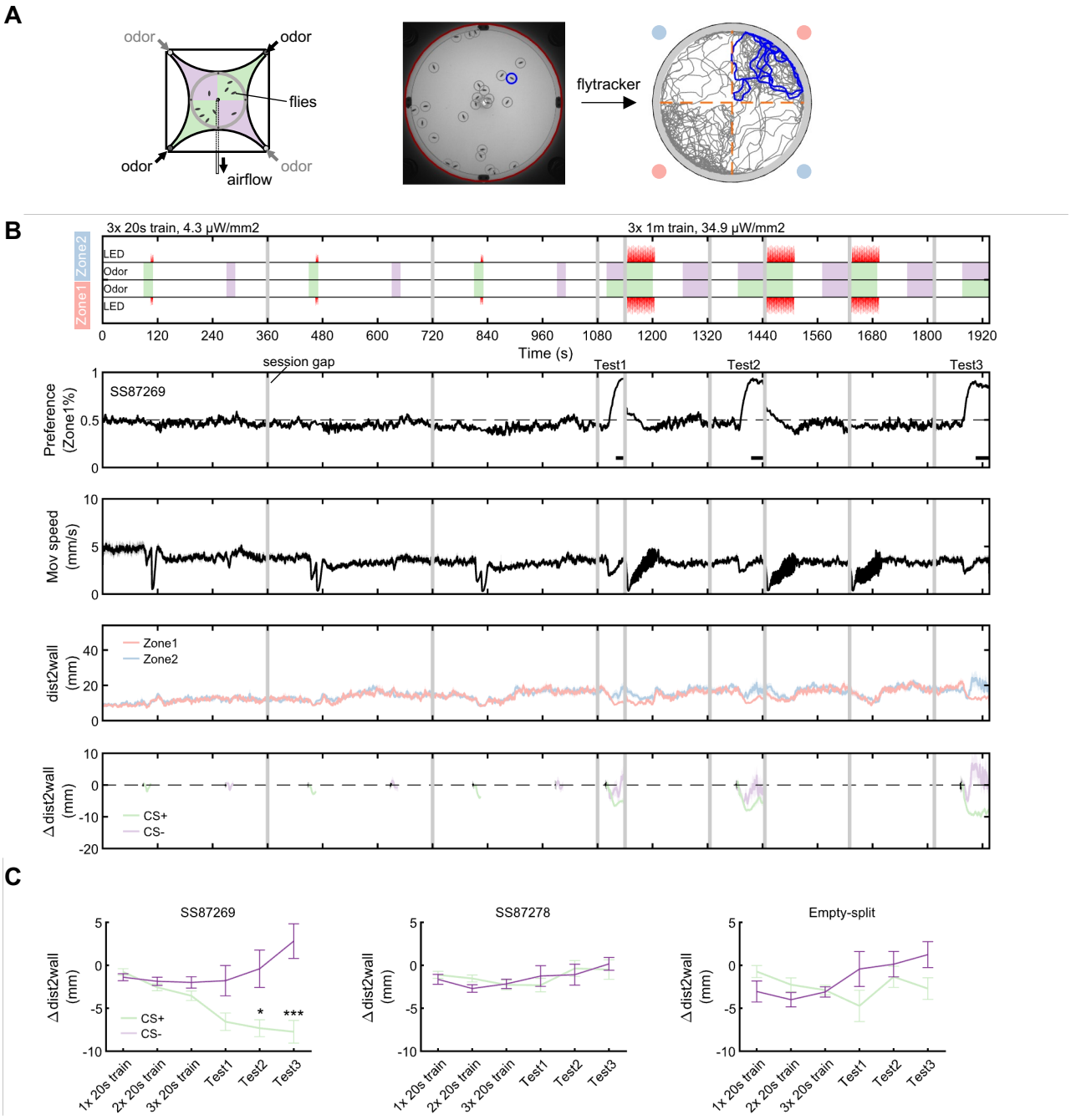

Figure 8-figure supplement 1 Olfactory arena learning experiment, fly tracking and data analysis

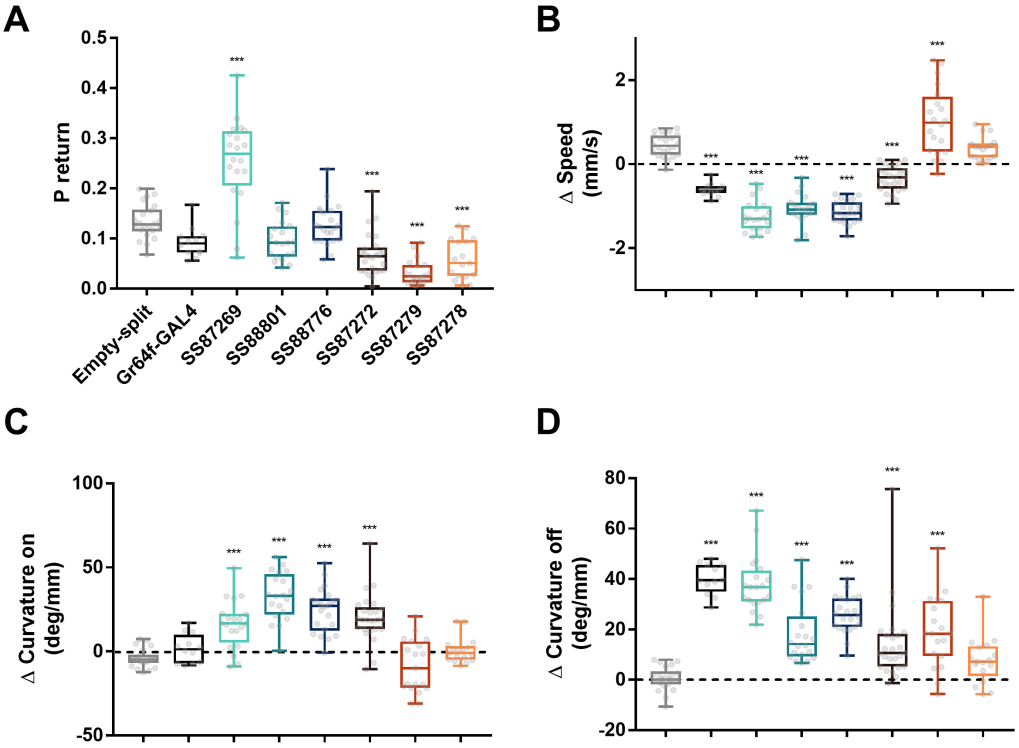

Figure 8-figure supplement 2 Summary data of Gr64f-split-Gal4 activation phenotypes

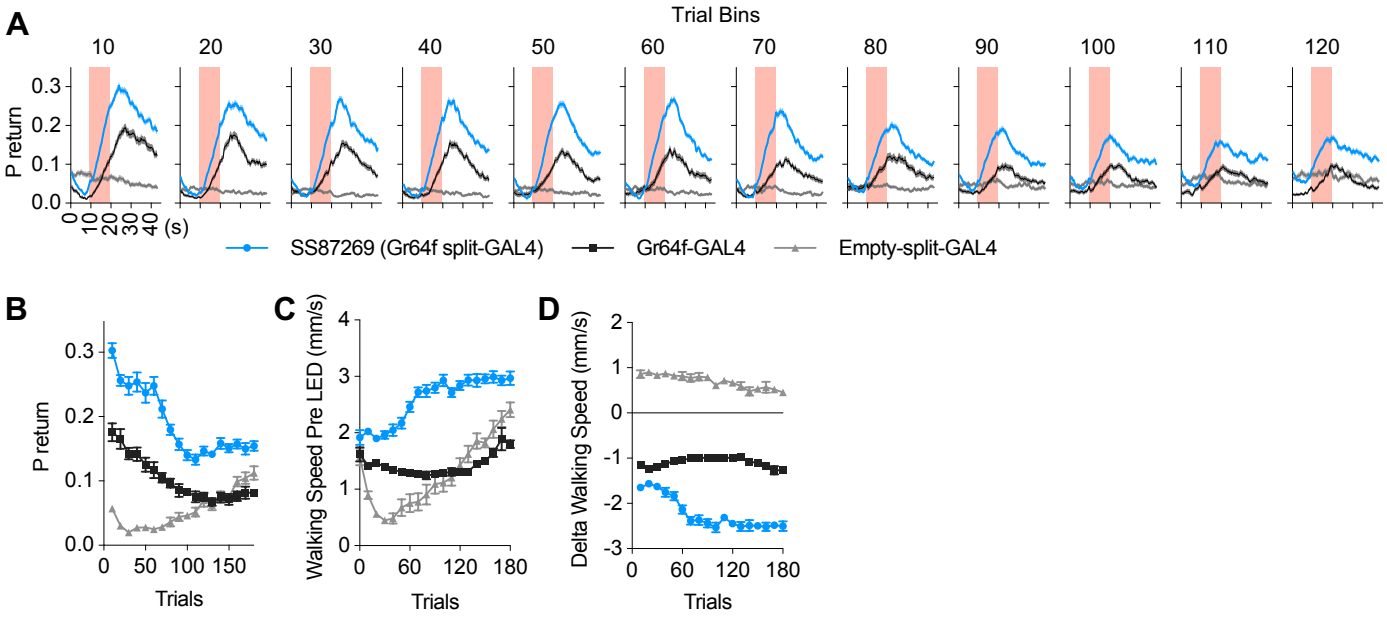

Figure 8-figure supplement 3 Consistency of Gr64f-split-GAL4 phenotypes over repeated activations

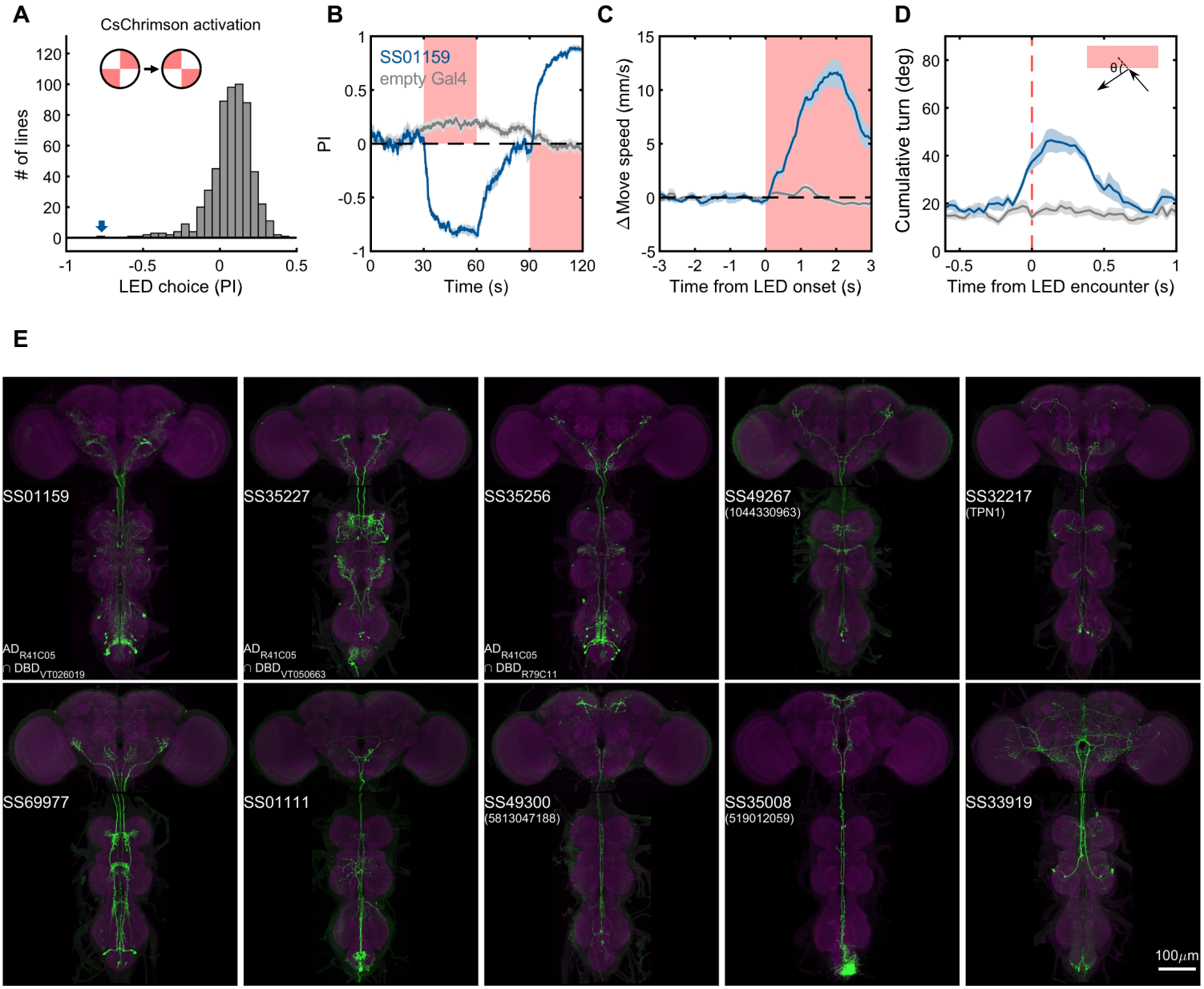

Figure 9 Examples of covered ascending neurons

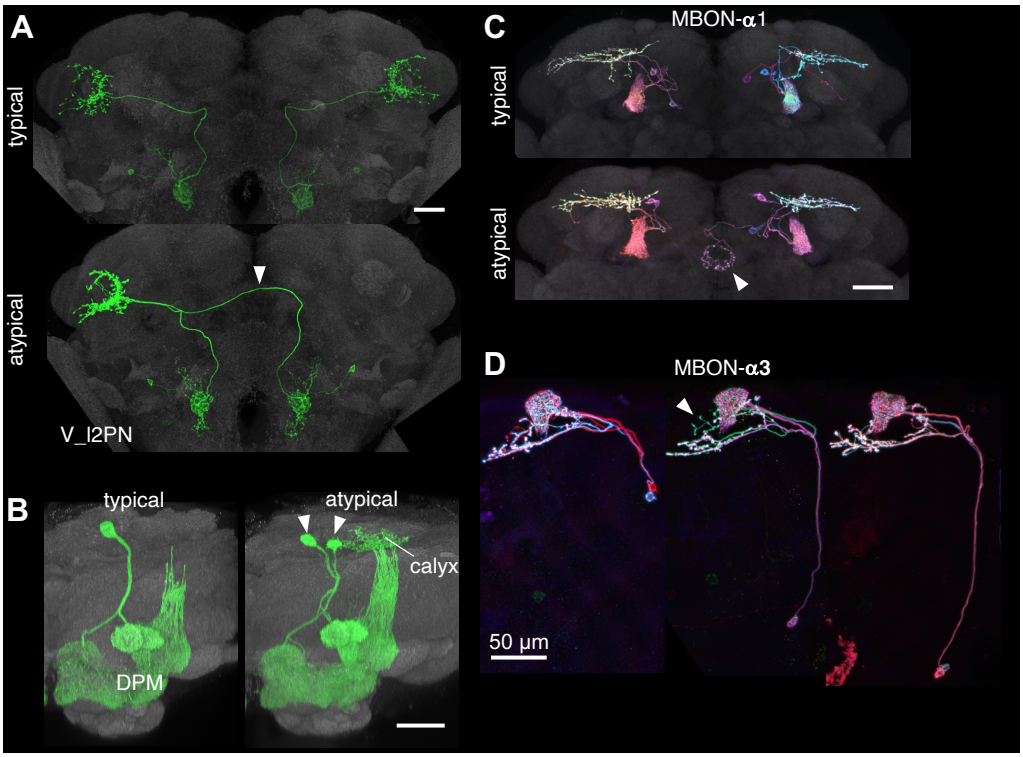

E

Cell Type	MB compartments	N hemisphere examined	Typical number of cells	Different number of cells (%)	Mislocalization (%) Dendrite	Mislocalization (%) Axon	mode of errors
MBON01	Y5, β'2a	16	1	0.0	0.0	12.5	mislocalization of axons
MBON02	β2, β'2a	96	1	1.0	1.0	1.0	mislocalization of axons
MBON03	β'2mp	56	1	0.0	0.0	0.0	
MBON05	Y4	50	1	0.0	0.0	0.0	
MBON06	β1	38	1	0.0	0.0	0.0	
MBON07	α1	105	2	0.0	22.9	1.9	dendrites outside the MB axon in the ellipsoid body third soma without neurites
MBON08/09	Y3, β'1	338	2	0*	*	0.6	see Figure 11
MBON11	Y1, pedc	136	1	0.7	0.7	1.5	dendrites in Y2 axon in the calyx lack of axon in α3
MBON12	Y2, α'1	106	2	0.0	0.0	0.0	
MBON13	α'2	82	1	0.0	1.2	0.0	dendrites outside the MB
MBON14	α3	44	1	0.0	0.0	2.3	additional axon branch
MBON18	α2sc	36	1	0.0	0.0	0.0	
MBON19	α2p3p	34	2	0.0	0.0	0.0	
MBON22	calyx	56	1	1.8	17.9	0.0	dendriets outside the calyx
MB-DPM	all	48	1	8.3	4.2	4.2	Second DPM axons/dendrites in the calyx

Figure 10 Stereotypy and erroneous projections

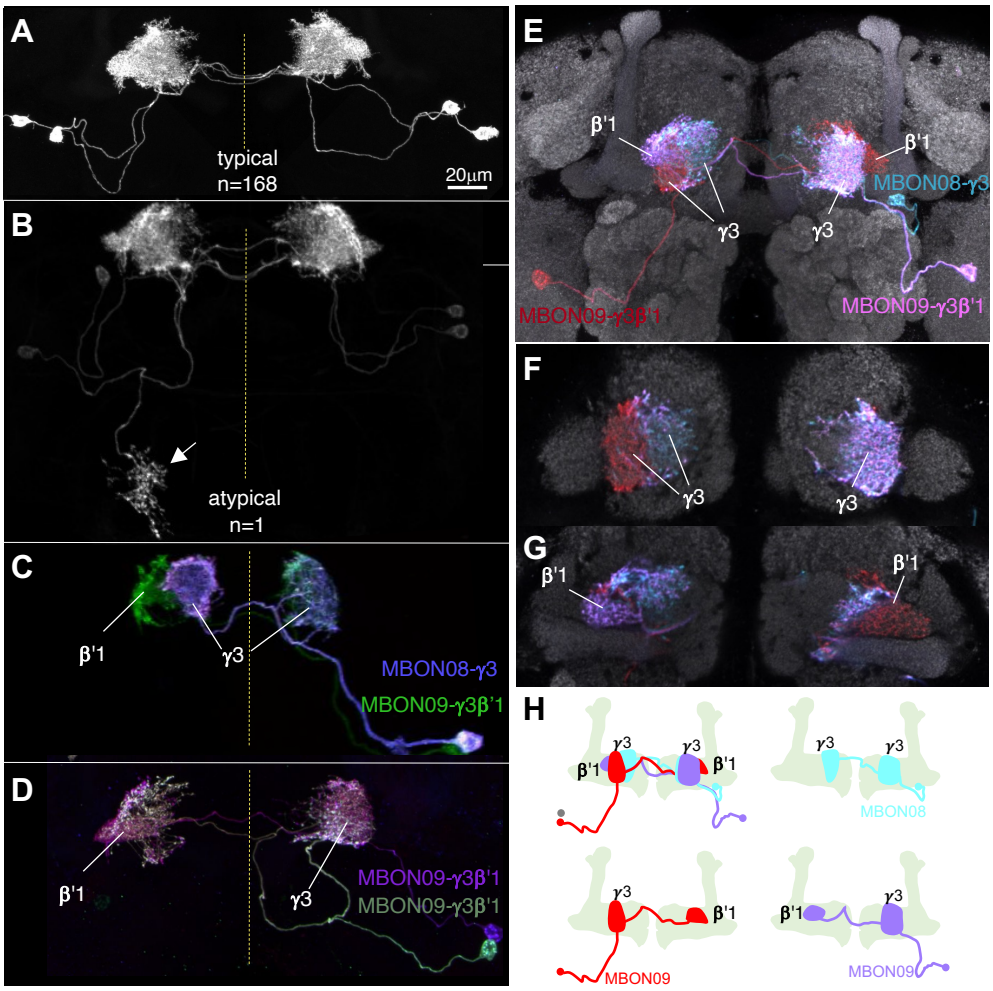

I

	Female	Male	Total
MBON08	7	14	21
MBON09	102	86	188
% MBON08	6.4	14.0	10.0
P only MBON09	0.77	0.55	0.65
P at least One MBON08	0.23	0.45	0.35

J

Left 2 cells	Right 2 cells	Left γ3	Left β'1	Right γ3	Right β'1	Estimated Probability (%)	
08/08	08/08	+		+		0.01	No occurrence in 169 flies
08/08	08/09	+	+	+		0.18	
08/08	09/09	+	+	+		0.82	
08/09	08/08	+		+	+	0.18	
09/09	08/08	+		+	+	0.82	
08/09	08/09	+	+	+	+	3.27	No occurrence in MCFO
08/09	09/09	+	+	+	+	14.63	
09/09	08/09	+	+	+	+	14.63	
09/09	09/09	+	+	+	+	65.47	
MBON type		MB compartments					

Figure 11 Individuality and asymmetry of MBON08 and MBON09

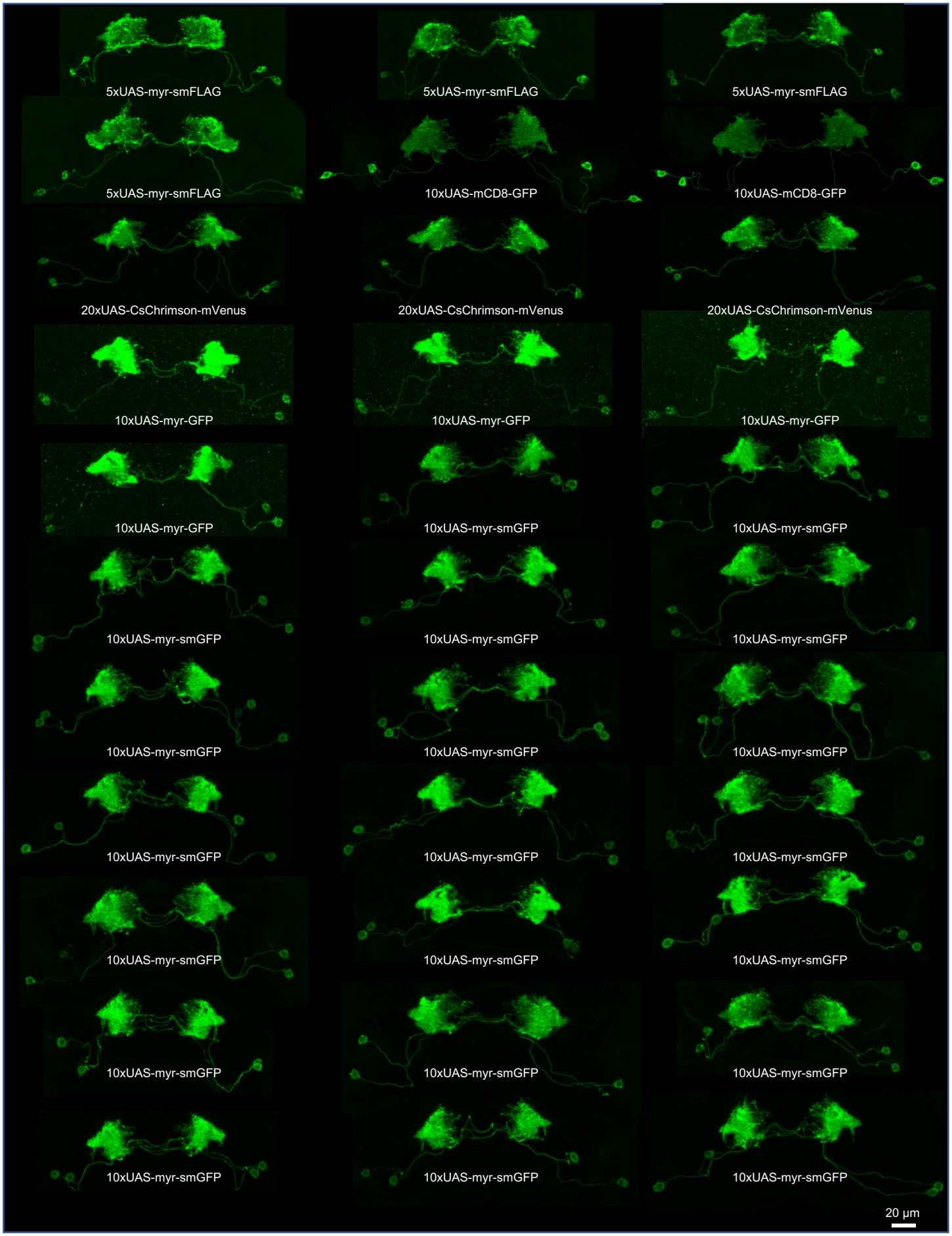

Figure 11 – figure supplement 1 MB083C invariantly label two MBONs

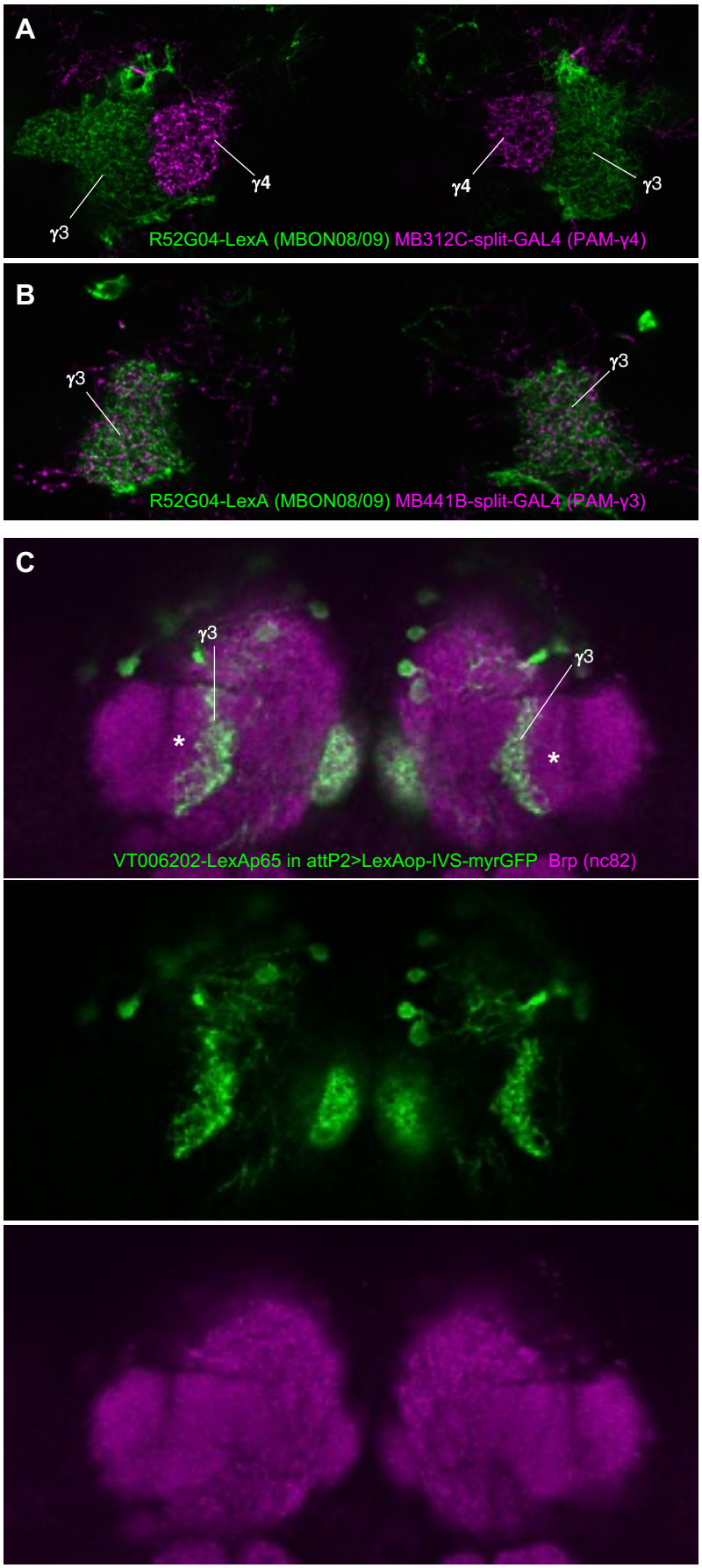

Figure 11 – figure supplement 2 Subdivisions of medial and lateral γ3 compartments

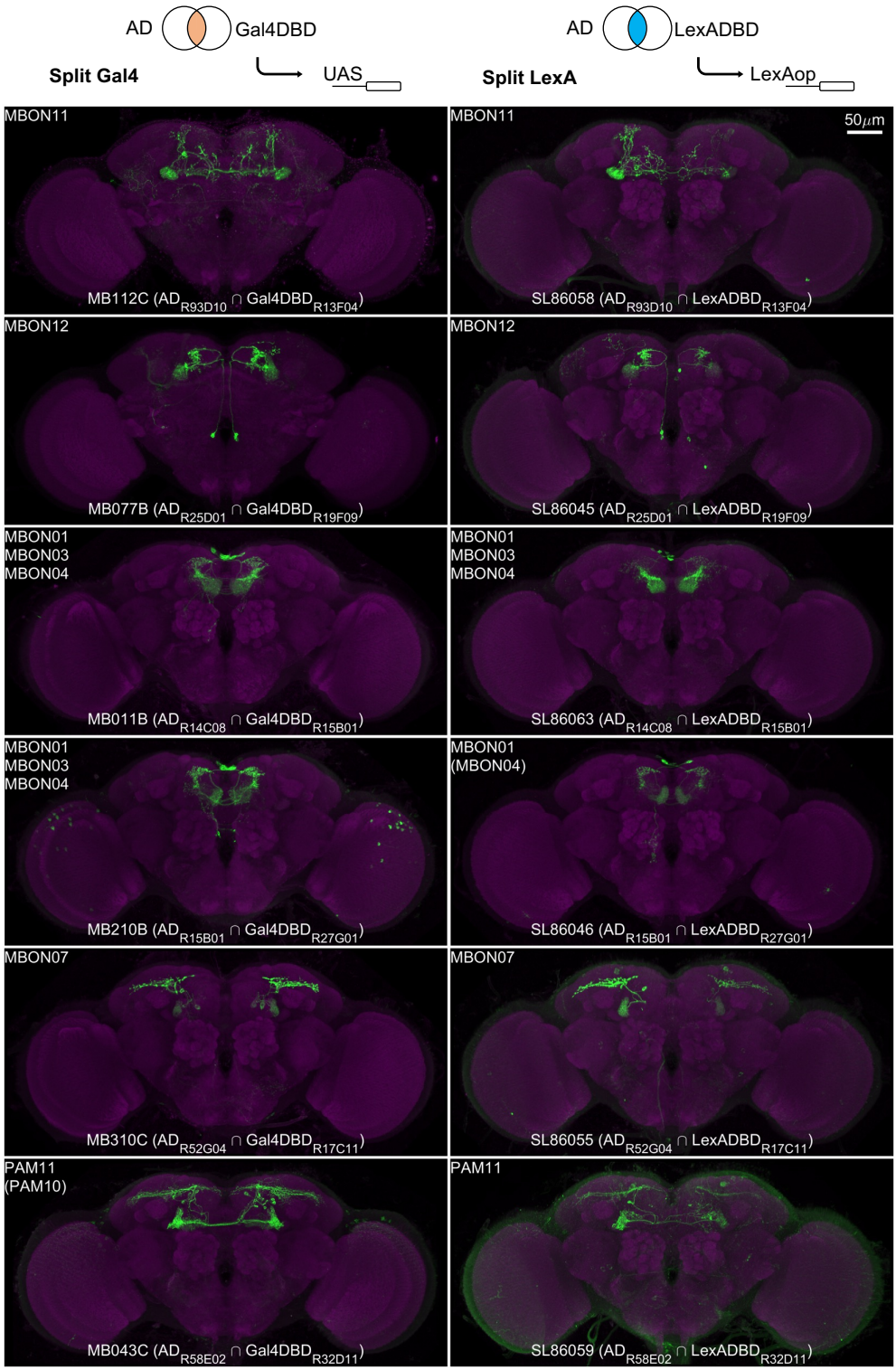

Figure 12 Examples of split-LexA conversion